

APPLICATION OF SUPERPARAMAGNETIC MESOPOROUS SILICATES ON  
NALIDIXIC ACID REMOVAL

Miss Vichuda Tipsunave

A Thesis Submitted in Partial Fulfillment of the Requirements  
for the Degree of Master of Science Program in Environmental Management  
(Interdisciplinary Program)  
Graduate School  
Chulalongkorn University  
Academic Year 2010  
Copyright of Chulalongkorn University

การประยุกต์ใช้เมโซพอร์สซิลิเกตที่มีสมบัติซูเปอร์พาราแมกเนติกในการกำจัดกรดนาลิติซิก

นางสาว วิชชุดา ทิพย์สุนาวี

วิทยานิพนธ์นี้เป็นส่วนหนึ่งของการศึกษาตามหลักสูตรปริญญาวิทยาศาสตรมหาบัณฑิต

สาขาวิชาการจัดการสิ่งแวดล้อม (สหสาขาวิชา)

บัณฑิตวิทยาลัย จุฬาลงกรณ์มหาวิทยาลัย

ปีการศึกษา 2553

ลิขสิทธิ์ของจุฬาลงกรณ์มหาวิทยาลัย



วิชาดา ทิพย์สุนาวี: การประยุกต์ใช้เมโซพอร์ซิลิเกตที่มีสมบัติซูเปอร์พาราแมกเนติกในการกำจัดกรดนาลิติซิก (APPLICATION OF SUPERPARAMAGNETIC MESOPOROUS SILICATES ON NALIDIXIC ACID REMOVAL) อ. ที่ปรึกษาวิทยานิพนธ์หลัก: ผศ.ดร. ปฏิภาณ ปัญญาพกุล, 96 หน้า.

งานวิจัยนี้มีวัตถุประสงค์เพื่อศึกษาประสิทธิภาพในการกำจัดกรดนาลิติซิกในน้ำเสียสังเคราะห์ที่มีความเข้มข้นสูง (0-30 มิลลิกรัมต่อลิตร) ด้วยกระบวนการดูดซับบนตัวกลางเมโซพอร์ซิลิเกตที่มีสมบัติซูเปอร์พาราแมกเนติก และศึกษาผลกระทบของสนามแม่เหล็กต่อการสะสมตัวของชั้นเค้กของตัวกลางดูดซับในการแยกโดยกระบวนการอัลตราฟิลเตรชัน (UF) หมู่ฟังก์ชันต่างๆ 5 ชนิดได้ถูกต่อติดบนพื้นผิวของตัวกลางเมโซพอร์ซิลิเกตที่มีสมบัติซูเปอร์พาราแมกเนติก ซึ่งได้แก่หมู่ silanol (HMS-SP), 3-aminopropyltrimethoxy- (A-HMS-SP), 3-mercaptopropyltrimethoxy- (M-HMS-SP), n-octyldimethyl- (OD-HMS-SP), 4-triethoxysilyl butyronitrile- (N-HMS-SP) และ phenyltrimethoxy- (PTM-HMS-SP) จลนพลศาสตร์การดูดซับกรดนาลิติซิกโดยตัวกลางดูดซับทุกชนิดสอดคล้องกับสมการอันดับสองเหมือน และถูกควบคุมโดยกระบวนการแพร่ภายในอนุภาค จากไอโซเทอมการดูดซับพบว่าตัวกลางดูดซับชนิดไม่ชอบน้ำได้แก่ OD-HMS-SP และ PTM-HMS-SP มีประสิทธิภาพการดูดซับสูงสุดเมื่อเปรียบเทียบกับตัวกลางดูดซับชนิดชอบน้ำ แต่ยังคงมีประสิทธิภาพน้อยกว่าถ่านกัมมันต์ชนิดผง นอกจากนี้แนวทางประจุไฟฟ้ามีบทบาทสำคัญต่อปรากฏการณ์การดูดซับกรดนาลิติซิก

ความต้านทานชั้นเค้ก ( $R_c$ ) ลดลงอย่างมากเนื่องจากสนามแม่เหล็กภายนอกส่งผลทำให้การสะสมตัวของชั้นเค้กของตัวกลางดูดซับบนพื้นผิวเมมเบรนเกิดขึ้นช้าลง นอกจากนี้แนวทางประจุไฟฟ้าระหว่างตัวกลางดูดซับและพื้นผิวของเมมเบรนส่งผลกระทบต่อค่าความต้านทานชั้นเค้กของตัวกลางดูดซับ และกรดนาลิติซิกส่งผลต่อแนวทางประจุระหว่างตัวกลางดูดซับและพื้นผิวเมมเบรน

สาขาวิชา การจัดการสิ่งแวดล้อม ลายมือชื่อนิสิต.....

ปีการศึกษา 2553

ลายมือชื่อ อ.ที่ปรึกษาวิทยานิพนธ์หลัก.....

# # 5287571020: MAJOR ENVIRONMENTAL MANAGEMENT

KEYWORDS: NALIDIXIC ACID / SUPERPARAMAGNETIC MESOPOROUS SILICATES / ADSORPTION / ULTRAFILTRATION / CAKE RESISTANCE

VICHUDA TIPSUNAVE: APPLICATION OF SUPERPARAMAGNETIC MESOPOROUS SILICATES ON NALIDIXIC ACID REMOVAL.

ADVISOR: ASST. PROF. PATIPARN PUNYAPALAKUL, Ph.D., 96 pp.

The main objective of this research is to evaluate removal efficiency of nalidixic acid (NAL) residues in synthetic wastewater at high concentration (0-30 mg/L) by adsorption on functionalized superparamagnetic mesoporous silicates (F-HMS-SP) and to study effect of magnetic field on cake formation of adsorbents removal by ultrafiltration(UF). Five types of surface functional groups (3-aminopropyltrimethoxy-, 3-mercaptopropyltrimethoxy-, n-octyldimethyl-, 4-triethoxysilyl butyronitrile- and phenyltrimethoxy functional group) were grafted on pristine superparamagnetic mesoporous silicates (HMS-SP) via post-grafting method denoted as A-HMS-SP, M-HMS-SP, OD-HMS-SP, N-HMS-SP and PTM-HMS-SP respectively. NAL adsorption kinetic of all adsorbents were compatible with the pseudo-second order model and implied the intraparticle diffusion as a rate limiting step. Hydrophobic surface of OD-HMS-SP and PTM-HMS-SP provided highest adsorption capacity comparing with hydrophilic adsorbents; however, it was still lower than PAC. Moreover, electrostatic interaction played an important role for NAL adsorption mechanism.

Greatly reduction of cake resistance ( $R_c$ ) was observed due to magnetic system which caused a slow-down of the cake built-up. Moreover, electrostatic interaction between adsorbent and membrane surface was found to affect on  $R_c$  value. The presence of NAL adsorbed on F-HMS-SP can affect electrostatic interaction between adsorbent and UF membrane surface.

Field of Study : Environmental management Student's Signature.....  
Academic Year : 2010 Advisor's Signature.....

## ACKNOWLEDGEMENTS

I would like to express my sincere appreciation and gratitude to my thesis advisor, Assistant Professor Patiparn Punyapalakul, Ph.D., the committees including Assistant Professor Chantra Tongcumpou, Ph.D, Associate Professor Jin Anotai, Ph.D., Assistant Professor Chawalit Ngamcharussrivichai, Ph.D. and Punjaporn Weschayanwiwat, Ph.D. for their encouragements and constructive suggestions throughout this work.

Funding of this work was provided through the National Research Center for Environmental and Hazardous Waste Management (NRC-EHWM) Program, Chulalongkorn University, Thailand. Moreover, the preparation of this important document would not have been possible without the support of Department of Environmental Engineering, Faculty of Engineering, Chulalongkorn University, Thailand.

Lastly, I offer my regards and blessings to Assistant Professor Manaskorn Rachakornkij, Ph.D. for introducing this master program. Thanks to my family, Chartchai Tipsunave, Vonvipa Tipsunave, Vantane Tipsunave, P'Bank, P'Palm, P'Tron, P'Preaw, P'Net, P'Rung, P'Ped, P'Nun, Friend, Eew, Kiaw, Kong, Jing, Gap and all of those who supported me in any respect during the completion of the project.

# CONTENTS

	<b>Page</b>
ABSTRACT (THAI).....	iv
ABSTRACT (ENGLISH).....	v
ACKNOWLEDGEMENTS.....	vi
CONTENTS.....	vii
LIST OF TABLES.....	xi
LIST OF FIGURES.....	xiv
ABBREVIATION.....	xvii
NOMENCLATURE.....	xix
CHAPTER I INTRODUCTION.....	1
1.1 State of Problems .....	1
1.2 Objectives.....	3
1.3 Hypotheses .....	3
1.4 Scopes of the Study.....	3
CHAPTER II THEORETICAL BACKGROUND AND LITERATURE REVIEW.....	5
2.1 Pharmaceutical Residues in the Environment.....	5
2.2 Distributions of antibiotics residues.....	6
2.3 Nalidixic acid (NAL) .....	6
2.3.1 Pharmaceuticals Properties .....	8
2.3.2 Toxicological Information of Nalidixic Acid .....	8
2.4 Mesoporous Silicate Materials.....	10
2.5 Mesoporous Silicates Synthesis Route .....	10
2.6 Hexagonal Mesoporous Silica (HMS).....	12
2.7 Surface Functionalization of Ordered Mesoporous Silicates.....	13

	<b>Page</b>
2.7.1 Post-synthesis (grafting) Method .....	14
2.7.2 Direct Synthesis (co-condensation) Method .....	14
2.8 Core-shell Magnetic Silica Microspheres .....	14
2.9 Superparamagnetic Iron Oxide Nanoparticles (SPIONs) .....	16
2.9.1 SPIONs Synthesis .....	17
2.10 Synthesis of SP Porous Silicates .....	17
2.11 Adsorption Mechanism .....	18
2.12 Factors Influence the Adsorptive Capacity .....	19
2.13 Adsorption Kinetic .....	19
2.13.1 Pseudo-first Order Model .....	19
2.13.2 Pseudo Second-order Model .....	20
2.13.3 Intraparticle Diffusion Model .....	20
2.14 Adsorption Isotherm .....	21
2.14.1 Langmuir Isotherm .....	21
2.14.2 Freundlich Isotherm .....	22
2.14.3 Redlich-Peterson Isotherm .....	22
2.14.4 Sips Isotherm .....	22
2.15 Membrane Filtration .....	23
2.15.1 Dead-end Filtration .....	24
2.15.2 Cross-flow Filtration .....	24
2.16 Factors of Filtrate Flux .....	25
2.17 Membrane Fouling .....	26
2.18 Cake Building Filtration .....	27
2.19 Magnetic System Enhance Ultrafiltration .....	27
2.20 Literature Reviews: .....	28



	<b>Page</b>
2.20.1 Currently Wastewater Treatment Process for Nalidixic Acid Removal .....	28
2.20.2 Adsorption Treatment Process for Removing Nalidixic Acid .....	28
2.20.3 Magnetic Field Enhanced Cake Filtration of Superparamagnetic Polyvinyl Acetate Particles (PVAc) .....	30
<b>CHAPTER III MATERIALS AND METHODS .....</b>	<b>31</b>
3.1 Materials.....	31
3.1.1 Chemical Reagents .....	31
3.1.2 Instruments .....	31
3.2 Experimental Procedure .....	32
3.2.1 Adsorbents Synthesis .....	32
3.2.2. Characterization for Physico-chemical Properties of Adsorbents..	34
3.2.3 Adsorption Study .....	35
3.2.4. Separation Process by Magnetic System Applied to Enhance..... Ultrafiltration.....	39
<b>CHAPTER IV RESULTS AND DISCUSSION .....</b>	<b>43</b>
4.1 Characterization for Physico-chemical Properties of Adsorbents .....	43
4.1.1 Pore Structure .....	44
4.1.2 Surface Area and Pore Size .....	44
4.1.3 Surface Functional Groups.....	46
4.1.4 Surface Charge .....	48
4.1.5 Morphology .....	49
4.1.6 Hydrophobicity .....	50
4.2 Adsorption Kinetic .....	52
4.2.1 The Pseudo-first and Pseudo-second Order Model.....	52

	<b>Page</b>
4.2.2 Intraparticle Diffusion Model .....	55
4.3 Adsorption Isotherm .....	57
4.3.1 Effect of Surface Functional Groups at pH = 6.8 – 7.2.....	57
4.3.2 Effects of pH .....	60
4.4 Separation Process by Magnetic System Applied to Enhance Ultrafiltration.....	67
4.4.1 Magnetic System Reducing Specific Cake Resistance .....	67
4.4.2 Effects of NAL on Magnetic System Applied on Ultrafiltration ...	70
4.4.3 Effects of Electrostatic Interaction Changing by pH between Adsorbate, Adsorbents, and Membrane.....	72
CHAPTER V CONCLUSION AND RECOMMENDATIONS .....	76
5.1 Conclusion .....	76
5.2 Recommendations.....	77
REFERENCES .....	79
APPENDICES .....	85
Appendix A .....	86
Appendix B .....	87
Appendix C .....	90
Appendix D .....	94
BIOGRAPHY.....	96

## LIST OF TABLES

	<b>Page</b>
<b>Table 2.1</b> Nalidixic Acid Properties.....	8
<b>Table 2.2</b> Toxicological Information of Nalidixic Acid .....	9
<b>Table 2.3</b> Synthesis of Various Structures Under Different Reaction Conditions...	11
<b>Table 2.4</b> Advantages and Disadvantages of	
Grafting and Co-condensation Method .....	15
<b>Table 2.5</b> Properties of Membrane Separation Systems .....	24
<b>Table 2.6</b> Currently Wastewater Treatment Process for	
Nalidixic Acid Removal.....	29
<b>Table 3.1</b> Analysis Methods of the Physico-chemical Characteristics	
of Synthesized Adsorbents .....	34
<b>Table 3.2</b> The Studied Parameters in Adsorption Kinetic Study .....	36
<b>Table 3.3</b> The Studied Parameters in Adsorption Isotherm Study .....	37
<b>Table 3.4</b> The Determined Parameters in Study of pH Effects.....	38
<b>Table 3.5</b> The Determined Parameters in Study of	
Magnetic System Reducing Specific Cake Resistance .....	39

	<b>Page</b>
<b>Table 3.6</b> The Determined Parameters in Study of Effects of NAL on Magnetic System Applied on Ultrafiltration .....	40
<b>Table 3.7</b> The Determined Parameters in Study of Effects of Electrostatic Interaction Changing by pH Between Adsorbate, Adsorbents, and Membrane .....	42
<b>Table 4.1</b> Summary of Chemical Structure of which Functional Group on F-HMS-SP Surface and Expected Interaction .....	43
<b>Table 4.2</b> BET Surface Area, Pores Volumes, and Pore Diameter of the Studied Adsorbents .....	45
<b>Table 4.3</b> Summary of FT-IR Spectra of HMS-SP and F-HMS-SP .....	47
<b>Table 4.4</b> $pH_{zpc}$ of Adsorbents Used in this Study .....	49
<b>Table 4.5</b> Chemical Structure and Contact Angle ( $\Theta$ ) of Adsorbents .....	51
<b>Table 4.6</b> Kinetics Values Calculated for NAL Adsorption on Adsorbents .....	54
<b>Table 4.7</b> Intraparticle Diffusion Parameters Plotted on adsorbents .....	57
<b>Table 4.8</b> Electrostatic Interaction between Adsorbents and NAL at Varying pH	61
<b>Table 4.9</b> Parameters of Linear, Langmuir and Freundlich Isotherm Model .....	66

	<b>Page</b>
<b>Table 4.10</b> Parameters for the Cake Building Equation Calculation .....	68
<b>Table 4.11</b> The Filter Media Resistance and the Specific Cake Resistance at pH = 5±0.2 .....	69
<b>Table 4.12</b> NAL Concentration of Initial and Filtrate Volume at pH = 5±0.2.....	71
<b>Table 4.13</b> Electrostatic Interaction of each Material at pH = 5±0.2 and 7±0.2....	72
<b>Table 4.14</b> NAL Concentration of Initial and Filtrate Volume at pH = 5±0.2 and 7±0.2.....	73
<b>Table 4.15</b> The Filter Media Resistance and the Specific Cake Resistance .....	74

## LIST OF FIGURES

	<b>Page</b>
<b>Figure 2.1</b> Distributions of Antibiotics in the Environment. ....	7
<b>Figure 2.2</b> Synthesis Pathways with Different Interaction of Surfactant and Inorganic Molecule .....	12
<b>Figure 2.3</b> The Synthesis Route of HMS Mesoporous Molecular Sieves.....	13
<b>Figure 2.4</b> Dead-end Filtration and Cross-flow Filtration .....	25
<b>Figure 2.5</b> Concentration Polarization (left) and Cake Layer (right).....	26
<b>Figure 2.6</b> Magnetic Field Effects: Effect of External Magnetic Force (Left), Effect of Interparticulate Magnetic Force (Right).....	30
<b>Figure 4.1</b> Nitrogen Adsorption-desorption Isotherms of Adsorbents .....	44
<b>Figure 4.2</b> FT-IR Spectra of HMS-SP and F-HMS-SP.....	47
<b>Figure 4.3</b> Surface Charges of HMS-SP and Functionalized HMS-SP .....	48

	<b>Page</b>
<b>Figure 4.4</b> Scanning Electron Microscopy (SEM) Images of HMS-SP(a), A-HMS-SP(b), M-HMS-SP(c), OD-HMS-SP(d), N-HMS-SP(e) and PTM-HMS-SP(f).....	50
<b>Figure 4.5</b> Schematic Drawing of Contact Angle ( $\Theta$ ) between Adsorbent Surface and Water .....	51
<b>Figure 4.6</b> Adsorption Kinetic Results of NAL (at 25oC, IS = 0.01 M and pH = 7±0.2) .....	53
<b>Figure 4.7</b> Intraparticle Diffusion Plotted of NAL Adsorption on Adsorbents .....	56
<b>Figure 4.8</b> NAL Adsorption Capacities of Synthesized Adsorbents .....	58
<b>Figure 4.9</b> NAL Adsorption Capacities of PAC .....	58
<b>Figure 4.10</b> NAL Adsorption Capacities per Specific Surface Area of Synthesized Adsorbents (at 25°C, IS = 0.01 M and pH = 7±0.2) ....	59
<b>Figure 4.11</b> NAL Adsorption Capacities per Specific Surface Area of PAC .....	60
<b>Figure 4.12</b> Effects of pH on NAL Adsorption Capacity on Adsorbents .....	62
<b>Figure 4.13</b> FT-IR Spectra of HMS and NAL- HMS which Adsorbed NAL in Hexane Solution.....	64

	<b>Page</b>
<b>Figure 4.14</b> Relations between Filtrate Volume and Time per Filtrate Volume....	68
<b>Figure 4.15</b> Relations between Filtrate Volume Versus Time, at pH = $5 \pm 0.2$ .....	69
<b>Figure 4.16</b> Surface Charges of Regenerated Cellulose UF Membrane .....	72
<b>Figure 4.17</b> Relations between Filtrate Volume and Time per Filtrate Volume....	73
<b>Figure 4.18</b> Relations between Filtrate Volume Versus Time, at pH = $5 \pm 0.2$ and $7 \pm 0.2$ .....	75



## ABBREVIATION

A-HMS-SP	3-aminopropyltrimethoxy Functional Group Grafted on Superparamagnetic Mesoporous Silicates
APTES	3-aminopropyltriethoxysilane
DDA	Dodecylamine
F-HMS-SP	Functionalized Superparamagnetic Mesoporous Silicates
HMS-SP	Superparamagnetic Mesoporous Silicates
IUPAC	International Union of Pure and Applied Chemistry
LCM	Liquid-crystal Templating
MCM	The Mobil Composite of Matter
MF	Microfiltration
M-HMS-SP	3-mercaptopropyltrimethoxy Functional Group Grafted on Superparamagnetic Mesoporous Silicates
MTS	Mesoporous Templated Silicates
NAL	Nalidixic Acid
N-HMS-SP	4-triethoxysilyl butyronitrile Functional Group Grafted on Superparamagnetic Mesoporous Silicates
NPs	Nanoparticles
OD-HMS-SP	N-octyldimethyl Functional Group Grafted on Superparamagnetic Mesoporous Silicates
ONDCP	Office of National Drug Control Policy
PAC	Powder Activated Carbon
PTM-HMS-SP	Phenyltrimethoxy Functional Group Grafted on Superparamagnetic Mesoporous Silicates
RO	Reverse Osmosis
SI	Ionic Strength
SP	Superparamagnetic
SPIONs	Superparamagnetic Iron Oxide Nanoparticles

STPs	Sewage Treatment Plants
TEOS	Tetraethylorthosilicate
UF	Ultrafiltration

## NOMENCLATURE

$C_e$	=	The equilibrium concentration (mg/L)
$C_0$	=	The initial concentration (mg/L)
$h$	=	The initial adsorption rate (mg/g min)
$k$	=	The concentration coefficient (dimensionless)
$k_f$	=	Freundlich constants related to sorption capacity of the adsorbent (dimensionless)
$k_i$	=	The intraparticle diffusion rate (mg/g min <sup>0.5</sup> )
$k_l$	=	Langmuir constant related to the affinity of the binding sites (dimensionless)
$k_1$	=	First order rate constant (1/min)
$k_2$	=	Second order rate constant (g/mg min)
$q_e$	=	The amount of sorbate adsorbed at equilibrium time (mg/g)
$q_t$	=	The amount of sorbate adsorbed at time (mg/g)
$n$	=	Freundlich constants related to sorption intensity of the adsorbent
$R_c$	=	The cake resistance (1/m <sup>2</sup> )
$R_m$	=	The membrane resistance (1/m)
$t$	=	Time (min)
$V$	=	Filtrate volume (mL)
$\mu$	=	The dynamic viscosity of the liquid phase (Pa·s)
$\Delta p$	=	The transmembrane pressure drop (Pa)

# CHAPTER I

## INTRODUCTION

### 1.1 State of Problems

During the past decade, much attention has been paid to antibiotic residues due to their adverse effects and ability to induce bacterial resistance, even at low concentrations. Nalidixic Acid (NAL) is a synthetic antibacterial agent, used in treating urinary tract infections and can be detected in ppm level in pharmaceutical industrial wastewater (Nakada, et al. 2006; Sirtori, et al. 2009; Mascolo, et al. 2010).

However, current biological wastewater treatment processes still have many drawbacks and limitations. Conventional sewage treatment plants cannot remove NAL because of its non-biodegradability (Mascolo, et al. 2010). Various available physico-chemical treatment processes have been applied to remove NAL from aqueous phase, but their own limitations and effects could not be neglected. For example, degradation by UV process required high UV energy and cost. Enhancement of NAL degradation by adding  $H_2O_2$  during UV process could reduce UV energy but degradation by-products and their toxicities have not been investigated yet. Moreover, photo-fenton process was applied as pre-treatment to enhance biodegradation of conventional wastewater treatment process. However, it takes long retention time with heavy hydrogen peroxide consumption to eliminate and/or detoxify the organic compounds in wastewater.

Up to now, adsorption process is widely applied in wastewater treatment due to its efficiency in removing various target pollutants in wastewater even at low concentration, simple to install and easy to operate and maintain. (Shepherd, et al. 2001) Nevertheless, well-known adsorbent, Powdered Activated Carbon (PAC) still establish the major drawback which is its low selectivity. Moreover, regeneration by thermal treatment of used PAC cannot be applied on micro-pollutant which contains halogen atom. As a result, higher selectivity and conveniently separate from water are desired properties for ideal adsorbent which should be further investigated.

Thus, superparamagnetic (SP) nano-materials, which have magnetism only under magnetic field, are widely used in adsorption process due to their separation or recovery efficiencies with external magnetic field. However, adsorption efficiencies of target pollutants strongly depend on surface characteristics such as surface area, functional groups and porosity. Hence, surface modification on SP nano-materials by porous silicate coating is suggested to enhance adsorption efficiency due to active surface area and increase possibility to modified surface functional groups. In particular, the functionalization on adsorbents surface might increase an opportunities for selective removal of target pollutant from wastewater. Several research works have described the synthesis method of magnetic mesoporous silica nanocomposites by using mesoporous silica coating and/or encapsulating superparamagnetic iron oxide nanoparticles (SPIONs) (Deng, et al. 2008; Mahmoudi, et al. 2010). Hence, SP porous silicates are very attractive adsorbent and have high possibility to be applied for organic pollutants adsorption systems combining with magnetic recovery by various physical separation processes.

Comparing with the traditional separation, membrane technology can be operated under the normal temperature and stated pressure. But physical change and hydraulic performance might be a major drawback which related to energy consumption and operation cost. Thus, magnetic field is suggested to apply in membrane filtration process in order to reduce membrane fouling by slow-down cake formation due to formation of chainlike agglomerates and the filtrate can run through the filter media almost without resistance. This application was included in this research to evaluate the decreasing of specific cake resistance comparing with conventional ultrafiltration (UF) process.

In this study, NAL adsorption efficiencies of functionalized superparamagnetic mesoporous silicates (F-HMS-SP) and their effects on pH were investigated and described adsorption mechanism. Moreover, effect of magnetic field on reducing of specific cake resistance on ultrafiltration process was studied.

## 1.2 Objectives

The main objective of this research is to evaluate removal efficiency of nalidixic acid (NAL) residues in synthetic wastewater by adsorption on functionalized superparamagnetic mesoporous silicates (F-HMS-SP) and to study effect of magnetic field on cake formation of ultrafiltration (UF). The sub objectives are as follow;

1. To determine adsorption capacities of Nalidixic acid (NAL) on functionalized superparamagnetic mesoporous silicates at high concentration (0-30 mg/L).
2. To determine the impact of surface functional groups and pH on Nalidixic acid (NAL) adsorption capacity.
3. To enhance particle separation by membrane ultrafiltration process by using external magnetic force to slow-down cake formation of applied superparamagnetic (SP) adsorbents.

## 1.3 Hypotheses

1. Hydrophobic surfaces functional groups might perform higher adsorption capacity of NAL than hydrophilic surfaces.
2. NAL adsorption capacity might be affected by electrostatic interaction due to changing of pH.
3. Magnetic system applied to F-HMS-SP can slow-down cake formation and decrease specific cake resistance on membrane filtration.

## 1.4 Scopes of the Study

1. Adsorption and membrane filtration experiment were conducted by using synthesized wastewater containing Nalidixic acid (NAL) in order to investigate the adsorption capacities and mechanisms comparing with powdered activated carbon (PAC).

2. Synthesized adsorbents were superparamagnetic hexagonal mesoporous silicates (HMS-SP) which were modified surface by grafting with five types of surface functional groups (3-aminopropyltrimethoxy-, 3-mercaptopropyltrimethoxy-, n-octyldimethyl-, 4-triethoxysilyl butyronitrile- and phenyltrimethoxy functional group) via post-grafting method due to good preservation of the mesoporous structure. The obtained materials were single-functional group mesoporous silicates denoted as A-HMS-SP, M-HMS-SP, OD-HMS-SP, N-HMS-SP and PTM-HMS-SP respectively.
3. Synthesized adsorbents were investigated physico-chemical characteristics, such as surface area, pore size, pore structure and surface charge.
4. Adsorption kinetics and isotherms were conducted under batch experiments under controlled temperature (25 °c) and ionic strength (0.01 M). Effects of electrostatic interaction were investigated by varying pH from 5 to 9 of solution. Obtained results were analyzed with various mathematic model such as the pseudo-first order model, pseudo-second order model, intraparticle diffusion model, Linear, Langmuir and Freundlich isotherm models, were used to analyze the experiment data.
5. Appropriate adsorbents and adsorption conditions obtained from previous experiments were selected and applied for study effects of specific cake resistance ( $R_c$ ). External magnetic field was applied in dead-end flow of regenerated cellulose ultrafiltration (UF). The transmembrane pressure drop across membrane was controlled to be stable at 1 bar and the filtrate volume versus time was determined. The specific cake resistance ( $R_c$ ) can be calculated and compared to the conventional UF. Moreover, effect of NAL in on specific cake resistance ( $R_c$ ) was also determined. NAL remained in filtrate flux was determined by UV-visible spectrophotometer at 260 nm.

## CHAPTER II

### THEORETICAL BACKGROUND AND LITERATURE REVIEW

#### 2.1 Pharmaceutical Residues in the Environment

Pharmaceuticals have been produced for commercial and therapeutic uses in large quantities both for humans and veterinary treatment. During the past decade, the adverse effects caused by pharmaceuticals which are released to the environment have become a potentially concerns. A survey of the current literature on the topic 'drugs in the environment' shows that antibiotics, antiparacetic agents, agents and hormones are investigated for environmental impacts (Jùrgensen and Halling-Sùrensen 2000). These compounds reach the environment resulting from the improper disposal of the expired drugs, as well as through wastewater. According to several studies, many pharmaceuticals are not completely metabolized in humans or animals and then are excreted with urine. Since sewage treatment plants, historically, are not designed to remove these residues, pharmaceuticals are not eliminated when they are released to the environment. These pharmaceuticals are also discharged from chemical and pharmaceutical industries due to a limited efficiency of a conventional wastewater treatment. Moreover, some of pharmaceuticals have been reported as non-biodegradable and might persistence in the environment. As a consequence, pharmaceuticals have been recently detected in surface water and groundwater up to the level of  $\mu\text{g/L}$  around the world, such as in Austria, Brazil, Canada, Croatia, England, Germany, and US (Heberer 2002; Lorphensri, et al. 2006; Lin, et al. 2009; Mascolo, et al. 2010).

Although they have been reported in a little amount, their adverse effect and persistence are not negligible. In particular, much attention has been paid to antibiotics as they can induce bacterial resistance, even at low concentrations (Sirtori, et al. 2009).



## **2.2 Distributions of antibiotics residues**

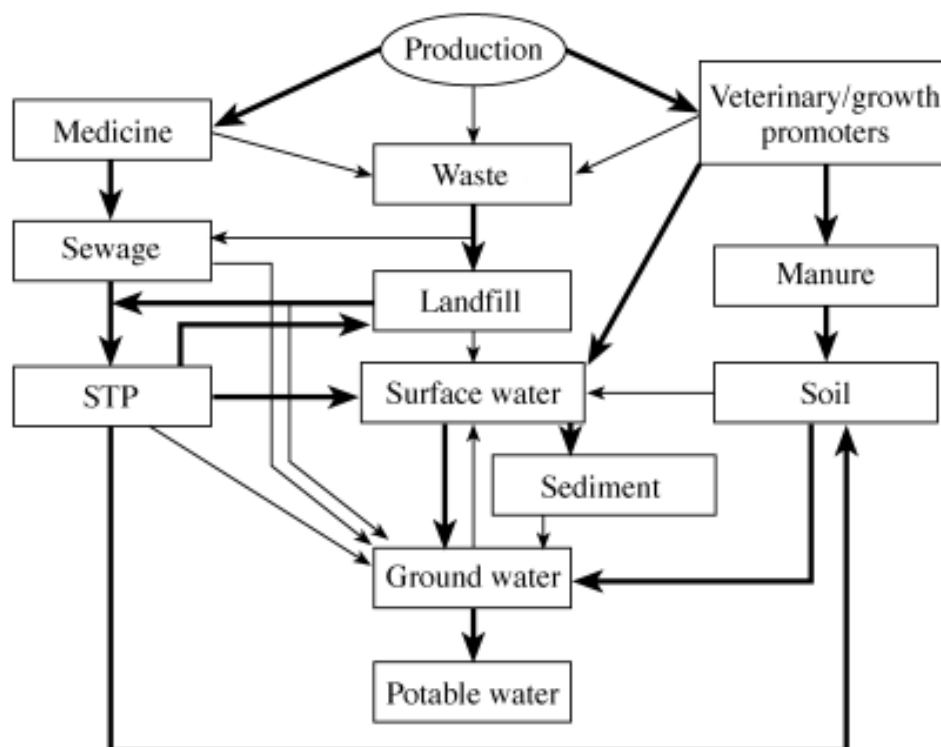
Beyond antibiotic consumption evidences, their sources have been identified which mainly include manufacturers, hospitals, private households, veterinary treatment and landfills (Jørgensen and Halling-Sørensen 2000; Kümmerer 2009). Considering their distributions, many of antibiotic compounds, which are disposed of into the sewage system including from mentioned sources, are not eliminated during sewage treatment due to a limitation of conventional sewage treatment plant. In addition, several pharmaceutical compounds are not degraded even in soil or in other environmental compartments. Under test conditions in aquatic systems, only a few of the compounds were partially biodegraded while most were persistent. There have been verified that the genotoxicity of compounds such as quinolones or metronidazole was not removed during the test (Al-Ahmad, et al. 1999; Kümmerer, K., Al-Ahmad, A., and Mersch-Sundermann 2000; Kümmerer 2003). Thus, they remain persistence and tend to reach surface water, ground water, and, potentially, drinking water. Unmetabolized antibiotic substances are often passed into the aquatic environment in wastewater. Antibiotics used for veterinary purposes or as growth promoters are excreted and end up in manure that is used as an agricultural fertilizer. As a result, the antibiotics seep through the soil and become contaminated in groundwater and surface water as well as compounds leaching from landfills shown as Figure 2.1 (Kümmerer 2003). Therefore, antibiotics have been detected in the  $\mu\text{g/L}$  range in municipal sewage, the effluent of sewage treatment plants (STPs), surface water and in ground water. These included quinolones such as ciprofloxacin, sulphonamides, roxythromycin, dehydrated erythromycin and others (Kümmerer 2003).

## **2.3 Nalidixic acid (NAL)**

Nalidixic acid (NAL) is a synthetic antibacterial agent, which is a member of fluoroquinolones. NAL is effective against both gram-positive and gram-negative bacteria. At lower concentrations, it acts in a bacteriostatic manner that inhibits

growth and reproduction. On the other hand, at high concentrations, it is bactericidal which kills bacteria instead of merely inhibiting their growth. NAL is especially used in treating urinary tract infections, caused by, for example, *Escherichia coli*, *Proteus*, *Shigella*, *Enterobacter*, and *Klebsiella*. Taken by mouth, NAL does not accumulate in body tissue but it is concentrated in urine. NAL has been one of the most common agents used for the treatment of shigellosis, especially in children. Recently, a growing resistance of *Shigella* subgroups, for examples, *Shigella dysenteriae* and *Shigella boydii* to NAL have been reported in some studies (Mamishi, et al. 2009).

Therefore, the occurrence of NAL in the environment through varieties of sources, which can induce bacterial resistance, should be taken into account, especially when NAL is non-biodegradable. To illustrate, this indicated that if the prevention of releasing NAL to the environment has never been conducted, antibiotics will lose their efficiency in the future. Moreover, NAL in various wastewater treatment plants can be found in ranges of 100 µg/L (for municipal wastewater) to 222 mg/L (for pharmaceuticals wastewater) (Nakada, et al. 2006; Sirtori, et al. 2009; Mascolo, et al. 2010).

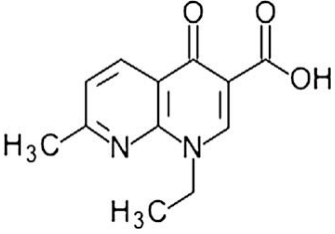


**Figure 2.1** Distributions of Antibiotics in the Environment (Kümmerer 2003).

### 2.3.1 Pharmaceuticals Properties

The properties of NAL are summarized in Table 2.1.

**Table 2.1** Nalidixic Acid Properties (Wanitkorkul, et al. 2005)

Pharmaceutical Properties	Nalidixic Acid
Structure	
CAS number	389-08-2
Mol formula	C <sub>12</sub> H <sub>12</sub> N <sub>2</sub> O <sub>3</sub>
Mol weight	232.24
Melting point	229.5°C
Water solubility at 25°C (mg/L)	100
Molecular diameter (Å)	10.907
Log Kow	1.59
Vapor Pressure at 25°C (mm Hg)	3.56×10 <sup>-7</sup>
pKa	6.33
Henry's constant (atm-m <sup>3</sup> /mole)	5.12×10 <sup>-16</sup>

### 2.3.2 Toxicological Information of Nalidixic Acid

Table 2.2 summarizes toxicities of NAL reported by the office of national drug control policy (ONDCP).

**Table 2.2** Toxicological Information of Nalidixic Acid

([http://www.whitehousedrugpolicy.gov/drugfact/factsht/proper\\_disposal.html](http://www.whitehousedrugpolicy.gov/drugfact/factsht/proper_disposal.html))

Toxicity of NAL	Toxicological Information
<p>Routes of entry</p> <p>Toxicity to animals</p> <p>Mutagenic effects</p> <p>Developmental toxicity</p> <p>Special remarks on chronic effects on humans</p> <p>Acute potential health effects on humans</p>	<ul style="list-style-type: none"> <li>• Inhalation and ingestion</li> <li>• Acute oral toxicity (LD50): 572 mg/kg (Mouse)</li> <li>• Mutagenic for bacteria and/or yeas</li> <li>• Classified reproductive system/toxin/ female,Reproductive system/toxin/male (suspected). May cause damage to the following organs: the nervous system, the reproductive system, liver, central nervous system (CNS)</li> <li>• May affect genetic material (mutagenic)</li> <li>• May cause cancer. May cause adverse reproductive effects and birth defects (teratogenic)</li> <li>• May cause skin irritation</li> <li>• May cause eye irritation</li> <li>• May cause respiratory tract irritation</li> <li>• It may cause sweating, gastrointestinal tract irritation with nausea, vomiting, diarrhea, stomach pains.</li> <li>• It may cause metabolic acidosis.</li> <li>• May affect behavior/central nervous system (somnolence, lethargy, toxic psychosis, convulsions, headache, dizziness, confusion, weakness, drowsiness), brain (increased intracranial pressure)</li> </ul>

## 2.4 Mesoporous Silicate Materials

Porous materials have ability to interact with atoms, ions and molecules not only at their surfaces, but throughout the bulk of the material. As a result they recently become attractive for many chemical applications. According to IUPAC definition, porous materials are classified into three classes depending on the predominant pore size: microporous with the pore sizes  $< 2.0$  nm, macroporous with pore sizes  $> 50.0$  nm, and mesoporous with pore sizes between  $2.0 - 50.0$  nm (Hu, B.S. et al. 2009). Since microporous material applications are limited by the relatively small pore openings, mesoporous are preferable (Ciesla and Schüth 1999). Especially in many fields of chemistry, well-ordered hexagonal mesoporous silicates have been made to expand the range of applications of silica materials by utilizing their high surface area, controllable pore size, and narrow pore size distribution. These structural characteristics are desirable for surface modifications with various kinds of supports through chemical attachment that have proven to be an effective and important method for improving the interaction of such surfaces with the environment. So far, mesoporous silicates are attractive for developing adsorbents for toxic ions in the environment (Pérez-Quintanilla, et al. 2006).

## 2.5 Mesoporous Silicates Synthesis Route

In 1992, scientists at Mobil Oil Corporation announced the direct synthesis of the first broad family of mesoporous templated silicates (MTS), the Mobil composite of matter (MCM), based on a liquid-crystal templating (LCM) mechanism. Following this method, highly porous solids with pores  $> 2$  nm, surface areas reaching  $> 1000$  m<sup>2</sup>/g and other desirable properties are prepared. There has been impressive progress in the development of many new mesoporous materials based on a similar mechanism of templating. Surfactant molecules is commonly used as a template for preparation of ordered mesoporous silicates due to its synthesis parameters resistance for example, aging time, pH of synthesis medium and initial inorganic ratios in surfactant or

silicate mesostructure synthesis. Surfactant template mesoporous materials is generally synthesized with 2 steps which are forming the surfactant or inorganic mesostructure, then removing the surfactant from the mesoporous structure to achieve mesoporous materials (Wang, et al. 2010). Depending on the synthesis conditions and the inorganic precursor species (I) or the type of surfactant (S) used, many other mesoporous materials can be synthesized with properties different than those of MCM as reflected in Table 2.3.

**Table 2.3** Synthesis of Various Structures under Different Reaction Conditions  
(Linssen, et al. 2003)

Reaction Medium	Template	Mesophase Name
<b>Strong (electrostatic) interactions</b>		
Direct interaction      pH >7	Ammonium surfactants      S <sup>+</sup> T	KIT-1, PCH, MCM-41, 48 and FSM-16
Anion mediated interaction      pH <7	Ammonium surfactants      S <sup>+</sup> XT <sup>+</sup>	SBA-1, 2, 3
	Triblock copolymers      (S <sup>0</sup> H <sup>+</sup> )XT <sup>+</sup>	SBA-15, 16
	Ethylene oxides	SBA-11, 12, 14
<b>Weak (van der Waals) interactions</b>		
Hydrogen bonding interaction pH >7	Amine surfactants      S <sup>0</sup> T <sup>0</sup>	HMS
Hydrogen bonding interaction pH 7	Non-ionic ethylene oxides      N <sup>0</sup> T <sup>0</sup>	MSU-n

An overview of all types of MTS materials is given in Table 2.5 and mesostructure which can be disordered or ordered to be lamellar, cubic, or hexagonal phase depending up on the synthesis route are shown in Figure 2.2.

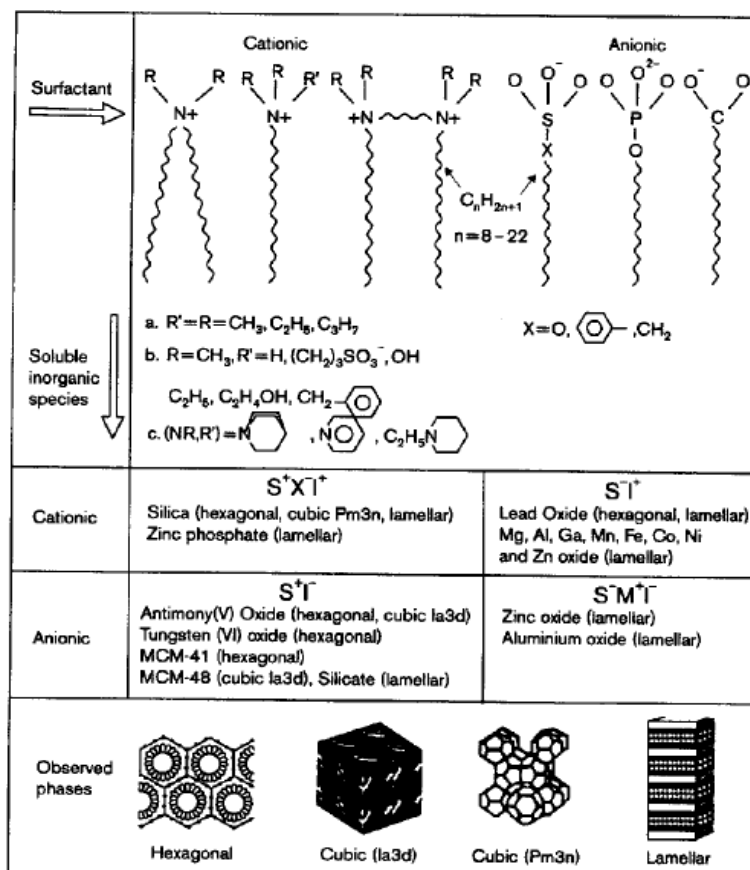


**Figure 2.2** Synthesis Pathways with Different Interaction of Surfactant and Inorganic Molecule (Beck and Vartuli 1996).

## 2.6 Hexagonal Mesoporous Silica (HMS)

Hexagonal Mesoporous Silica (HMS) is a kind of mesoporous molecular sieves generated through hydrogen bonding pathway first synthesized by Tanev and Pinnavaia (1996). It has been interested in the area of catalysis because of its thicker framework wall, which improves its thermal stability, and the wormhole framework structure. Due to their mesostructure, they can let the molecule trap internal surface so that their adsorption capacity is high. To synthesis HMS, a neutral synthesis pathway ( $S^0I^0$ ) was proposed as shown in Figure 2.3. Dodecylamine (DDA) was used as the template. Mixture of water and ethanol was used as solvent to improve template solubility and tetraethylorthosilicate (TEOS) was used as silica source.

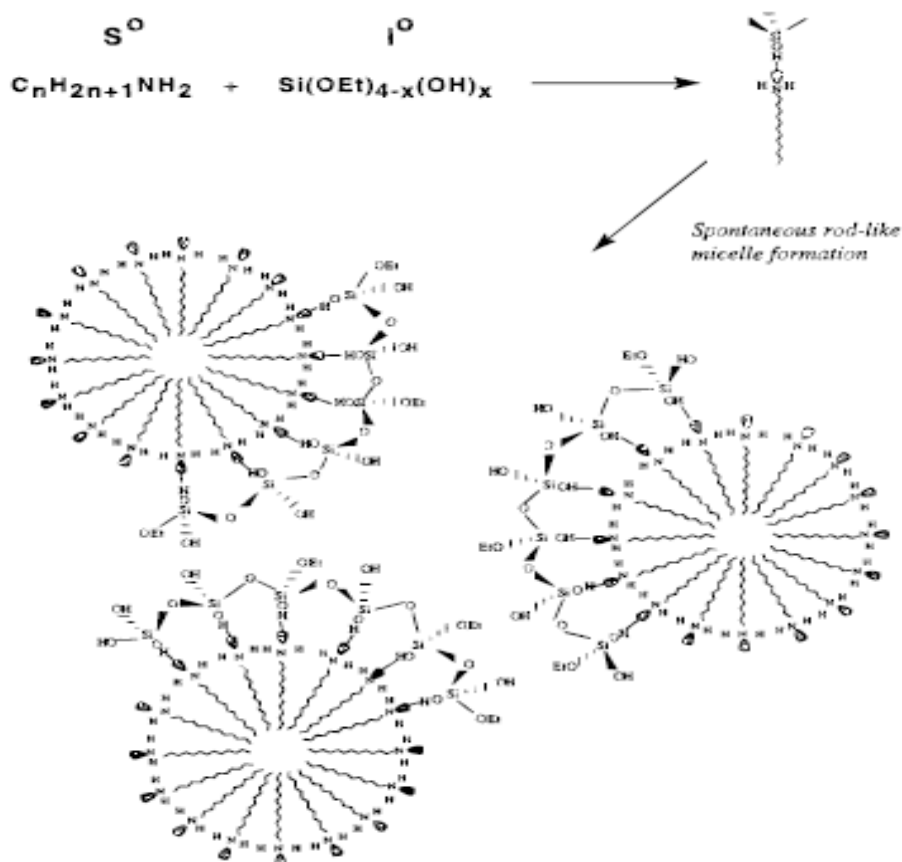


**Figure 2.3** The synthesis Route of HMS Mesoporous Molecular Sieves (Tanev and Pinnavaia 1996).

## 2.7 Surface Functionalization of Ordered Mesoporous Silicates

Surface functionalization can extend the limit in application of pure silicate component, for example, increase in the hydrophobicity of surface causes the increasing in hydrothermal of material. These properties can apply in novel catalysis, adsorbents and advanced materials. To enhance specific characteristic of ordered mesoporous silicates, their surface can be modified with organosilane generally through 2 approaches which are post-synthesis (grafting) and direct synthesis (co-condensation).



### **2.7.1 Post-synthesis (grafting) Method**

There are two steps involved in this method, including pre-synthesis of a parent mesostructure, followed by post-treatment which consists of reaction of a suitable organosilane with surface silanol groups (Si-OH) using an appropriate solvent under reflux conditions. During post-treatment process, the silanol groups react with the organosilane to form a layer of covalently coupled surface functional groups.

Post-synthesis method provides low density and non uniformity of functionality compared to direct synthesis method. However, a good preservation of mesostructure after the functionalization provided by this method is predominant desirable.

### **2.7.2 Direct Synthesis (co-condensation) Method**

This method consists of one-step co-condensation of tetraalkoxysilanes such as tetraethyl orthosilicate (TEOS) with organosilanes such as 3-aminopropyltriethoxysilane (APTES). The resultant materials from co-condensation method provide a higher and more uniform surface coverage of functional groups and a better control over the surface properties.

Each advantages and disadvantages is summarized in Table 2.4.

## **2.8 Core-shell Magnetic Silica Microspheres**

Since ordered mesoporous materials have gained much attention for the applications in catalysis, adsorption, and separation. The integration of mesoporous silica with magnetic particles to form core shell composite microspheres is undoubtedly of great interest for practical applications in various fields. Magnetic microspheres are consisted of an iron oxide core and silica shell. They have attracted particular attention due to unique magnetic responsivity, low cytotoxicity, and chemically

modifiable surface. The core-shell magnetic silica microspheres have shown great potential in bioseparation, enzyme immobilization, diagnostic analysis, and so on.

**Table 2.4** Advantages and Disadvantages of Grafting and co-condensation method  
(Chong, et al. 2004)

<b>Grafting Method</b>	<b>Co-condensation Method</b>
<b>Advantages</b>	<b>Advantages</b>
<ul style="list-style-type: none"> <li>• Good preservation of the mesostructure afterpost-modification</li> </ul>	<ul style="list-style-type: none"> <li>• Higher and more uniform surface coverage of functionality</li> <li>• Capable control in surface properties</li> </ul>
<b>Disadvantages</b>	<b>Disadvantages</b>
<ul style="list-style-type: none"> <li>• Reduce pore size and pore volume</li> <li>• A limited loading level of the Functional groups can be grafted because of the limited density of the reactive surface silanols</li> <li>• Time-consuming process</li> <li>• Difficult to control over the loading level and uniformity of the functional groups</li> <li>• Ineffective due to partial cross-linking of the functional groups with the silica-surface silanol groups</li> </ul>	<ul style="list-style-type: none"> <li>• Loss in original structure ordering such as aminopropyltriethoxysilane (APTES) functionalization</li> </ul>

The core-shell magnetic silica microspheres is suggested to enhance adsorption efficiency due to easy to separation or regeneration with external magnetic field. This integration also provides active surface area and increase possibility to modified surface functional groups. In particular, the functionalization of adsorbents surface might yield an opportunities for selective removal of target pollutant from wastewater. Up to now, several papers have reported the synthesis of magnetic mesoporous silica nanocomposites which mesoporous silica is used for coating or encapsulating superparamagnetic iron oxide nanoparticles (SPIONs). It's applications has been reported as Controlled drug delivery, removal of mercury from industrial effluent, support for enzyme immobilisation for bio-catalysis, fluorescence, isolation of genomic and plasmid DNA (Deng, et al. 2008; Mahmoudi, et al. 2010).

## **2.9 Superparamagnetic Iron Oxide Nanoparticles (SPIONs)**

Nanoparticles (NPs) have unique physical and chemical properties compared with their bulk counterparts, therefore the case of magnetic NPs is especially interesting. The NP size is comparable to the size of a magnetic domain, which would result in unusual magnetic phenomena known as superparamagnetism. Magnetite ( $\text{Fe}_3\text{O}_4$ ), maghemite ( $\gamma\text{-Fe}_2\text{O}_3$ ) and hematite ( $\alpha\text{-Fe}_2\text{O}_3$ ) are three main iron oxides that fall under the category of SPIONs. Ferrites, which are mixed oxides of iron and other transitionmetal ions (e.g. Cu, Co, Mn, and Ni), have also been reported to be superparamagnetic (SP). However, this review article focuses mostly on pure iron oxide NPs with SP properties. Magnetite ( $\text{Fe}_3\text{O}_4$ ) is an important kind of magnetic material having cubic inverse spinel structure. It has been attracting increasing attention due to the wide use in magnetic recording, ferrofluid, catalyst and biomedical applications, such as magnetic resonance imaging (MRI), bio-separation, drug targeting and hyperthermia.

### 2.9.1 SPIONs Synthesis

So far, various chemical methods have been applied to fabricate magnetic NPs, such as sol-gel technique, co-precipitation process, reverse micelle method, and hydrothermal/solvothermal treatment (Yan, et al. 2008).

- *Co-precipitation Method*

Massart 1981 reported the most common method, in which the addition of base to an aqueous solution of ferrous ( $\text{Fe}^{2+}$ ) and ferric ( $\text{Fe}^{3+}$ ) ions in a 1:2 stoichiometry produced a black precipitate of spherical magnetite NPs of uniform sizes. To protect the oxidation of these NPs in the presence atmospheric oxygen and also to stop their agglomeration, the particles are usually coated with some surfactant like the oleic acid or sodium dodecylsulfate (NaDS) and then dispersed in some carrier liquid like ethanol, methanol, ammonia, etc. depending upon the nature of the NPs to be dispersed. The advantage over the others of this method is that the production rate of the NPs, its size and size distribution is relatively easy and there is no need of extra mechanical or microwave heat treatments. (Maaz, et al. 2009; Mahmoudi, et al. 2010)

### 2.10 Synthesis of SP Porous Silicates

Researches for preparation of magnetic mesoporous materials were centered on three approaches:

1. Dispersing magnetic NPs in the pores of mesoporous silicas.
2. Grafting magnetic NPs on the outer surface of mesoporous silicas.
3. Coating mesoporous silicas onto the monodisperse magnetic nanoparticles to compose core-shell structured microspheres.

Compared with the synthesis methods of 1 and 2, coating mesoporous silicas onto the monodisperse magnetic NPs can provide uniform shape and size which are favorable to respond to magnetic field well. The 3<sup>rd</sup> method produces the materials

with higher surface area and pore volume, that are beneficial to the adsorption process (Tian, et al. 2009). Therefore, in this paper, the coating method is chosen to synthesize a novel magnetic mesoporous silica material consisting of  $\text{Fe}_3\text{O}_4$  core and HMS (hexagonal mesoporous silica) shell.

### **2.11 Adsorption Mechanism**

Adsorption can be described as the inter-phase accumulation of substances at a surface or interface, which can occur at an interface of any two phases, such as liquid-liquid, gas-solid, or liquid-solid interfaces. The imbalance between these two phases is the driving force of the process. Surface adsorption phenomena can be classified as physical adsorption and chemisorption. For the physical adsorption, the solute molecules are attracted to the solid by relatively weak force (i.e. covalent, electrostatic, and Van der Waals force). On the other hand, chemisorption is associated with much stronger force than those of physical sorption such as metals chelation.

“The mechanism of adsorption is generally considered to involve three steps, one or any combination of which can be the rate-controlling mechanism.

1. Mass transfer across the external boundary layer film of liquid surrounding the outside of the particle
2. Adsorption at a site on the surface (internal or external) and the energy will depend on the binding process (physical or chemical); this step is often assumed to be extremely rapid
3. Diffusion of the adsorbate molecules to an adsorption site either by a pore diffusion process through the liquid filled pores or by a solid surface diffusion mechanism.” (Cheung, et al. 2007)

## 2.12 Factors Influence the Adsorptive Capacity

The adsorptive capacity for solutes on the adsorbents depends on 3 groups of factors.

1. Properties of sorbent materials: surface area, surface charge, charge density, pore size, etc.
2. Properties of sorbates: chemical structure,  $pK_a$  values, functional groups contained, molecular weight, etc.
4. Conditions of the solution: temperature, pH, ionic strength, presence of other ions.

## 2.13 Adsorption Kinetic

To get important information for designing and modeling the process, the adsorption rate which received from kinetic study is necessary to be identified. Sorption kinetic mechanisms can be based on chemical reaction kinetics. Two kinetic models including the pseudo-first order model and pseudo-second order model equations will be applied to investigate the controlling mechanism of adsorption processes such as chemical reaction.

### 2.13.1 Pseudo-first Order Model

A simple kinetic of sorption is the pseudo-first order model as expressed in Equation (2.1):

$$q_t = q_e(1 - \exp(-k_1 t)) \quad (2.1)$$

Where  $q_e$  and  $q_t$  (mg/g) are the amount of sorbate adsorbed at equilibrium and at time (hr) and  $k_1$  is first order rate constant for adsorption (1/min).

### 2.13.2 Pseudo Second-order Model

Pseudo-second-order equation is based on a chemisorption. The second order equation can be expressed as equation (2.2):

$$q_t = \frac{q_e k_2 t}{1 + q_e k_2 t} \quad (2.2)$$

Where  $q_e$  and  $q_t$  (mg/g) are the amount of sorbate adsorbed at equilibrium and at time (hr) and  $k_2$  is second order rate constant for adsorption (g/mg.min).

### 2.13.3 Intraparticle Diffusion Model

“Rate of sorption is frequently used to analyze nature of the ‘rate-controlling step’ and the use of the intraparticle diffusion model has been greatly explored in this regard which is represented by the following Weber and Morris equation (2.3) (Weber and Morris 1963)

$$q_t = k_i t^{0.5} + C \quad (2.3)$$

Where,  $C$  is the intercept, related to the thickness of the boundary layer; the larger the intercept, greater the contribution of the surface sorption in the rate controlling step.  $k_i$  is the intraparticle diffusion rate constant. According to this model, if adsorption of a solute is controlled by the intraparticle diffusion process, a plot of  $q_t$  versus  $t^{0.5}$  gives a straight line.” (Chakrapani, et al. 2010).

## 2.14 Adsorption Isotherm

For sorption isotherms, the equilibrium adsorption capacity ( $q$ ) and the final equilibrium concentration of the residual solute remaining in the solution ( $C_e$ ) are plotted to study their relationship. The capacity  $q$  (mg/g) can be calculated by equation(2.4):

$$q_e = \frac{V(C_0 - C_e)}{M} \quad (2.4)$$

where  $q_e$  is the adsorption capacity (mg/g),  $C_0$  and  $C_e$  are the initial and equilibrium concentration (mg/L), respectively.  $V$  is the volume of the solution (liter) and  $M$  is the mass of adsorbent (g).

The adsorption isotherm relationship can also be mathematically expressed by many models. However, Langmuir and Freundlich isotherm are the most commonly used.

### 2.14.1 Langmuir Isotherm

Langmuir model considers sorption as a chemical phenomenon. It is assumed that the sorption is restricted to a monolayer. Since the forces between sorbent and sorbate are exerted by chemically unsaturated atoms and assumed to not extend further than the diameter of one sorbed molecule. This model can be written as equation (2.5):

$$q_e = \frac{q_m k_l C_e}{1 + k_l C_e} \quad (2.5)$$

Where  $q_m$  (mg/g) is the maximum amount of the adsorbate per unit weight of the adsorbent to form a complete monolayer on the surface,  $k_l$  is Langmuir constant related to the affinity of the binding sites.



### 2.14.2 Freundlich Isotherm

Freundlich isotherm is an empirical equation which does not indicate a limited sorption capacity of the sorbent. This model is based on sorption on the heterogeneous surfaces and multilayer sorption of the sorbate. Freundlich model can be written as equation (2.6):

$$q_e = k_f C_e^{1/n} \quad (2.6)$$

Where  $k_f$  and  $n$  are Freundlich constants related to sorption capacity and sorption intensity of the adsorbent, which represent the quantity of organic adsorbed onto adsorbent for a unit equilibrium concentration. A value for  $1/n$  below one indicates a normal Langmuir isotherm while  $1/n$  above one is indicative of cooperative adsorption.

### 2.14.3 Redlich-Peterson Isotherm

The Redlich-Peterson equation is expressed as equation (2.7) (i.e. features of both Langmuir and Freundlich isotherm assumptions):

$$q_e = \frac{k_{RP} C_e}{1 + \alpha_{RP} C_e^\beta} \quad (2.7)$$

Where  $k_{RP}$  (L/g) and  $\alpha_{RP}$  (L/mg)<sup>B</sup> are Redlich-Peterson isotherm constants and  $\beta$  is the exponent which lies between 1 and 0.

### 2.14.4 Sips Isotherm

The Sips isotherm, at low sorbate concentrations, reduces to the Freundlich isotherm. At high sorbate concentrations, Sips model predicts monolayer sorption capacity,

which is a distinctiveness of the Langmuir isotherm. Also, for  $\gamma = 1$ , the Sips equation reduces to the Langmuir model, as evident from the values of parameters. The Sips isotherm fitted for the experimental equilibrium data overlaps with the Freundlich isotherm, thus, indicating a good fit. The Sips isotherm is expressed as equation (2.8):

$$q_e = \frac{q_m(k_s C_e)^\gamma}{1 + (k_s C_e)^\gamma} \quad (2.8)$$

Where  $k_s$  is Sips model isotherm constant  $(L/mg)^{1/\gamma}$  and  $\gamma$  is Sips isotherm model exponent.

## 2.15 Membrane Filtration

Membrane separation technology adopts the selective multi-hole membrane as separation medium. The separated fluid driving by the outside pressure goes through the surface of the membrane with stated pore size which allows certain components of the feed liquid to pass. The fluid that passes through the membrane is called *permeate* and the fluid retained on the feed side is called *retentate*. There are different membrane separation systems including microfiltration (MF), ultrafiltration (UF) and reverse osmosis (RO) which are summarized their properties in Table 2.5. In this paper ultrafiltration membrane (UF) will be selected.

Compared with the traditional separation, membrane technology is running under the normal temperature. The membrane separation process only happen the physical change, the energy consumption and operation cost will be lower and the second pollution never exists. The common membrane separation process is running under the stated pressure and can be completed in a moment. The systems are simple and compact, easier for operation and the automatic control.

There are two ways to operate membrane separation process; dead-end filtration and cross-flow filtration.

**Table 2.5** Properties of Membrane Separation Systems (Wankat 1944)

	Membrane Processes		
	Microfiltration (MF)	Ultrafiltration (UF)	Reverse Osmosis(RO)
<b>Separation Mechanism</b>	Sieving	Sieving	Solution diffusion
<b>Driving Force</b>	$\Delta p$	$\Delta p$	Partial pressure
<b>Flow Ddriven by</b>	$\Delta p$ 100-500 kPa	$\Delta p$ 100-800 kPa	$\Delta p$ 1-10 MPa
<b>Feed/Product</b>	Liquid/Liquid	Liquid/Liquid	Liquid/Liquid
<b>Material Removed</b>	Small particles	Macro molecules	Ions molecules
<b>Approximate Size</b>	400-20000 Å	30-1100 Å	3-20 Å
<b>Application</b>	Food processing Water purific	Food processing Water purific	Desalination Chemicals
<b>Membrane Materials</b>	Polysulfone	Polysulfone Cellulose acetate acrylonitrile	Cellulose acetate composites poliamides

### 2.15.1 Dead-end Filtration

All of the feed solution is forced through the membrane by an applied pressure. Then retained particles are collected on or in the membrane. The feed flow direction is vertical with the surface of the filtration membrane. The permeate direction which pass the membrane is identical with the feed flow. The retained particles in the feed solution will be adhered the surface of membrane, which causes the cartridge filter have to be replaced frequently and life time is shorter. Most type of cartridge filters cannot be reused by cleaning.

### 2.15.2 Cross-flow Filtration

The fluid to be filtered is pumped across the membrane parallel to its surface. Cross-flow produces two solutions which are a clear filtrate (permeate) and a retentate containing most of the retained particles in the solution. By maintaining a high velocity across the membrane, the retained material is swept off the membrane surface. Thus, cross-flow is used when significant quantities of material will be retained by the membrane, resulting in plugging and fouling. The life of the module

will be longer, maybe 12 months to 3 years according to different material of membrane.

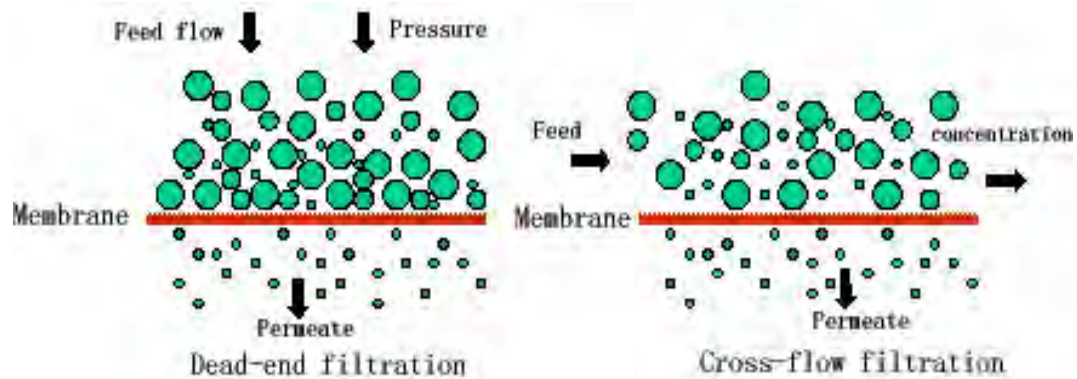


**Figure 2.4** Dead-end Filtration and Cross-flow Filtration

(<http://www.hydrotech.cn/English/index.asp>).

## 2.16 Factors of Filtrate Flux

The filtrate flux is affected by three factors including membrane materials properties, solute properties and operating parameter.

1. Membrane materials properties: hydrophilicity, surface topography, charge on membrane, pore size.
2. Solute properties: pH, ionic strength, shear.
3. Operating parameter: temperature, flow rate, flow characteristic (turbulence), pressure.

It is difficult to predict flux because of so many affecting factors, complicated mechanisms and different conditions of different liquid systems and membranes. According to Darcy's Law, for a laminar flow of a Newton fluid through an incompressible packed bed the flux of dead-end UF can be expressed as follows:

$$J(t) = \frac{\Delta p}{\mu (R_m + R_b + R_c)} \quad (2.9)$$

Where  $J(t)$  is the instantaneous permeate flux ( $\text{m}^3/\text{m}^2\text{s}$ ),  $\Delta p$  is the transmembrane pressure drop (Pa),  $\mu$  is the feed liquids viscosity (Pa·s),  $R_m$  is the membrane resistance ( $1/\text{m}$ ),  $R_b$  is concentration polarization boundary layer resistance ( $1/\text{m}$ ) and  $R_c$  is the cake resistance ( $1/\text{m}^2$ ). According to equation (2.9), factors of filtrate flux consist of the transmembrane pressure drop, liquid viscosity, membrane resistance and resistance of concentration polarization and deposition (cake) resistance.

## 2.17 Membrane Fouling

Filtration performance is often limited due to the buildup of retained solutes at the membrane surface that cause flux decline. This buildup may be classified into two categories: (1) concentration polarization (CP), and (2) formation of a “cake” between CP layer and the membrane surface. However, in most practical applications, the effect of CP on permeate flux is rarely measurable because the transition from CP to cake formation occurs almost immediately (Kim and Hoek 2002). Thus, for this paper, the CP layer resistance is assumed negligible in the presence of a cake, and thus the focus of flux decline models is on the cake resistance.

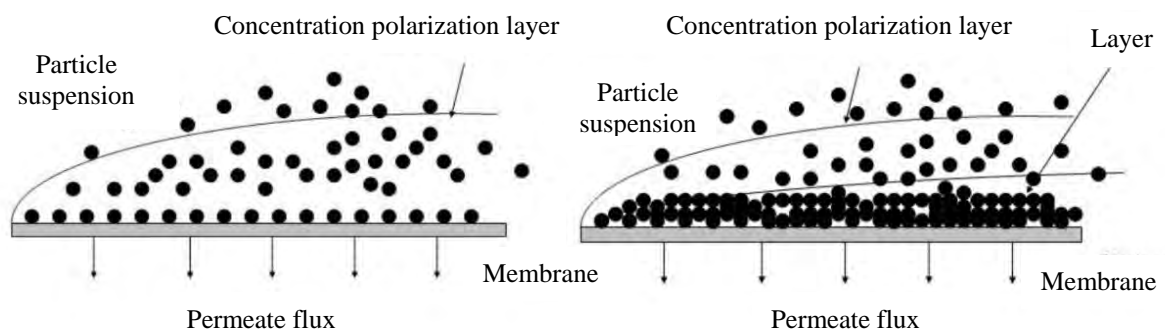


**Figure 2.5** Concentration Polarization (Left) and Cake Layer (Right)

(Chen, et al. 1997).

## 2.18 Cake Building Filtration

From Darcy's law the typical linear equation of cake building filtration (Ruth's law) can be derived ( Ruth, B., Montillo, G., and Montonna, H. 1933) shown in equation (2.10). This linear function correlates the ratio  $t/V_l$  with the filtrate volume  $V_l$

$$t = \frac{\mu k R_c}{2 \Delta p A^2} V_l + \frac{\mu R_m}{\Delta p A} = a V_l + b \quad (2.10)$$

Where  $V_l$  is the filtrate volume ( $\text{m}^3$ ),  $t$  is the time (s),  $A$  is the filter area ( $\text{m}^2$ ),  $\mu$  is the dynamic viscosity of the liquid phase (Pa·s),  $\Delta p$  is the transmembrane pressure drop (Pa),  $R_m$  is the membrane resistance (1/m),  $R_c$  is the cake resistance (1/m) and  $k$  is the concentration coefficient (dimensionless). By experimentally determining slope  $a$  and intercept  $b$  the filter media resistance and the specific cake resistance can be calculated. Incompressibility of the filter cake is significant assumption for this equation; however, the results are acceptable for slightly compressible cakes. The integral values for the porosity are helpful in the latter case. (Eichholz, et al. 2008)

## 2.19 Magnetic System Enhance Ultrafiltration

In the UF process membrane fouling, which is an integrated phenomenon including solute and particles adsorbed and deposited on membrane surface, can cause a decline in membrane flux, decrease the efficiency of the membrane module, and even shorten membrane longevity. These problems increase production costs and price (Wang, et al. 2006). Thus, magnetic system which consists of SP adsorbent with external magnetic field is suggested to apply in UF process in order to reduce membrane fouling by slow-down cake formation. This application will be conducted in this research to determine the specific cake resistance which is expected to be less than of which conventional UF process.

## 2.20 Literature Reviews:

### 2.20.1 Currently Wastewater Treatment Process for Nalidixic Acid Removal

According to several reports, detected NAL concentration are varied from level of ng/L to mg/L, while pharmaceutical industrial and hospital wastewater have been frequently found NAL in higher concentration (mg/L) than municipal wastewater. Conclusions of several current treatment processes conducted in different wastewater treatment plants are shown in Table 2.6.

Conventional sewage treatment plants usually cannot remove NAL which is non-biodegradable. Although other available technologies have individual advantages, all remain their own limitations.

### 2.20.2 Adsorption Treatment Process for Removing Nalidixic Acid

**Lorphensri, et al. 2006** prepared two pure minerals and a hydrophobic medium which selected to study sorption of NAL. Alumina and silica were selected to represent positively charged and negatively charged aquifer mineral surfaces at neutral pH, respectively, while Porapak P (a cross-linked polymer of divinylbenzene/styrene) was selected to represent the hydrophobic organic content of an aquifer medium. This study investigated that NAL, which has a carboxyl functional group and performs anionic charges at neutral pH, showed significant adsorption to the positively charged alumina. The maximum adsorption of NAL to alumina occurred near its pKa (pH~6), where the combination of cationic alumina (PH<sub>ZPC</sub> 8.8) and anionic NAL produced maximum adsorption. Porapak P gave higher adsorption capacity than silica but still much lower compare to alumina. This research states that the adsorption of ionizable pharmaceuticals is strongly dependent on the system pH, the pharmaceutical properties (pKa and hydrophobicity), and the nature of the surface charge (point of zero charge). This paper concluded that the electrostatic attraction had a greater influence on the sorption of NAL than hydrophobic interaction.

**Table 2.6** Currently Wastewater Treatment Process for Nalidixic Acid Removal.

<b>Wastewater Treatment Processes</b>	<b>NAL Concentration (mg/l)</b>	<b>Advantages</b>	<b>Limitations</b>	<b>References</b>
Aerobic biological treatment	$1 \times 10^{-4}$ to 222	<ul style="list-style-type: none"> <li>• Conventional system.</li> <li>• Low cost.</li> </ul>	<ul style="list-style-type: none"> <li>• Limited removal efficiency, since Nalidixic acid is non-biodegradable.</li> </ul>	(Nakada, et al. 2006; Mascolo, et al 2010)
UV process	4 to $148 \times 10^{-6}$	<ul style="list-style-type: none"> <li>• Well known for oxidizing and mineralizing capacity to almost any organic contaminant.</li> </ul>	<ul style="list-style-type: none"> <li>• High UV energy required which much higher than application in disinfection process for wastewater treatment plant.</li> <li>• High cost required for UV process.</li> <li>• Studies of byproduct potential toxicity remain not available.</li> </ul>	(Nakada, et al. 2006; Kim, Ilho, Yamashita, Naoyuki, and Tanaka, Hiroaki. 2009; Sirtori, et al. 2009)
UV/H <sub>2</sub> O <sub>2</sub> process	4 to $148 \times 10^{-6}$	<ul style="list-style-type: none"> <li>• Reduce UV energy required.</li> </ul>	<ul style="list-style-type: none"> <li>• Cost is considered to be the commercial application obstruct.</li> <li>• None of byproduct has been investigated for measuring potential toxicity.</li> </ul>	(Nakada, et al. 2006; Kim, Ilho, Yamashita, Naoyuki, and Tanaka, Hiroaki. 2009; Sirtori, et al. 2009)
Solar photo-Fenton following by biological treatment.	45	<ul style="list-style-type: none"> <li>• The use of renewable energy sources to reduce cost of Advanced Oxidation Processes (AOP).</li> <li>• Successfully enhanced the wastewater biodegradability.</li> </ul>	<ul style="list-style-type: none"> <li>• Long treatment with heavy consumption of hydrogen peroxide, but without decreasing toxicity.</li> <li>• Required suitable selection of the photo-Fenton treatment time and hydrogen peroxide in order to achieve its efficiency and detoxify wastewater.</li> </ul>	(Sirtori, et al. 2009)



### 2.20.3 Magnetic Field Enhanced Cake Filtration of Superparamagnetic Polyvinyl Acetate Particles (PVAc)

**Eichholz, et al. 2008** studied combination of two classical separation methods, cake filtration and magnetic field driven separation. This paper discusses about the results of magnetic filtration experiments of non-functionalized particles. A special configuration of the magnet system leads to a slow down of the cake built-up which influenced by an external magnetic force and interparticulate magnetic force as shown in Figure 2.6. The result is an increase of the overall filtrate mass flow and therefore an improvement of filtration kinetics.

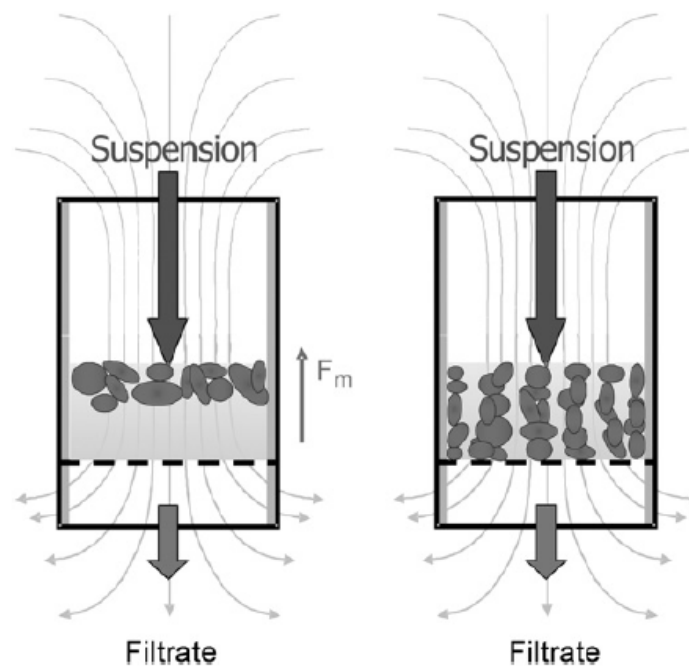


**Figure 2.6** Magnetic Field Effects: Effect of External Magnetic Force (Left), Effect of Interparticulate Magnetic Force (Right) (Eichholz, et al. 2008).

## CHAPTER III

### MATERIALS AND METHODS

#### 3.1 Materials

##### 3.1.1 Chemical Reagents

1. Dodecylamine	98%	ACROS ORGANICS
2. Tetraethoxysilane	98%	ACROS ORGANICS
3. 3-aminopropyltriethoxysilane	>98%	Fluka
4. 3-mercaptopropyltrimethoxysilane	>98%	Fluka
5. N-Octyldimethylchlorosilane	97%	Fluka
6. Phenyltrimethoxysilane	97%	Sigma Aldrich
7. 4-(Triethoxysilyl)butyronitrile	98%	Sigma Aldrich
8. Powdered activated carbon	ShirasakiS-10	Japan enviroChemicals, Ltd.
9. Ethyl alcohol absolute	RPE-ACS	CARLO ERBA
10. Hydrochloric acid	37%	CARLO ERBA
11. Sulfuric acid	98%	LAB SCAN
12. Potassium dihydrogenphosphate	AR grade	Riedel-de-Haen
13. Dipotassium hydrogenphosphate	AR grade	Riedel-de-Haen
14. Nalidixic acid	98%	Sigma Aldrich
15. Ammonium hydroxide	28-30%	J.T. Baker

##### 4.1.2 Instruments

1. Fourier transform Infrared Spectroscopy: Spectrum one (Perkin Elmer)

2. Inductively coupled plasma atomic emission spectroscopy (ICP-AES): Sulfer determinator model SC-132
3. UV- visible spectrophotometer: GENESYS<sup>TM</sup> 10S UV Vis with 1 cm quartz cells
4. Zeta potential analyzer
5. Shaker: Green Striker II
6. Magnetic stirrer : AS ONE Rexim RS 6D model
7. Scanning Electron Microscope (SEM): JSM -6400
8. pH meter: Sartorius PB-10 model
9. A Dataphysics DCAT-11 tensiometer: a powder contact angle mode
10. Regenerated cellulose membrane: 30,000 Da (Millipore)
11. Diaphragm pump: Deng yuan TYP-2500N
12. Permanent-magnet 0.4 T

## 3.2 Experimental Procedure

### 3.2.1 Adsorbents Synthesis

- *Synthesis of Superparamagnetic Iron Oxide Nanoparticles (Fe<sub>3</sub>O<sub>4</sub> NPs)*

Fe<sub>3</sub>O<sub>4</sub> NPs was prepared following the method which reported by Qu et al. (2010) (Qu, et al. 2010). A mixture of FeCl<sub>3</sub>.6H<sub>2</sub>O (0.046 mol) and FeSO<sub>4</sub>.7H<sub>2</sub>O (0.023 mol) was dissolved into 150 mL deionized water in 250 mL three-necked flask and Ar was imported for 3 min to extrude the air. Then 20 mL ammonium hydroxide (25%) was added quickly into the iron solution under vigorous stirring. After 30 min 3 mL of oleic acid was added into the mixture to modify the Fe<sub>3</sub>O<sub>4</sub> NPs and the mixture was heated to 75 °C. Keep this temperature for 1 h under Ar protection then cool down to room temperature. The Fe<sub>3</sub>O<sub>4</sub> NPs was collected through magnetic separation and washed with deionized water and ethanol three times, respectively, then dried at vacuum conditions.

- *Synthesis of Superparamagnetic Hexagonal Mesoporous Silicates (HMS-SP)*

Fe<sub>3</sub>O<sub>4</sub> NPs obtained from previous synthesis was encapsulated in mesoporous silica through a packing approach, forming core-shell structured Fe<sub>3</sub>O<sub>4</sub>@HMS microspheres following Tian et al. (2009)(Tian, et al. 2009) with some modifications. Briefly, 0.50 g of Fe<sub>3</sub>O<sub>4</sub> NPs was dispersed in 250mL of 0.1M HCl aqueous solution by ultrasonication for 10 min to reduce agglomerations. Then the result materials was separated and washed with deionized water. 0.35 g of dodecylamine was dissolved into a mixture of 3.94 g of ethanol and 27.36 g of H<sub>2</sub>O. Then the as-treated Fe<sub>3</sub>O<sub>4</sub> particles were added into the system. After vigorous stirring for 0.5 h, 2.0 g of tetraethylorthosilicate (TEOS) was added dropwise to the mixed solution. The reaction mixture was then stirred at ambient temperature for 24 h, collected with a magnet and washed with deionized water and ethanol to remove nonmagnetic by-products. Finally, the resulting powders was extracted by refluxing with 200mL ethanol at 80 °C for 6 h.

The extraction was repeated for twice to remove the surfactant templates completely. Finally, the product was washed with deionized water, and denoted as HMS-SP.

- *Synthesis of Single-functional SP-HMS (A-HMS-SP, M-HMS-SP, OD-HMS-SP, PTM-HMS-SP, N-HMS-SP and PTM-HMS-SP)*

SP-HMS obtained from previous synthesis will be grafted with 3-aminopropyltriethoxy-, 3-mercaptopropyl-, n-octyldimethyl-, 4-triethoxysilyl butyronitrile- and phenyltrimethoxy-, functional group by post-grafting method as following (Lee, et al. 2001 and Punyapalakul and Takizawa 2004 for n-octyldimethyl- functional group): 0.5 g of calcined SP-HMS was dehydrated at 120°C for 20 hr, and then stirred in 30 mL of toluene containing 0.5 g of each organosilane (such as of 3-aminopropyltriethoxysilane (APTES), 3-mercaptopropyltriethoxysilane (MPTMS) and n-octyldimethylchlorosilane, etc.) under refluxing condition for 24 hr. After that the product was filtrated and

thoroughly washed with 50 mL of toluene. Then the materials were washed with 50 mL of ethanol except for SP-OD and SP-CN. The latter materials were washed with 50 mL of acetone instead. Then, the sample was dried under vacuum at 85 °C for 2 hr. HMS-SP, A-HMS-SP, M-HMS-SP, OD-HMS-SP, N-HMS-SP and PTM-HMS-SP were obtained, respectively.

### 3.2.2. Characterization for Physico-chemical Properties of Adsorbents

To determine their physico-chemical properties, the synthesized adsorbents were analyzed through various methods as summarized in Table 3.1.

**Table 3.1** Analysis Methods of the Physico-chemical Characteristics of Synthesized Adsorbents

Parameter	Instrument/Analysis
Surface area, pore size and pore structure	Nitrogen adsorption-desorption measurement
Functional group	Fourier transform infrared spectroscopy (FT-IR)
Sulfur content	Inductively coupled plasma atomic emission spectroscopy (ICP-AES)
Surface charge	Zeta potential analyzer
Surface appearance	Scanning Electron Microscopy (SEM)
Hydrophobicity	Tensiometer

### 3.2.3 Adsorption Study

- *Adsorption kinetic*

1. HMS-SP of 0.02 g was transferred into 150 ml Erlenmeyer flask with 20 mg/l NAL solution for 20 ml. The pH value and ionic strength of solution were controlled at 7 and 0.01 M by using phosphate buffer.
2. Shaking the flasks in controlled temperature at  $25 \pm 2$  °C.
3. The samples were taken at time interval until reach 48 h, and then filtered through the GF/C filter paper. The filtered solution was analyzed for NAL concentration by applying an UV-visible spectrophotometer at 260 nm.
4. The procedure was repeated with changing adsorbents, including A-HMS-SP, M-HMS-SP, OD-HMS-SP, N-HMS-SP, PTM-HMS-SP and PAC.

- *Adsorption isotherm*

1. HMS-SP of 0.02 g was transferred into 150 ml Erlenmeyer flask with various range of NAL concentration from 1 to 30 mg/L for 20 ml in volume each. The pH value of solution was controlled at 7 and 0.01 M ionic strength by using phosphate buffer.
2. Shaking the flasks in controlled temperature at  $25 \pm 2$  °C.
3. The sample was taken at the contact time obtained from adsorption kinetic. The sample was filtered through the GF/C filter paper, and then analyzed for NAL concentration by applying an UV-visible spectrophotometer at 260 nm.
4. The procedure was repeated with changing adsorbents, including A-HMS-SP, M-HMS-SP, OD-HMS-SP, N-HMS-SP, PTM-HMS-SP and PAC.

The considered variables in adsorption kinetic can be concluded in Table 3.3.

**Table 3.2** The Studied Parameters in Adsorption Kinetic Study

<b>Studied Parameters</b>	<b>Values</b>
<ul style="list-style-type: none"> <li>• Time</li> <li>• Adsorbent types</li> <li>• Pollutant types</li> </ul>	<ul style="list-style-type: none"> <li>• 0, 1, 2, 3, 4,5,10,15,20,25,30,45, 60 min and then every 2 h until reach 48 h</li> <li>• HMS-SP, A-HMS-SP, M-HMS-SP, OD-HMS-SP, N-HMS-SP, PTM-HMS-SP and PAC</li> <li>• Nalidixic acid (NAL)</li> </ul>
<b>Analytical Parameters</b>	<b>Analytical Method</b>
<ul style="list-style-type: none"> <li>• Concentration of NAL</li> </ul>	<ul style="list-style-type: none"> <li>• UV-visible spectrophotometer (1 cm quart cell)</li> </ul>
<b>Controlled Parameters</b>	<b>Values</b>
<ul style="list-style-type: none"> <li>• pH</li> <li>• Ionic strength</li> <li>• Temperature</li> <li>• Adsorbent weight</li> <li>• Solution volume</li> </ul>	<ul style="list-style-type: none"> <li>• pH value 7 controlled by phosphate buffer</li> <li>• 0.01M</li> <li>• <math>25 \pm 2</math> °C</li> <li>• 0.02 g</li> <li>• 20 ml</li> </ul>

- *Effects of pH*

1. HMS-SP of 0.02 g was transferred into 150 ml Erlenmeyer flask with various range of NAL concentration from 1 to 30 mg/L for 20 ml in volume each. The pH value of solution was controlled at 5, 7, 9 and 0.01 M ionic strength by using phosphate buffer.
2. Shaking the flasks in controlled temperature at  $25 \pm 2$  °C.

3. The sample was taken at the contact time obtained from adsorption kinetic. The sample was filtered through the GF/C filter paper, and then analyzed for NAL concentration by applying an UV-visible spectrophotometer at 260 nm.
4. The procedure was repeated with changing adsorbents, including A-HMS-SP, M-HMS-SP, OD-HMS-SP, N-HMS-SP, PTM-HMS-SP and PAC.

The considered variables in determining of pH effect can be concluded in Table 3.4.

**Table 3.3** The Studied Parameters in Adsorption Isotherm Study

<b>Studied Parameters</b>	<b>Values</b>
<ul style="list-style-type: none"> <li>• Adsorbent types</li> <li>• Pollutant types</li> </ul>	<ul style="list-style-type: none"> <li>• HMS-SP, A-HMS-SP, M-HMS-SP, OD-HMS-SP, N-HMS-SP, PTM-HMS-SP and PAC</li> <li>• Nalidixic acid (NAL)</li> </ul>
<b>Analytical Parameters</b>	<b>Analytical Method</b>
<ul style="list-style-type: none"> <li>• Concentration of NAL</li> </ul>	<ul style="list-style-type: none"> <li>• UV-visible spectrophotometer (1 cm quart cell)</li> </ul>
<b>Controlled Parameters</b>	<b>Values</b>
<ul style="list-style-type: none"> <li>• pH</li> <li>• Ionic strength</li> <li>• Temperature</li> <li>• Adsorbent weight</li> <li>• Solution volume</li> <li>• Time</li> </ul>	<ul style="list-style-type: none"> <li>• pH value 7 controlled by phosphate buffer</li> <li>• 0.01 M</li> <li>• <math>25 \pm 2</math> °C</li> <li>• 0.02 g</li> <li>• 20 ml</li> <li>• As obtain from adsorption kinetic</li> </ul>



**Table 3.4** The Determined Parameters in Study of pH Effects

<b>Studied Parameters</b>	<b>Values</b>
<ul style="list-style-type: none"> <li>• Adsorbent types</li> <li>• Pollutant types</li> </ul>	<ul style="list-style-type: none"> <li>• HMS-SP, A-HMS-SP, M-HMS-SP, OD-HMS-SP, N-HMS-SP, PTM-HMS-SP and PAC</li> <li>• Nalidixic acid (NAL)</li> </ul>
<b>Analytical Parameters</b>	<b>Analytical Method</b>
<ul style="list-style-type: none"> <li>• Concentration of NAL</li> </ul>	<ul style="list-style-type: none"> <li>• UV-visible spectrophotometer (1 cm quart cell)</li> </ul>
<b>Controlled Parameters</b>	<b>Values</b>
<ul style="list-style-type: none"> <li>• pH</li> <li>• Ionic strength</li> <li>• Temperature</li> <li>• Adsorbent weight</li> <li>• Solution volume</li> <li>• Time</li> </ul>	<ul style="list-style-type: none"> <li>• pH value 5, 7,9 controlled by phosphate buffer</li> <li>• 0.01 M</li> <li>• <math>25 \pm 2</math> °C</li> <li>• 0.02 g</li> <li>• 20 ml</li> <li>• As obtain from adsorption kinetic</li> </ul>

- *Investigate Hydrogen Bonding Reaction between NAL and HMS-SP*

1. HMS of 0.1 g was transferred into 150 ml Erlenmeyer flask with NAL concentration of 30 mg/L for 20 ml. The NAL solution was prepared in hexane to eliminate effect of water that can cause hydrogen bonding to the adsorbent.
2. Shaking the flasks in controlled temperature at  $25 \pm 2$  °C.
3. The sample was taken at the contact time obtained from adsorption kinetic. The sample was filtered through the GF/C filter paper, and then analyzed for NAL concentration by applying an UV-visible spectrophotometer at 260 nm.

- The filtrated HMS was collected and analyzed by FTIR to compared O-H stretching peak with the pristine HMS to confirm hydrogen bonding reaction of NAL adsorption on HMS surface.

### 3.2.4. Separation Process by Magnetic System Applied to Enhance Ultrafiltration

- Magnetic System Reducing Specific Cake Resistance*

- From 3.2.3, PTM-HMS-SP under pH5 was selected to perform this experiment. The of solution of PTM-HMS-SP 1g/L, controlled at pH 5 and 0.01 M ionic strength by using phosphate buffer, was prepared and mixing for 2 hours.
- The completely mixed of solution was feed to the dead-end flow membrane system while pressure head was controlled to be 1 bar by valve of by-pass line (temperature at  $25 \pm 2$  °C).
- The filtrate volume versus time was detected until filtrate volume reached 90 mL.
- The procedure was repeated withluxh addition of external magnetic field (using permanent-magnet with 0.4T maximum field strength).
- The procedure 1.-3.was repeated with changing feed solution to be DI water controlled at pH 5 and 0.01 M ionic strength by using phosphate buffer.

**Table 3.5** The Determined Parameters in Study of Magnetic System Reducing Specific Cake Resistance

Controlled Parameters		Experimental Parameters	
pH	5	PTM-HMS-SP 1g/L	Magnetic System 0.4 T
Ionic strength	0.1 M	/	
Temperature	$25 \pm 2$ °C	/	/
Pressure head	1 bar		

- *Effects of NAL on Magnetic System Applied on Ultrafiltration*

1. The of solution of 20 mg/L of NAL mixing with PTM-HMS-SP 1g/L, controlled at pH 5 and 0.01 M ionic strength by using phosphate buffer, was prepared and mixing for 2 hours.
2. The completely mixed of solution was feed to the dead-end flow membrane system while pressure head was controlled to be 1 bar by valve of by-pass line (temperature at  $25 \pm 2$  °C).
3. The filtrate volume versus time was detected until filtrate volume reached 90 mL.
4. The procedure was repeated with addition of external magnetic field (using permanent-magnet with 0.4T maximum field strength).
5. The procedure 1.-3.was repeated with changing feed solution to be 20 mg/L of NAL controlled at pH 5 and 0.01 M ionic strength by using phosphate buffer.
6. NAL remained in filtrate volume will be determined by UV-visible spectrophotometer at 260 nm.

**Table 3.6** The Determined Parameters in Study of Effects of NAL on Magnetic System Applied on Ultrafiltration

Controlled Parameters		Experimental Parameters		
pH	5	PTM-HMS-SP 1g/L	NAL 20 mg/L	Magnetic System 0.4 T
Ionic strength	0.1 M		/	
Temperature	$25 \pm 2$ °C	/	/	
Pressure head	1 bar	/	/	/

- *Effects of Electrostatic Interaction Changing by pH between Adsorbate, Adsorbents, and Membrane*

1. The of solution of PTM-HMS-SP 1g/L, controlled at pH 5, 7 and 0.01 M ionic strength by using phosphate buffer, was prepared and mixing for 2 hours.
2. The completely mixed of solution was feed to the dead-end flow membrane system while pressure head was controlled to be 1 bar by valve of by-pass line (temperature at  $25 \pm 2$  °C).
3. The filtrate volume versus time was detected until filtrate volume reached 90 mL.
4. The procedure 1.-3.was repeated with changing feed solution to be 20 mg/L of NAL mixing with PTM-HMS-SP 1g/L, controlled at pH 5, 7 and 0.01 M ionic strength by using phosphate buffer.
5. The procedure 1.-3.was repeated with changing feed solution to be DI water controlled at pH 5 and 0.01 M ionic strength by using phosphate buffer.
6. NAL remained in filtrate volume will be determined by UV-visible spectrophotometer at 260 nm.

**Table 3.7** The Determined Parameters in Study of Effects of Electrostatic Interaction Changing by pH Between Adsorbate, Adsorbents, and Membrane

Controlled Parameters		Experimental Parameters	
		<b>PTM-HMS-SP 1g/L</b>	<b>NAL 20 mg/L</b>
		<b>pH 5</b>	
		/	
Ionic strength	0.1 M		/
Temperature	$25 \pm 2$ °C	/	/
Pressure head	1 bar	<b>pH 7</b>	
		/	
			/
		/	/

Diagram of magnetic system applied to UF is shown in Figure 3.1

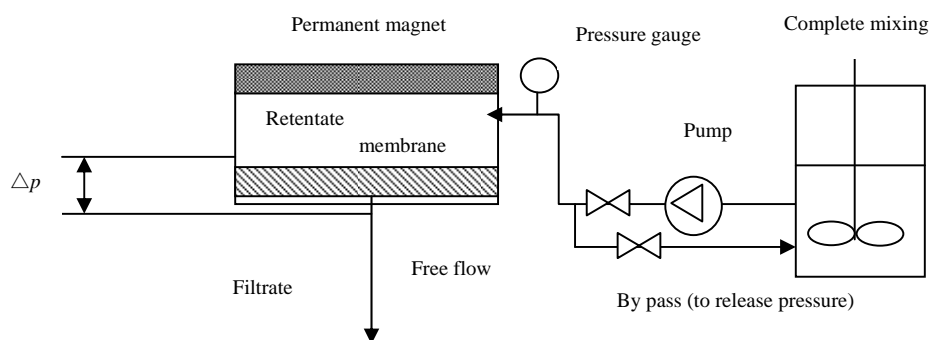


**Figure 3.1** Diagram of Magnetic System Applied to UF.

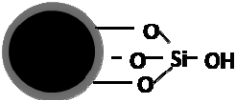
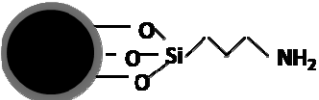
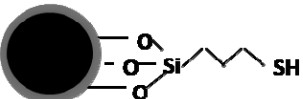
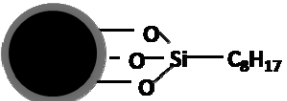
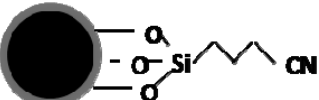
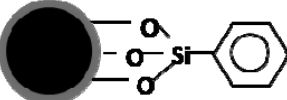
## CHAPTER IV

### RESULTS AND DISCUSSION

#### 4.1 Characterization for Physico-chemical Properties of Adsorbents

Synthesized adsorbents were investigated their physico-chemical characteristics. Summary of chemical structure of which functional group on F-HMS-SP surface (HMS-SP, A-HMS-SP, M-HMS-SP, OD-HMS-SP, N-HMS-SP and PTM-HMS-SP) and expected interaction are displayed in Table 4.1

**Table 4.1** Summary of Chemical Structure of which Functional Group on F-HMS-SP Surface and Expected Interaction

Surface Functional Group	Chemical Structure	Expected Interaction
Silanol (HMS-SP)		Hydrogen bonding
3-Aminopropyltriethoxy- (A-HMS-SP)		Weak hydrogen bonding Attraction electrostatic interaction
3-Mercaptopropyltrimethoxy- (M-HMS-SP)		Weak hydrogen bonding* Van der waals force due to hydrophobicity
n-Octyldimethyl- (OD-HMS-SP)		Weak hydrogen bonding* Van der waals force due to hydrophobicity
4-Triethoxysilyl butyronitrile- (N-HMS-SP)		Weak hydrogen bonding* Van der waals force due to hydrophobicity
Phenyltrimethoxy- (PTM-HMS-SP)		Weak hydrogen bonding* Van der waals force due to hydrophobicity

\*Weak hydrogen bonding was expected due to remaining silanol group after surface modifications of F-HMS-SP.

#### 4.1.1 Pore Structure

Figure 4.1 illustrates nitrogen adsorption-desorption isotherms of synthesized adsorbents. Type IV isotherm (IUPAC), and two capillary steps can be observed on the adsorption-desorption isotherms. All hysteresis loops occurred at similar relative pressure ( $p/p_0$ ) and showed mesoporous structure.

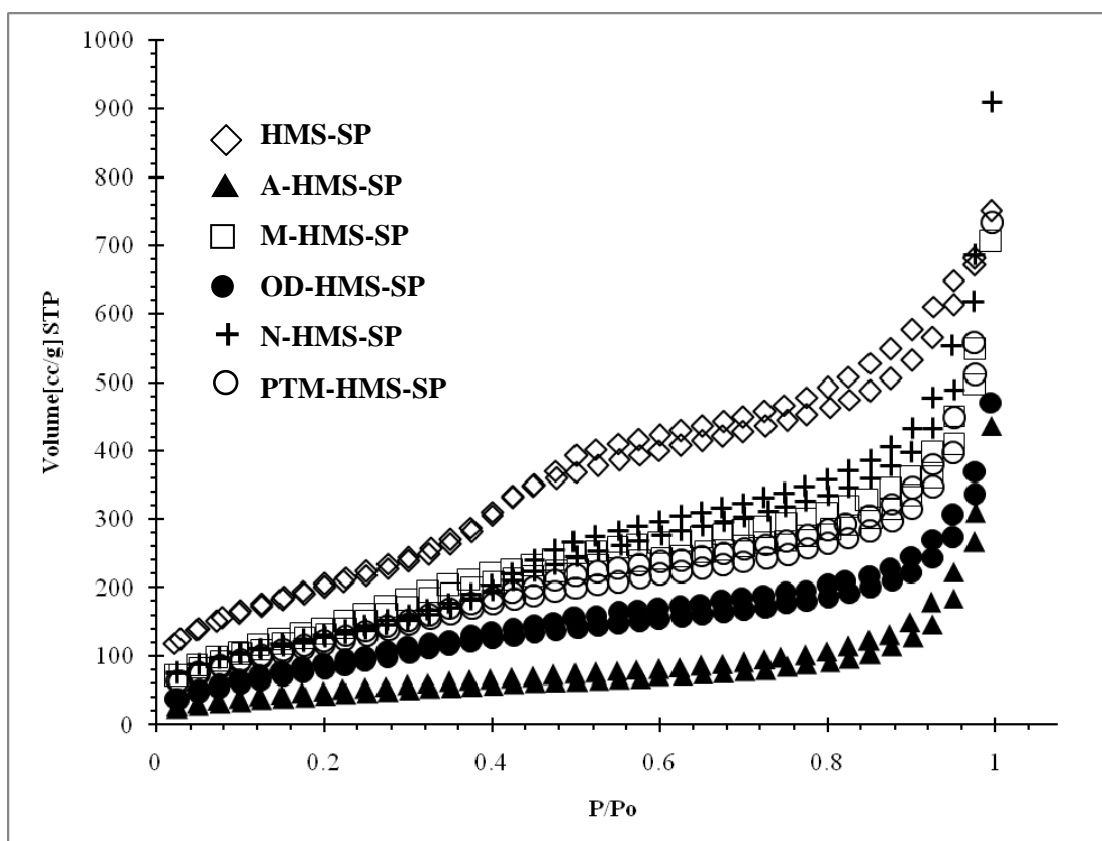


**Figure 4.1** Nitrogen Adsorption-desorption Isotherms of Adsorbents.

#### 4.1.2 Surface Area and Pore Size

To explain surface area, pore volumes, and pore size distributions of porous materials, the Brunauer-Emmett-Teller (BET) method was widely used for these purposes. The

BET equation was expressed in Equation 4.1 using nitrogen adsorption-desorption isotherm data. The nitrogen isotherms (BET) were measured at 77 K on a surface area and porosity analyzer.

$$\frac{p}{v(p_0 - p)} = \frac{1}{v_m c} + \frac{c-1}{v_m c} \cdot \frac{p}{p_0} \quad (4.1)$$

Where,  $v$  is volume of  $N_2$  adsorbed by the analyzed sample under pressure  $p$  and  $p_0$  is the saturated vapor pressure at the same temperature.  $v_m$  is the volume of  $N_2$  adsorbed when the surface is covered with a uni-molecular layer and  $c$  is constant for a given adsorbate.

The specific surface areas of samples were calculated from the adsorption data by Equation 4.2.

$$S = \frac{N_0 v_m A}{22414m} \quad (4.2)$$

Where  $S$  is specific surface area,  $N_0$  is Avogadro number,  $m$  is amount of solid adsorbent and  $A$  is cross-section of the gas molecules ( $16.2 \text{ \AA}^2$  for  $N_2$ ).

Using the BET model, the calculation of surface areas, pores volumes, and pores size of HMS-SP, functionalized HMSs, and PAC were shown in Table 4.2.

**Table 4.2** BET Surface Area, Pores Volumes, and Pore Diameter of the Studied Adsorbents

Adsorbents	Pore Diameter (Å)	BET Surface Area (m <sup>2</sup> /g)	Pore Volume (mm <sup>3</sup> /g)	Surface Functional Groups
HMS-SP	60.2	771	1,161	silanol
A-HMS-SP	167.1	162	676	3-aminopropyltriethoxy-
M-HMS-SP	80	542	1,091	3-mercaptopropyl-
OD-HMS-SP	84	344	729	n-octyldimethyl-
N-HMS-SP	117.3	480	1,406	4-triethoxysilyl butyronitrile-
PTM-HMS-SP	97.1	468	1,137	phenyltrimethoxy-
PAC	19	980	276	carboxyl, phenyl, and others



According to Table 4.2, the highest specific surface area of PAC comparing to the other adsorbents might yield highest NAL adsorption capacity. For pore size distribution, the smallest pore size among the others is performed by PAC. Average pore sizes of HMS-SP and functionalized HMS-SP (A-HMS-SP, M-HMS-SP, OD-HMS-SP, N-HMS-SP and PTM-HMS-SP) were conformed to the mesoporous structures category which in the range of 2 – 50 nm. Functionalized HMS-SP had smaller surface area and larger pore size comparing with non-grafted HMS-SP. This might be caused by the collapse of silicate structure during grafting processes, especially on A-HMS-SP.

### 4.1.3 Surface Functional Groups

Figure 4.2 showed surface functional groups of synthesized adsorbents that were investigated by Fourier Transform Infrared (FT-IR) to confirm the presence of functional groups on the adsorbents surface. According to Figure 4.2, hydrogen bonded Si-OH stretching band at wavenumber of  $3400 - 3500 \text{ cm}^{-1}$  can be observed for all adsorbents. This can indicate the presence of remaining silanol functional group of adsorbent surfaces. For functionalized HMS-SP, C-H stretching band and C-H bending of  $\text{CH}_2$ -methylene group can be observed by the band at less than  $3000 \text{ cm}^{-1}$  and  $1450 \text{ cm}^{-1}$  wavenumber, respectively. CN stretching band at  $2210-2260 \text{ cm}^{-1}$  wave number also can be detected and confirmed the presence of 4-triethoxysilyl butyronitrile functional group on material surface. Moreover, benzene ring was confirmed by  $>3000 \text{ cm}^{-1}$  stretching band. A-HMS-SP did not show N-H stretching band at wave number of  $3300 - 3400 \text{ cm}^{-1}$ , and the 3-mercaptopropyl- functional group of M-HMS-SP also cannot be detected the band of S-H stretching at  $2550-2600 \text{ cm}^{-1}$ . These might be caused by limitation of sensitivity of FT-IR to analyze N-H and S-H stretching. However, ICP-AES can determine 3.37% by weight of sulfur content on M-HMS-SP surface which indicated the presence of 3-mercaptopropyl- functional group. Table 4.3 summarizes FT-IR spectra of HMS-SP and F-HMS-SP. (<http://www.umsl.edu/~orglabdocuments/IRIR2.html>)

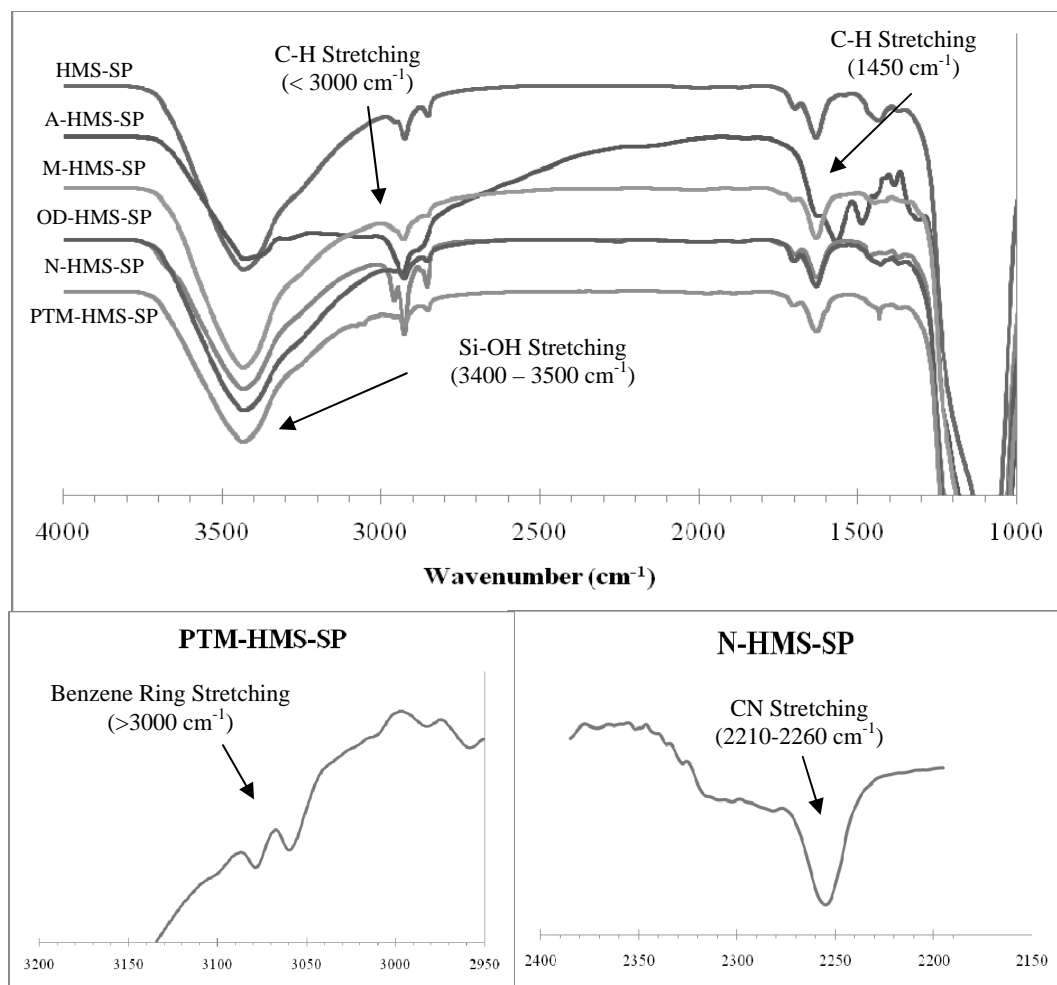


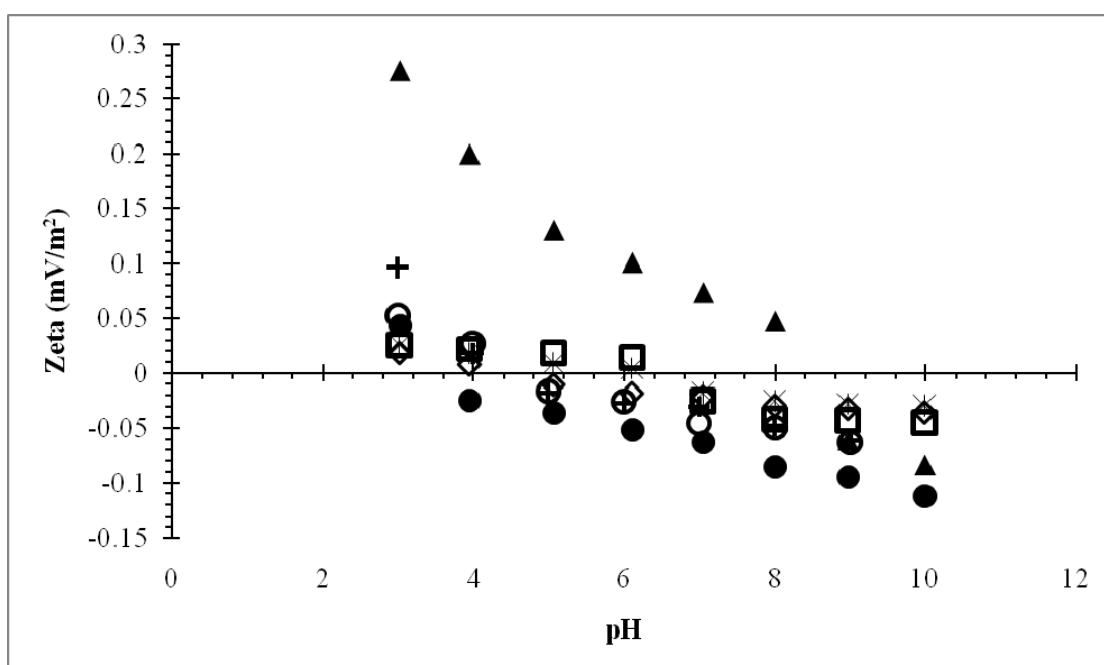
**Figure 4.2** FT-IR Spectra of HMS-SP and F-HMS-SP.

**Table 4.3** Summary of FT-IR Spectra of HMS-SP and F-HMS-SP

Stretching Band	Si-OH	C-H	C-H	Benzene Ring	CN	N-H	S-H
Wavenumber (cm <sup>-1</sup> )	3400 – 3500	< 3000	1450	>3000	2210-2260	3300 – 3400	2550-2600
<b>Adsorbents</b>							
HMS-SP	/	/	/				
A-HMS-SP	/	/	/				
M-HMS-SP	/	/	/				
OD-HMS-SP	/	/	/				
N-HMS-SP	/	/	/		/		
PTM-HMS-SP	/	/	/	/			

#### 4.1.4 Surface Charge

Zeta potential analyzer was applied for determining the surface charge of synthesized adsorbents. The surface charge of HMS-SP and functionalized HMS-SP (A-HMS-SP, M-HMS-SP, OD-HMS-SP, N-HMS-SP and PTM-HMS-SP) were displayed in Figure 4.3 as function of pH. The pH value at the zero point of charge ( $\text{pH}_{\text{zpc}}$ ) is summarized in Table 4.4.

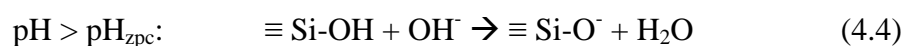
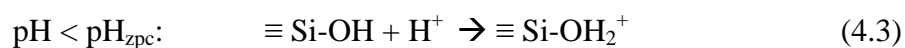
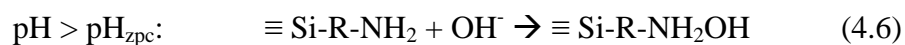
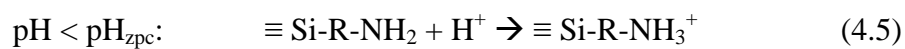
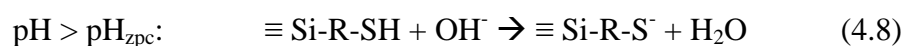


**Figure 4.3** Surface Charges of HMS-SP and Functionalized HMS-SP.

At  $\text{pH}_{\text{zpc}}$  value, Surfaces are balanced between the positive charge of cationic surface groups and the negative charge of anionic surface groups. Thus, adsorbents perform zero surface charge at  $\text{pH}_{\text{zpc}}$ . When the pH increased from acidic region to neutral pH or basic region range, the surface charge is decreased. Equation 4.3 and 4.4 showed protons gaining or losing from the silanol groups on the surface of HMS-SP that result in the variations of surface charge. (Punyapalakul and Sitthisorn 2010) The surfaces of HMS-SP are protonated at low pH, so the surfaces become positively charged. On the contrary, losing their protons, the surfaces become negatively charged at high pH.

**Table 4.4**  $\text{pH}_{\text{zpc}}$  of Adsorbents Used in this Study

Adsorbents	$\text{pH}_{\text{zpc}}$
A-HMS-SP	8.8
HMS-SP	5
M-HMS-SP	6.2
OD-HMS-SP	4
N-HMS-SP	4.5
PTM-HMS-SP	4.6
PAC	6.8

**HMS -SP:****A-HMS:****M-HMS:****4.1.5 Morphology**

Scanning Electron Microscope (SEM) was applied to inspect surface appearance of all adsorbents and showed uniform size distribution in ranges of nanometer diameter exhibited on Figure 4.4.

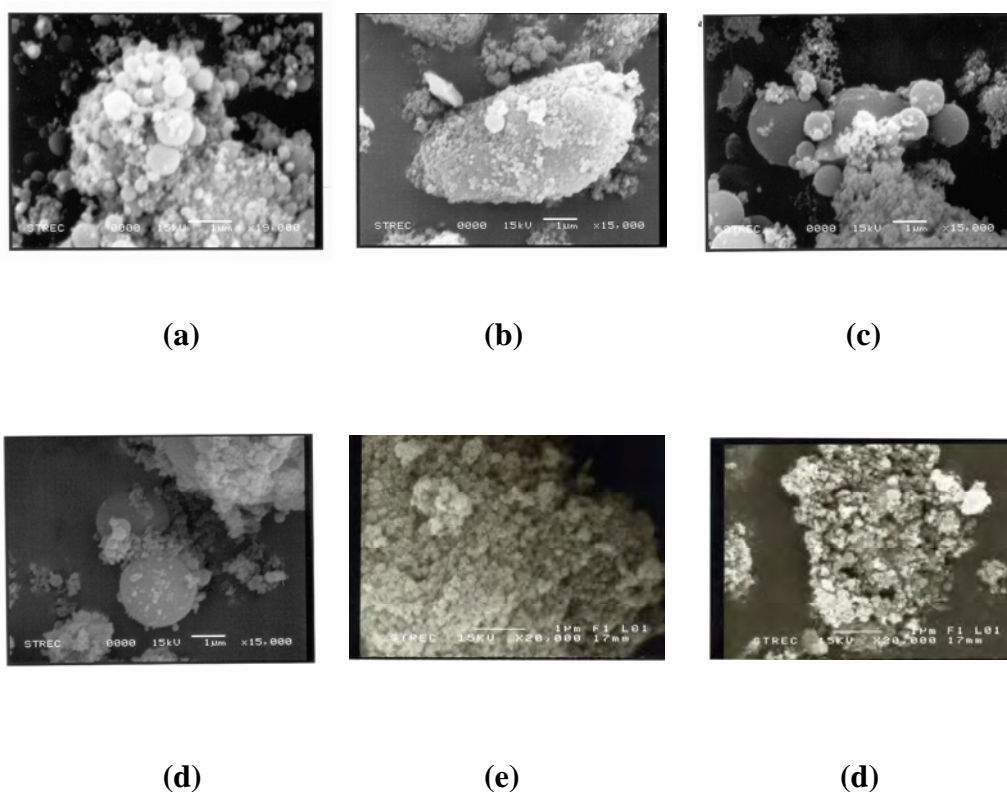


**Figure 4.4** Scanning Electron Microscope (SEM) Images of HMS-SP(a), A-HMS-SP(b), M-HMS-SP(c), OD-HMS-SP(d), N-HMS-SP(e) and PTM-HMS-SP(f).

Synthesized adsorbents can be categorized by their hydrophobicity. Silanol functional group of HMS-SP and 3-aminopropyltriethoxy functional group of A-HMS-SP performed hydrophilicity whereas other adsorbent surfaces are hydrophobic. The contact angle ( $\Theta$ ) between adsorbent and water surface as shown in Figure 4.5 can be used to indicate hydrophobicity. Larger contact angle ( $\Theta$ ) can be observed in adsorbent which had higher hydrophobicity. To compare hydrophobicity of each surface, contact angle ( $\Theta$ ) of hydrophobic surface adsorbents (M-HMS-SP, OD-HMS-SP, N-HMS-SP, PTM-HMS-SP and PAC) were analyzed by using a Dataphysics DCAT-11 tensiometer in a powder contact angle mode. The summary of contact angle ( $\Theta$ ) displayed on Table 4.5. indicated that OD-HMS-SP surface performed the highest hydrophobicity and agreed with aliphatic hydrocarbon chemical structure, following by PTM-HMS-SP, M-HMS-SP, PAC and N-HMS-SP

respectively. Moreover, to compare with hydrophilic surface, contact angle ( $\Theta$ ) of HMS-SP was determined. As anticipated, HMS-SP provided very low contact angle ( $\Theta$ ) which implied low hydrophobicity.

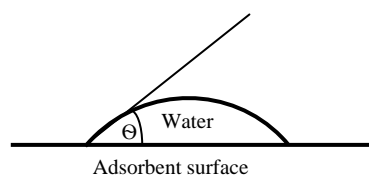


**Figure 4.5** Schematic Drawing of Contact Angle ( $\Theta$ ) between Adsorbent Surface and Water.

**Table 4.5** Chemical Structure and Contact Angle ( $\Theta$ ) of Adsorbents

Adsorbent	Chemical Structure	Contact Angle (Degree)	Error
OD-HMS-SP		89.46	$\pm 0.67$
PTM-HMS-SP		76.64	$\pm 0.02$
M-HMS-SP		59.97	$\pm 2.73$
N-HMS-SP		53.27	$\pm 0.66$
HMS-SP		45.06	-
PAC	-	58.34	$\pm 0.08$

## 4.2 Adsorption Kinetic

The NAL adsorption kinetic studies were performed at pH around  $7 \pm 0.2$  and 0.01 M ionic strength controlled by phosphate buffer. Figure 4.6 displays the NAL kinetic results on the applied adsorbents. The NAL concentrations were drastically decreased at first 5 minutes and reached equilibrium stage after 15 minutes, except for PTM-HMS-SP (20 min.) and PAC (3 hr.).

### 4.2.1 The Pseudo-first and Pseudo-second Order Model

The pseudo-first and pseudo-second order model were applied, to analyze the NAL adsorption rate on the applied adsorbents. The pseudo-first order and pseudo-second order kinetic models are expressed in Equation 4.9 and Equation 4.10.

$$\ln(q_e - q_t) = \ln q_e - k_1 t \quad (4.9)$$

$$\frac{t}{q_t} = \frac{1}{2k_2 q_e^2} + \frac{t}{q_e} \quad (4.10)$$

Where, $k_1$	=	Lagergen rate constant (1/min)
$k_2$	=	Pseudo-second order rate constant (g/mg min)
$q_e$	=	Amounts of targeted pollutant sorbed at equilibrium (mg/g)
$q_t$	=	Amounts of targeted pollutant sorbed at time t (mg/g)

Moreover, the initial adsorption rate can also be obtained from this model by calculated from Equation 4.11.

$$h = k_2 q_e^2 \quad (4.11)$$

Where,  $h$  is the initial adsorption rate ( $\mu\text{g/g}\cdot\text{min}$ ). The calculated  $k_2$  values indicated the adsorption rate of adsorbents.

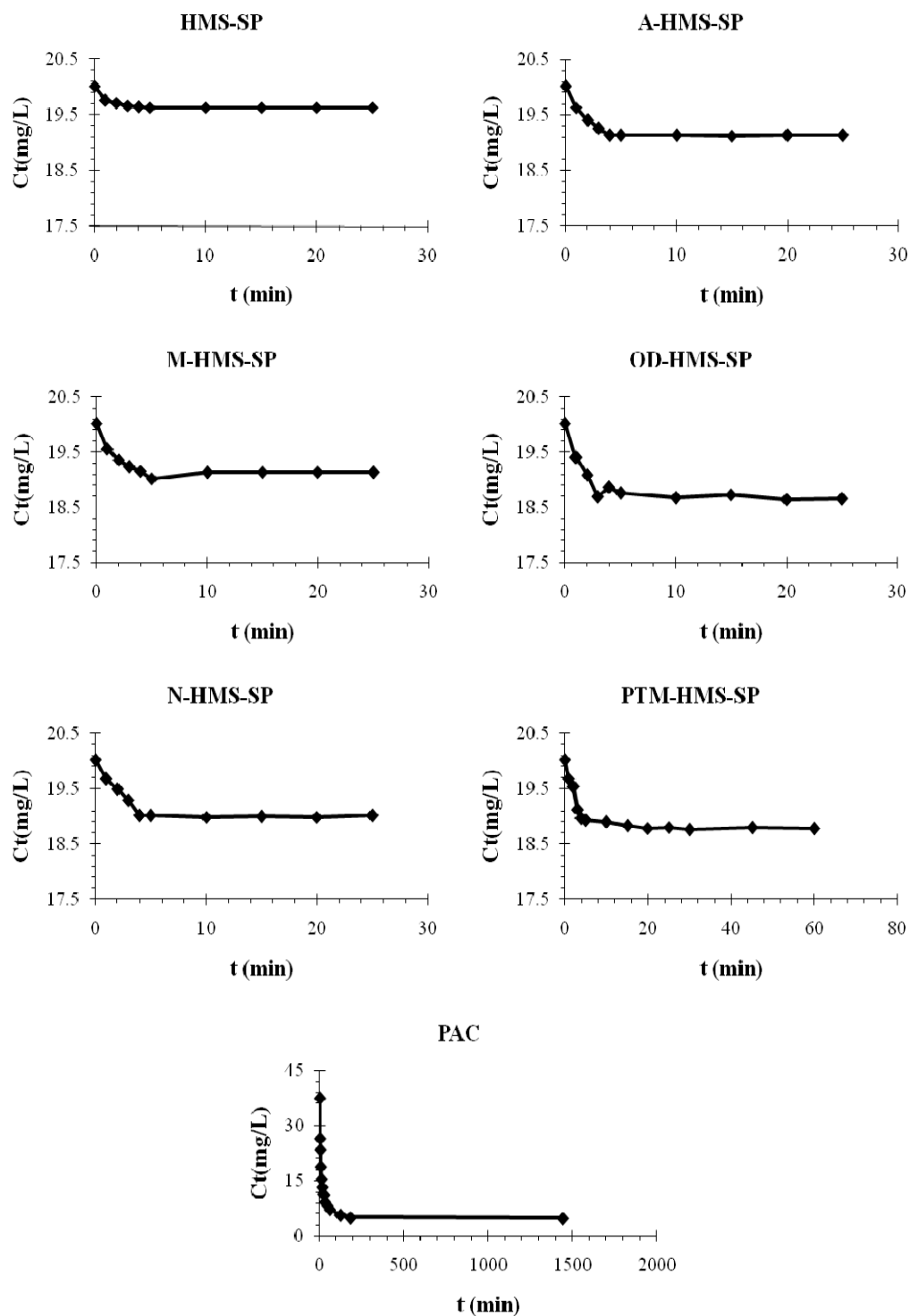


**Figure 4.6** Adsorption Kinetic Results of NAL  
(at 25°C, IS = 0.01 M and pH = 7±0.2).



The experimental data were plotted based on equations above. The calculated kinetic constants of each adsorbent are summarized in Table 4.6. The results showed that the experimental data were incompatible with pseudo-first order model but fitted with the pseudo-second order model. The experimental  $q_e$  and the calculated  $q_e$  were compared and it was found that the calculated  $q_e$  agreed with the experimental  $q_e$ . The adsorption phenomena of NAL were dependent on the quantity of adsorbed target compounds on the adsorbents' surface that can be described by the pseudo-second order model. Furthermore, high adsorption rate can be observed at the initial stage, and then performed slower adsorption rate versus time.

**Table 4.6** Kinetics Values Calculated for NAL Adsorption on Adsorbents

Adsorbent	Pseudo-first Order				Pseudo-second Order			
	$R^2$	Experimental $q_e$ (mg/g)	$k_1$ (1/min)	Calculated $q_e$ (mg/g)	$R^2$	$k_2$ (g/mg min)	Calculated $q_e$ (mg/g)	$h$ (mg/g min)
HMS-SP	0.025	0.376	0.007	0.012	0.999	14.585	0.366	1.957
A-HMS-SP	0.021	0.886	0.004	0.081	0.999	4.601	0.883	3.584
M-HMS-SP	0.001	0.874	0.001	0.179	0.999	5.646	0.876	4.329
OD-HMS-SP	0.366	1.368	0.015	0.166	0.999	1.545	1.370	2.899
N-HMS-SP	0.002	1.020	-	0.055	0.999	1.221	1.036	1.310
PTM-HMS-SP	0.323	1.230	0.014	0.393	0.999	0.765	1.245	1.187
PAC	0.159	32.515	0.000	5.702	1.000	0.007	33.333	8.264

Obtained results showed high adsorption rate and rapidly reach the saturation stage which can be implied by high  $k_2$  value. Whereas, the initial adsorption rate ( $h$ ) mentioned the rate of adsorption at the initial period, which can be implied to the drastically decrease of NAL concentration in the first 5 minutes occurred in this study. PAC performed the highest adsorption rate as seen in Table 4.5 that might be caused by very high surface area and high complexity of surface functional groups. Conversely, adsorption rate of HMS-SP, which also has high surface area, performed low value. This may implied the limitation of the smallest pore size of HMS-SP affected to adsorption rate.

### 4.2.2 Intraparticle Diffusion Model

Intraparticle diffusion model also has been applied in this study to analyze nature of the ‘rate-controlling step’ represented by the following Weber and Morris equation (4.12) (Weber and Morris 1963)

$$q_t = k_i t^{0.5} + c \quad (4.12)$$

Where,  $C$  is the intercept, related to the thickness of the boundary layer and  $k_i$  is the intraparticle diffusion rate constant. According to this equation, the results were plotted and displayed on Figure 4.7

As shown on Figure 4.7, there are 2 separate stages; the first linear portion (stage 1) and second plateau (stage 2) which occurred after achieve equilibrium time obtained from the results in Figure 4.6. The similar shape of intraparticle diffusion plot were normally found in the literature (Chakrapani, et al. 2010).

At stage 1 of all adsorbents except for PAC, the straight lines are plotted pass through the origin, which implied that the NAL adsorption is controlled by the intraparticle diffusion process. Though intraparticle diffusion renders straight lines (stage 1) with correlation co-efficients ( $>0.9$ ) for all sorbents as displayed on Table 4.7, the intercept of the line in PAC case fails to pass through the origin that may indicate some degree of boundary layer control. The deviation from the origin may be due to the variation of mass transfer in the initial and final stages of adsorption. (Theivarasu and Mylsamy 2010)

As seen in the Table 4.7, HMS-SP provided the lowest intraparticle diffusion rate constant that might be limited by small pore size compared to other adsorbents. On the other hand, the highest intraparticle diffusion rate constant was performed by the lowest pore size adsorbent which is PAC, that might be caused by very high surface area, large pore size distribution and high surface complexity of materials.

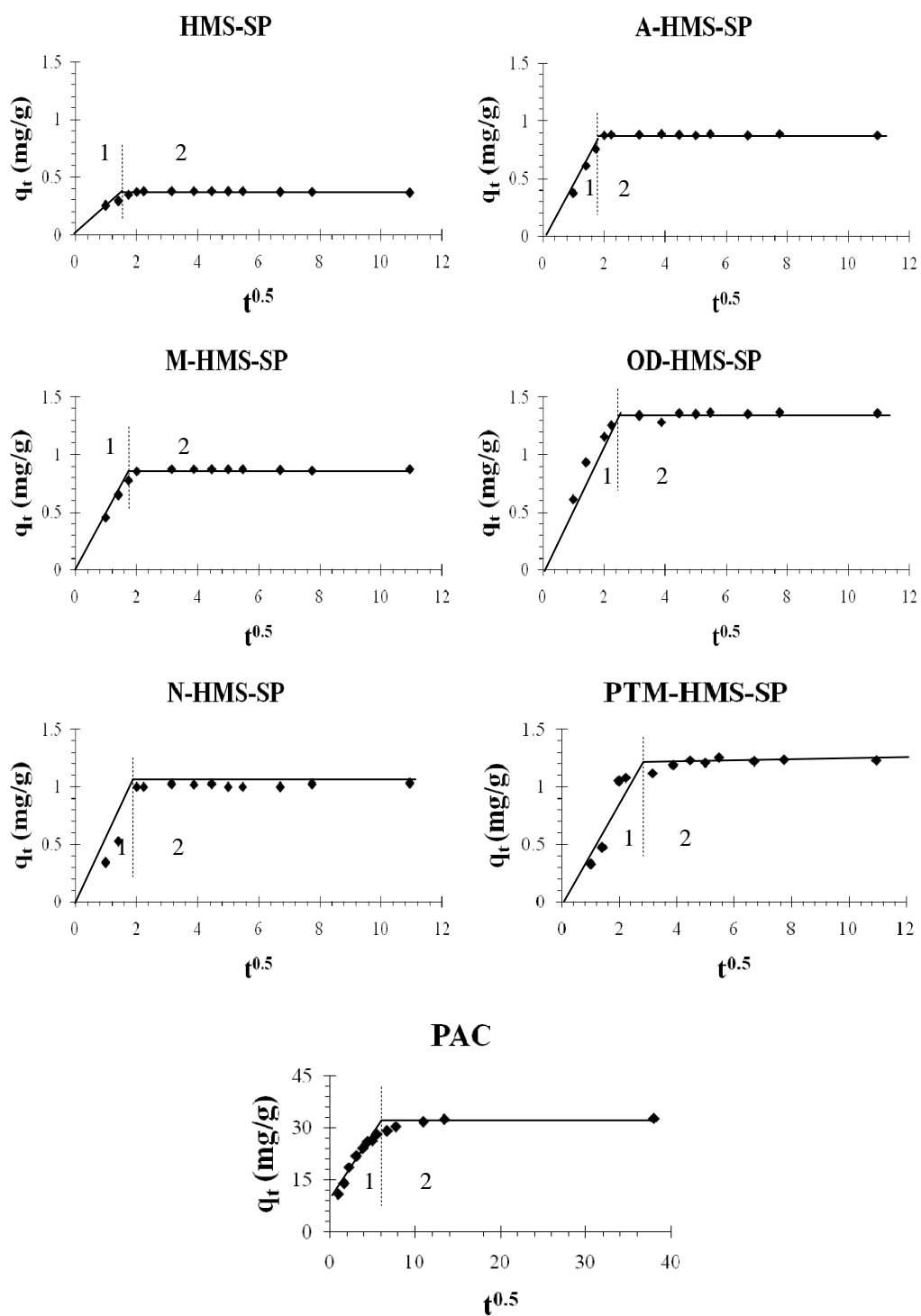


Figure 4.7 Intraparticle Diffusion Plotted of NAL Adsorption on Adsorbents.

**Table 4.7** Intraparticle Diffusion Parameters Plotted of NAL Adsorption on Adsorbents

Adsorbent	Stage 1			Stage 2
	$k_i(\text{mg/g min}^{0.5})$	Intercept	$R^2$	
HMS-SP	0.12	-	0.99	Equilibrium
A-HMS-SP	0.50	-	0.99	Equilibrium
M-HMS-SP	0.40	-	0.99	Equilibrium
OD-HMS-SP	0.50	-	0.97	Equilibrium
N-HMS-SP	0.52	-	0.99	Equilibrium
PTM-HMS-SP	0.77	-	0.94	Equilibrium
PAC	4.39	7.21	0.97	Equilibrium

### 4.3 Adsorption Isotherm

#### 4.3.1 Effect of Surface Functional Groups at pH = 6.8 – 7.2

NAL adsorption isotherms were investigated, at around  $7 \pm 0.2$ , 0.01 M ionic strength controlled by phosphate buffer, as shown in figure 4.8 and figure 4.9. PAC provided the highest adsorption capacity (up to 38 mg/g) due to very high surface area and varieties of surface functional groups. For the synthesized materials, OD-HMS-SP had highest adsorption capacity following with PTM-HMS-SP, M-HMS-SP, A-HMS-SP, N-HMS-SP and HMS-SP, respectively. Hydrophobic adsorbents (PTM-HMS-SP, OD-HMS-SP, M-HMS-SP and N-HMS-SP) had higher affinity to NAL than hydrophilic adsorbents (A-HMS-SP and HMS-SP). Moreover, attractive electrostatic interaction at pH 7 between 3-aminopropyltriethoxy- groups of A-HMS-SP and NAL molecule could enhance the adsorption capacity. The results agreed with kinetic study that van der waals force due to hydrophobicity of OD-HMS-SP performed highest adsorption capacity (1.37 mg/g) following by PTM-HMS-SP (1.28 mg/g) although under repulsive electrostatic interaction at pH 7. M-HMS-SP, which had lower hydrophobicity compared with OD-HMS and PTM-HMS-SP due to thio group (S-H),

performed lower adsorption capacity (0.89 mg/g). Thus, van der waals force due to hydrophobicity and attractive electrostatic interaction might be the major role to controlled NAL adsorption capacity.

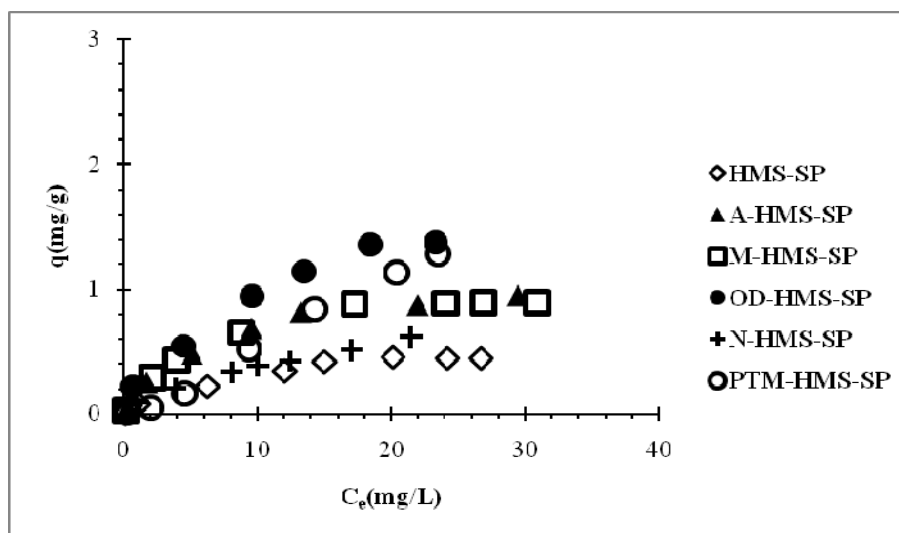


**Figure 4.8** NAL adsorption capacities of synthesized adsorbents (at 25°C, IS = 0.01 M and pH = 7±0.2).

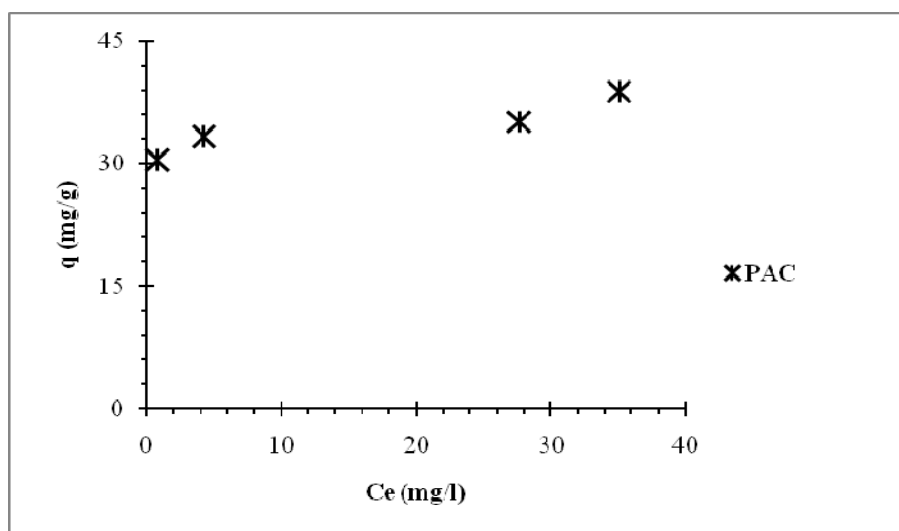


**Figure 4.9** NAL adsorption capacities of PAC (at 25°C, IS = 0.01 M and pH = 7±0.2).

Figure 4.10 and Figure 4.11 illustrates the adsorption capacities of all adsorbents per square meter of specific surface area in order to neglect the effect of surface area of adsorbents. PAC still performed very high adsorption capacity that might result from varieties of surface functional groups. For the synthesized adsorbents, the adsorption capacities of A-HMS-SP turned to be the highest. This case may be caused by strong attractive electrostatic interaction that was discussed in the effects of pH study in the next part.

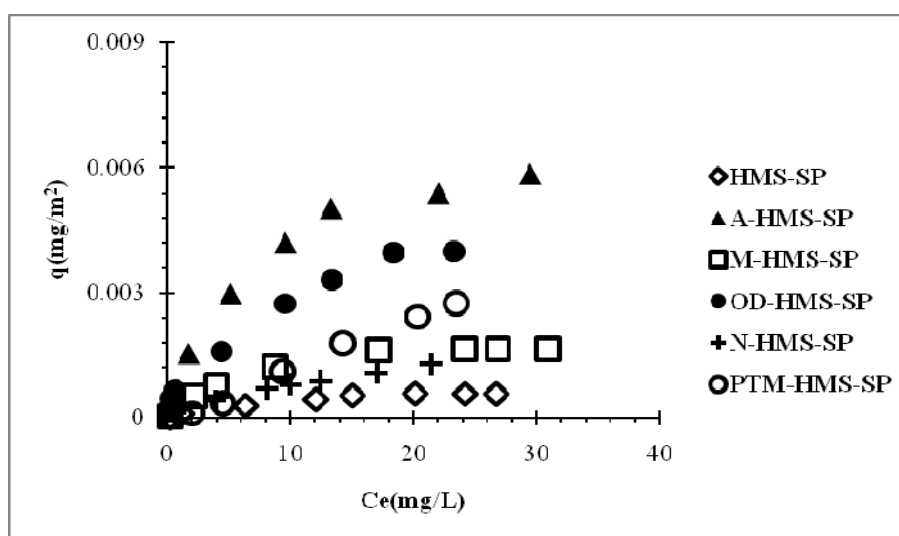


**Figure 4.10** NAL Adsorption Capacities per Specific Surface Area of Synthesized Adsorbents (at 25°C, IS = 0.01 M and pH = 7±0.2).

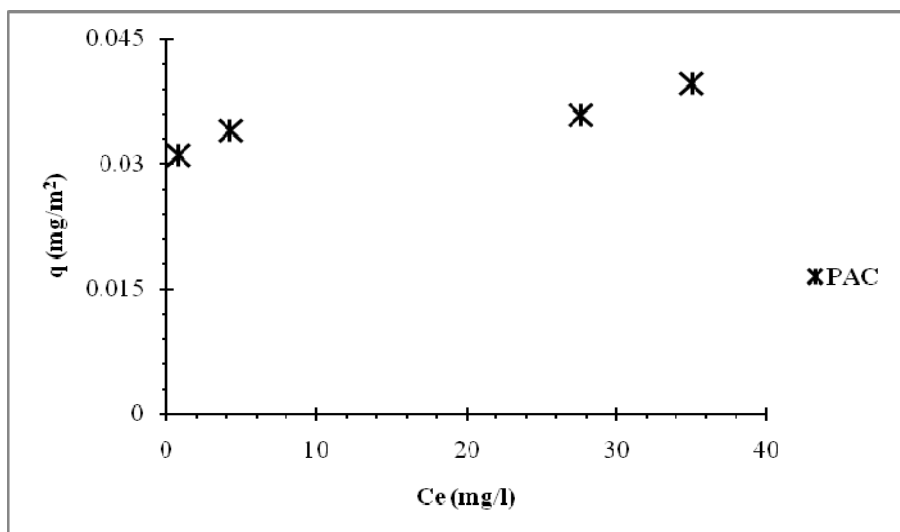


**Figure 4.11** NAL Adsorption Capacities per Specific Surface Area of PAC (at 25°C, IS = 0.01 M and pH = 7±0.2).

#### 4.3.2 Effects of pH

For NAL, the pKa establishes the fraction of protonated and deprotonated under given pH. The pH at which equal concentrations of protonated and deprotonated compound are present is called pKa of a monoprotic acid. “At one pH unit lower than the pKa, the functional groups exist predominately (91%) in the neutralized form, while at one pH unit higher than the pKa the functional groups exist predominately in the ionized form, as expressed by the Henderson–Hasselbalch equation” (4.13) (Watson 1999; Lorphensri, et al. 2006)

$$\frac{[A^-]}{[HA]} = 10^{(pH-pKa)} \quad (4.13)$$

Table 4.8 illustrated different electrostatic interactions between adsorbents and adsorbate depending on pH conditions. These interactions resulted from surface charges due to  $pH_{zpc}$  of synthesized adsorbents and pKa of NAL (6.33).

**Table 4.8** Electrostatic Interaction between Adsorbents and NAL at Varying pH

Adsorbents	pH <sub>zpc</sub>	Electrostatic Interaction		
		pH 7	pH 5	pH 9
A-HMS-SP	8.8	Attractive	Neutral	Repulsive
HMS-SP	5	Repulsive	Neutral	Repulsive
M-HMS-SP	6.2	Repulsive	Neutral	Repulsive
OD-HMS-SP	4	Repulsive	Neutral	Repulsive
N-HMS-SP	4.5	Repulsive	Neutral	Repulsive
PTM-HMS-SP	4.6	Repulsive	Neutral	Repulsive
PAC	6.8	Repulsive	Neutral	Repulsive

To study the importance of electrostatic interaction between target compounds and adsorbents, the effect of pH on the adsorption capacity of HMS-SP, A-HMS-SP, M-HMS-SP, OD-HMS-SP, N-HMS-SP, PTM-HMS-SP and PAC were determined by varying pH of solution to 5, 7, and 9 with 0.01 M, controlled by phosphate buffer.

According to Figure 4.12, A-HMS-SP (pH<sub>zpc</sub> 8.8) which had high adsorption capacity at pH7 due to attractive electrostatic interaction, cannot adsorb NAL under neither of neutral (pH 5) nor repulsive electrostatic state (pH 9). Thus, these results indicated that NAL adsorption capacity on A-HMS-SP strongly affected by attractive electrostatic interaction. On the other hand, effect of pH to adsorption capacity on PAC cannot be observed. Adsorption capacities of HMS-SP, M-HMS-SP, OD-HMS-SP, N-HMS-SP and PTM-HMS-SP could be increased by decreasing pH that might be caused by electrostatic interaction. Adsorption capacities at pH 7 and 9 could be interrupted by repulsive electrostatic interaction between negative charge of surface and NAL. At pH 5, NAL molecule become neutral due to pKa of NAL (6.33), that can reduce the effect repulsive electrostatic interaction and enhance adsorption capacity at pH 5. At this pH, PTM-HMS-SP performed higher adsorption capacity than OD-HMS-SP that may imply stronger van der waals force due to non-polar on chemical structure between NAL and benzene ring of phenyltrimethoxy functional group without interrupted by repulsive electrostatic interaction. However, adsorption capacities at pH 9 still could be detected even under stronger repulsive electrostatic interaction. That might indicate the stronger effect of van der waals force due to hydrophobicity comparing with electrostatic interaction.



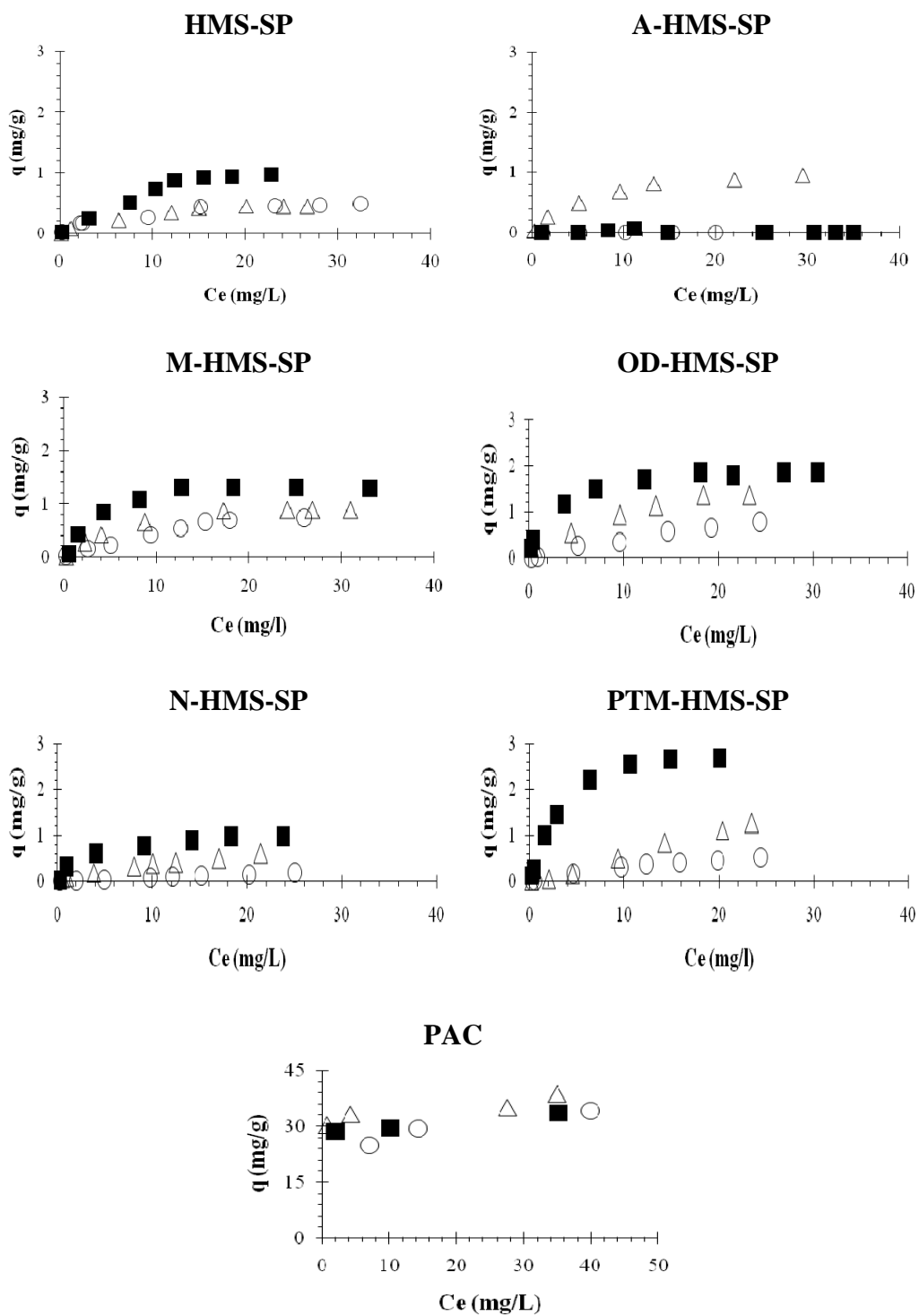


**Figure 4.12** Effects of pH on NAL Adsorption Capacity on Adsorbents (at 25°C, IS = 0.01 M, pH = 5±0.2 (■), 7±0.2 (△), 9±0.2 (○)).

In case of HMS-SP, hydrogen bonding (OH group) was suspected to react with NAL. Though HMS-SP performed lower adsorption capacity compared to hydrophobic surfaces, its adsorption capacity still exist even under repulsive electrostatic interaction. To prove the availability of hydrogen bonding (OH group), pristine HMS and HMS which adsorbed NAL on surface from hexane solution (NAL-HMS) were analyzed by FT-IR, and investigated the shift of silanol groups (free O-H stretching band) due to hydrogen bonding. The adsorption was performed in hexane solution to eliminate effect of water which can compete with NAL forming hydrogen bond to HMS surface. The results showed that free O-H stretching band of NAL-HMS was shifted compare to the pristine HMS ( $3746\text{ cm}^{-1}$  to  $3749\text{ cm}^{-1}$ ). Adsorption of NAL on HMS surface was also confirmed by  $0.4\text{ mg/g}$  NAL adsorption capacity. Moreover the new band at  $3600\text{-}3650\text{ cm}^{-1}$  was observed on NAL-HMS. This stretch was found as adsorption by hydrogen bonding. The FT-IR spectra implied that NAL was adsorped on HMS surface by hydrogen bonding but the adsorption capacity was still much lower than hydrophobic adsorbents. Effect of water which can compete with NAL forming hydrogen bond to HMS surface may play important roles on NAL adsorption capacity especially in low concentration (ppb level). (<http://www.umsl.edu/~orglabdocuments/IRIR2.html>).

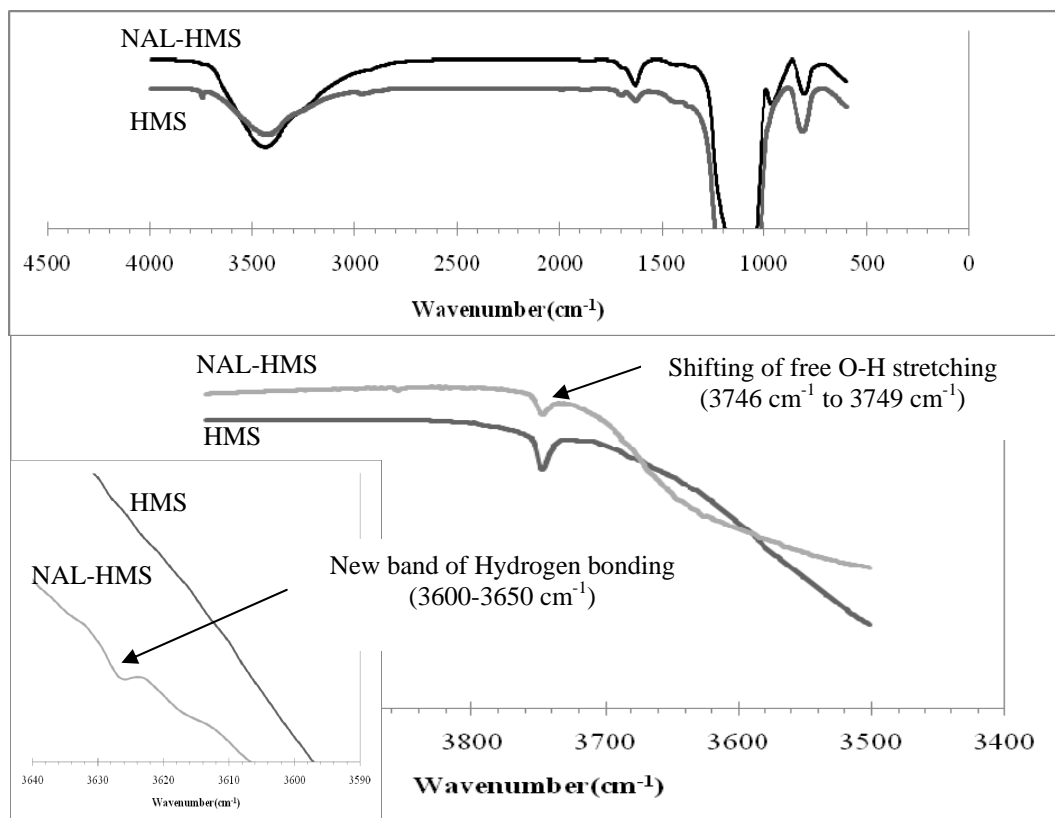


**Figure 4.13** FT-IR Spectra of HMS and NAL- HMS which Adsorbed NAL in Hexane Solution.

Table 4.9 indicated isotherm parameters of all adsorbents fitted to Langmuir, Freundlich and linear isotherm models. Most of adsorbent data can be fitted well with Langmuir, except M-HMS-SP at pH 9. At pH 7 and 9, OD-HMS-SP, N-HMS-SP, PTM-HMS-SP and PAC were more suitable with Freundlich isotherm model. The result of PAC adsorbent at pH 5 is suitable for linear isotherm models.

- *Comparison with other research*

Although comparison between other researches was necessary, unfortunately, there still lacks of NAL adsorption research. Compare to adsorbents (alumina, silica and Porapak P) in Lorphensri, et al. 2006, both electrostatic interaction and van der Waals force due to hydrophobicity were anticipated similar to this research. F-HMS-SP provided higher surface area that might yield more advantage on the real application.

In terms of adsorption capacity per square meter ( $\text{mg}/\text{m}^2$ ) which the effect of surface area of adsorbents can be neglected, attractive electrostatic interaction provided highest adsorption capacity as same as in this research. Alumina performed higher adsorption capacity ( $\text{mg}/\text{m}^2$ ) than A-HMS-SP that may caused by higher surface charge density. Silica and Porapak P. provided lower adsorption capacity than F-HMS-SP. Against to this research, Lorphensri, et al. 2006 concluded that electrostatic interaction had more effect on NAL adsorption capacity than van der waals force due to hydrophobicity. On the other hand, in this research, stronger effect of van der waals force due to hydrophobicity than electrostatic interaction was confirmed by high existing of NAL adsorption capacity on hydrophobic surface even in repulsive electrostatic interaction.

- *Effect of water in NAL adsorption under ppb level*

At high concentration of NAL (0-30 mg/L), synthesized adsorbents performed much lower adsorption capacity than PAC. In contrast, at low concentration (ppb level) which water drastically affected on the adsorption interaction, the results may be different. Low hydrophobicity of PAC compare to M-HMS-SP, OD-HMS-SP and PTM-HMS-SP as shown on the Table 4.5 may result in lower accessibility of NAL to PAC surface due to surrounding water molecules. Van der waals force due to hydrophobicity caused by PAC might yield lower adsorption capacity compare to adsorbent which had higher hydrophobicity at this ppb concentration. NAL adsorption under both high and low concentration should be investigated due to widely ranges of NAL found in environment and wastewater. Effect of water molecules in low concentration must be considered.

**Table 4.9** Parameters of Linear, Langmuir and Freundlich Isotherm Model for NAL Adsorption on Applied Adsorbents

Adsorbent	Linear		Langmuir			Freundlich		
pH	$a$ (slope)	$R^2$	$q_e$	$k_l$	$R^2$	$k_f$	$n$	$R^2$
HMS-SP								
5	0.044	0.856	1.703	0.069	0.969	0.171	1.694	0.940
7	0.017	0.854	0.649	0.095	0.983	0.090	1.943	0.958
9	0.013	0.828	0.574	0.141	0.956	0.110	2.296	0.947
A-HMS-SP								
5	N/A	N/A	N/A	N/A	N/A	N/A	N/A	N/A
7	0.029	0.759	1.164	0.149	0.995	0.232	2.295	0.949
9	N/A	N/A	N/A	N/A	N/A	N/A	N/A	N/A
M-HMS-SP								
5	0.031	0.530	1.530	0.285	0.971	0.462	2.966	0.826
7	0.025	0.775	1.112	0.161	0.991	0.235	2.413	0.941
9	0.030	0.883	1.369	0.052	0.975	0.105	1.586	0.951
OD-HMS-SP								
5	0.048	0.651	2.035	0.438	0.993	0.729	3.2890	0.926
7	0.053	0.908	2.119	0.087	0.978	0.282	1.914	0.977
9	0.032	0.974	2.108	0.025	0.993	0.069	1.303	0.990
N-HMS-SP								
5	0.026	0.977	1.090	0.345	0.985	0.328	2.663	0.939
7	0.036	0.743	1.090	0.056	0.981	0.090	1.605	0.997
9	0.008	0.989	540	0.000	0.989	0.007	0.954	0.990
PTM-HMS-SP								
5	0.127	0.731	3.286	0.299	0.955	0.871	2.394	0.926
7	0.058	0.993	7030	0.000	0.990	0.047	0.944	0.991
9	0.023	0.953	1.109	0.039	0.998	0.060	1.433	0.990
PAC								
5	0.157	0.992	32.280	3.559	0.124	26.900	17.489	0.688
7	0.192	0.791	36.436	6.130	0.554	30.758	18.561	0.791
9	0.260	0.826	29.497	0.000	0.500	17.938	5.642	0.965

## 4.4 Separation Process by Magnetic System Applied to Enhance Ultrafiltration

### 4.4.1 Magnetic System Reducing Specific Cake Resistance

The core-shell magnetic silica structure of synthesized materials provided advantages on adsorbent separation after NAL removal process. Magnetic system which consists of SP adsorbent with external magnetic field were applied in ultrafiltration (UF) in this study to separate adsorbents after adsorption process. This magnetic system is suggested to enhance UF by slow-down cake formation and reduce membrane fouling. The specific cake resistance ( $R_c$ ) of UF with magnetic system were determined. This value was expected to be less than of which conventional UF process to prove efficiency in reducing membrane fouling on UF.

From 4.3.2, PTM-HMS-SP under pH5 was selected for this experiment due to its highest adsorption capacity. The results exhibited on figure 4.14 were plotted follow the typical linear equation of cake building filtration (Ruth's law) can be derived (Ruth, et al. 1933) shown in equation (2.10).

$$t = \frac{\mu k R_c}{2 \Delta p A^2} V_l + \frac{\mu R_m}{\Delta p A} = a V_l + b \quad (2.10)$$

Where  $V_l$  is the filtrate volume ( $m^3$ ),  $t$  is the time (s),  $A$  is the filter area ( $m^2$ ),  $\mu$  is the dynamic viscosity of the liquid phase (Pa·s),  $\Delta p$  is the transmembrane pressure drop (Pa),  $R_m$  is the membrane resistance ( $1/m$ ),  $R_c$  is the cake resistance ( $1/m^2$ ) and  $k$  is the concentration coefficient (dimensionless). By experimentally determining slope  $a$  and intercept  $b$  the filter media resistance and the specific cake resistance can be calculated as shown in Table 4.10, 4.11.

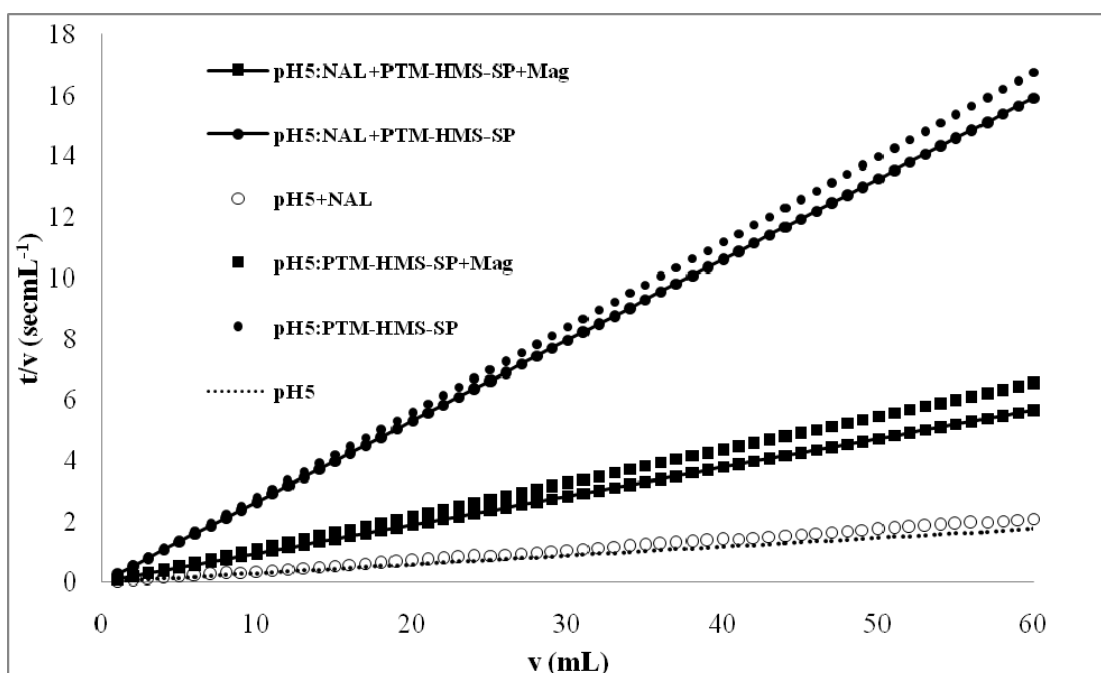


**Figure 4.14** Relations between Filtrate Volume and Time per Filtrate Volume, at 25°C, IS = 0.01 M, pH = 5±0.2.

**Table 4.10** Parameters for the Cake Building Equation Calculation

Parameter		Value
$A$	the filter area (m <sup>2</sup> )	0.0128
$\mu$	the dynamic viscosity of the water at 25°C (Pa s)	$8.9 \times 10^{-4}$
$\Delta p$	the transmembrane pressure drop (Pa)	$10^5$
$k$	the concentration coefficient (dimensionless)	0.001

**Table 4.11** The Filter Media Resistance and the Specific Cake Resistance at  $\text{pH} = 5 \pm 0.2$

Experiment	$R_c$ ( $1/\text{m}^2$ )	$R_m$ ( $1/\text{m}$ )
pH5	1.075	13.057
pH5:NAL	1.285	18.133
pH5:PTM-HMS-SP	10.294	5.079
pH5:PTM-HMS-SP+mag	4.021	15.238
pH5:NAL+PTM-HMS-SP	9.771	2.532
pH5:NAL+PTM-HMS-SP+Mag	3.479	10.790

$R_m$  values were not similar to each other which might result from recycling usage of UF membrane. The lines of pH5 and NAL under pH5 (without PTM-HMS-SP) almost performed no slope and very low  $R_c$  which confirmed no cake formation in the system. After applied PTM-HMS-SP to the system under pH5 (without NAL), magnetic field greatly reduced  $R_c$  from 10.29 to 4.02  $\text{m}^{-2}$  which imply the slow-down of the cake formation. Figure 4.15 shows that the filtrate volume of PTM-HMS-SP under pH5 increased after applied magnetic system. Moreover, the presence of NAL in the system did affect to  $R_c$  significantly. This might be confirmed the reducing membrane fouling.

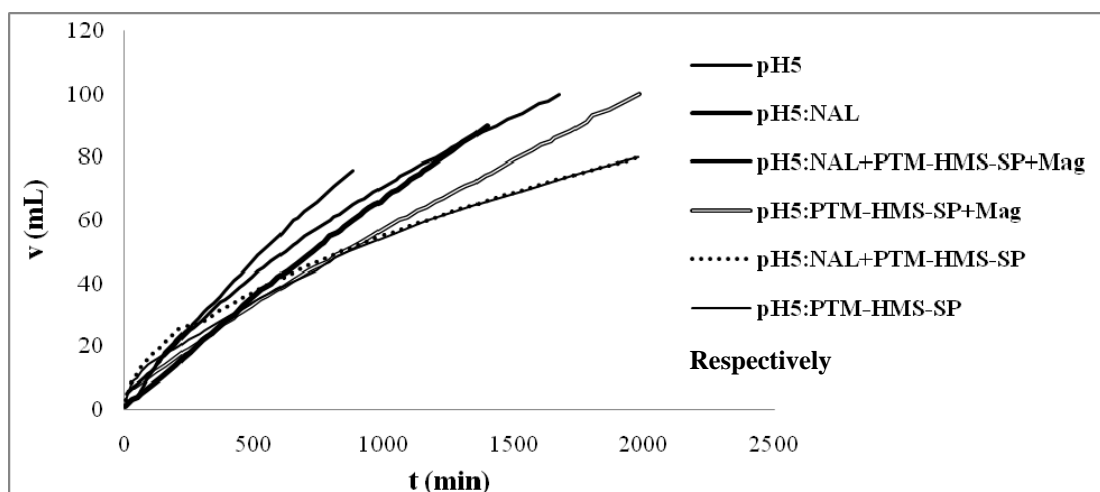


**Figure 4.15** Relations between Filtrate Volume Versus Time, at at  $25^\circ\text{C}$ ,  $\text{IS} = 0.01 \text{ M}$ ,  $\text{pH} = 5 \pm 0.2$ .



From these results, a special configuration of the magnet system leads to a slow down of the cake built-up can be described by an external magnetic force and interparticulate magnetic force as shown in Figure 2.6.

- *Effect of an External Magnetic Force*

Under inhomogeneous external magnetic field, the movement of the solid phase can be affected by the magnetic force. Thus its differential speed movement compared to the liquid phase can occur. Moreover, the uncoupling of movement of counterclockwise orientation of differential pressure and magnetic force can cause a slower cake formation. Therefore, the cake built-up at the beginning of a filtration process can be prevented under sufficient field strength. (Eichholz, et al. 2008)

- *Interparticulate Magnetic Force*

External magnetic field can affect to the filter cake structure that the particles formed North and South Poles when exposed to a magnetic field. The particles acted themselves as microscopic magnets result in interparticle forces upon approaching particles. Then the chainlike agglomerates formation in direction of the external magnetic field can be observed (Charles 1988). “The permeability of a cake with this channeled structure is obviously higher than a cake consisting of smaller pores, broadly distributed in size. These effects together result in a strong improvement of filtration kinetics and thus to a reduction of the filtration resistance, which can be seen in the slope of the cake building equation.” (Eichholz, et al. 2008)

#### **4.4.2 Effects of NAL on Magnetic System Applied on Ultrafiltration**

NAL were added to the system to determine effect of NAL adsorbed by PTM-HMS-SP on cake formation. The filtrate flux was detected, and remained NAL concentration and adsorption capacities are shown in Table 4.12. The results confirmed that UF membrane could not reduce NAL concentration. And reducing of NAL concentration should be caused by adsorption on PTM-HMS-SP surface. The

2.85 mg/g adsorption capacity of NAL was determined and consists of the results obtained from 4.3.2. From the data obtain from Table 4.11, the presence of NAL in the system did affect to  $R_c$  significantly.

**Table 4.12** NAL Concentration of Initial and Filtrate Flux at pH =  $5 \pm 0.2$

Experiment	NAL Concentration (mg/L)		NAL Adsorption Capacity (mg/g)
	Initial	Filtrate Volume	
pH5:NAL	20.52	20.48	-
pH5:NAL+PTM-HMS-SP	20.8	19.75	2.85

From Figure 4.14 and Table 4.11, adsorbed NAL on PTM-HMS-SP surface resulted slightly decreasing of  $R_c$  (10.29 to  $9.77 \text{ m}^{-2}$ ) which may caused by reducing interruption from attractive electrostatic interaction between materials and membrane surface. at pH5, surface charges of PTM-HMS-SP become slightly positive whereas regenerated cellulose membrane surface is negative (Kim, et al. 1996) Attractive electrostatic interaction between virgin PTM-HMS-SP and membrane surface can activate fouling. Once NAL which become neutral at pH5 were adsorbed on adsorbent surface, slightly positive charges of PTM-HMS-SP surface were decreased or covered. The reduction of attractive electrostatic interaction between materials and membrane surface due to adsorbed NAL may lead to decreasing of  $R_c$  value. Effect of membrane surface charge, adsorbent and existing of NAL were investigated further in 4.4.3. However, according to Figure 4.14 and Table 4.11, application of magnetic field can significantly reduce  $R_c$  value of PTM-HMS-SP which adsorbed NAL on the surface as well ( $9.77$  to  $3.48 \text{ m}^{-2}$ ). The results indicated that combination of magnetic system and existing of NAL on PTM-HMS-SP surface under pH5 can enhance UF by slow down cake formation.

#### 4.4.3 Effects of Electrostatic Interaction Changing by pH between Adsorbate, Adsorbents, and Membrane

From 4.4.2, electrostatic interaction was suggested to involve in cake formation on UF membrane surface. This experiment was established to study effect of membrane surface charge. As shown in Figure 4.16 reported that “The net charges of both regenerated cellulose membranes were negative in the measured pH range and became gradually more negative with increasing pH.” (Kim, et al. 1996)

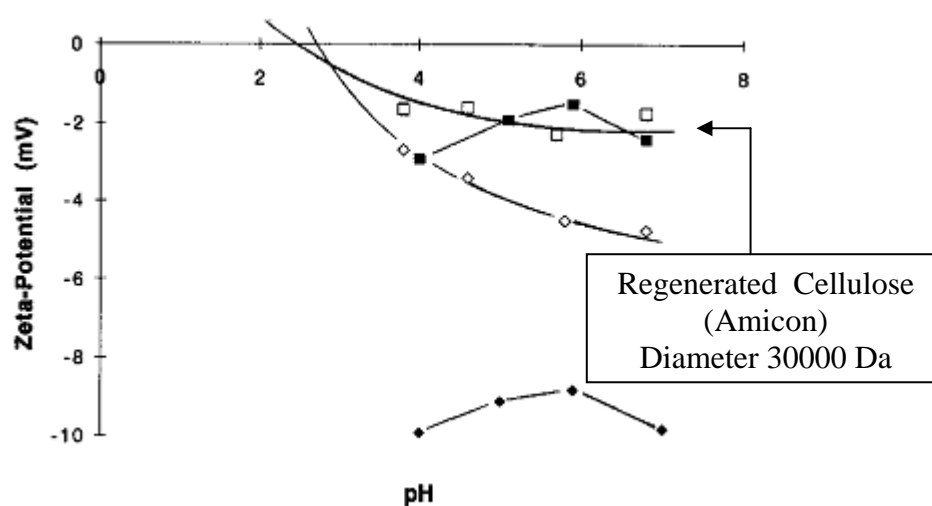


**Figure 4.16** Surface Charges of Regenerated Cellulose UF Membrane (Kim, et al. 1996).

Electrostatic interaction of applied membrane, adsorbents and NAL at pH 5 and 7 were summarized in Table 4.13. Table 4.14 confirmed that NAL cannot interact with UF membrane surface at both of pH 5 and 7. Thus only PTM-HMS-SP can interact with NAL in the system.

**Table 4.13** Electrostatic Interaction of each Material at pH = 5 $\pm$ 0.2 and 7 $\pm$ 0.2

pH	Electrostatic Charge		
	NAL	Regenerated Cellulose Membrane	PTM-HMS-SP
5	Neutral	Negative	Slightly Positive
7	Negative	Negative	Negative

**Table 4.14** NAL Concentration of Initial and Filtrate Volume  
at pH =  $5 \pm 0.2$  and  $7 \pm 0.2$

Experiment	NAL Concentration (mg/l)		NAL Adsorption Capacity (mg/g)
	Initial	Filtrate Volume	
pH5:NAL	20.52	20.48	-
pH5:NAL+PTM-HMS-SP	20.8	19.75	2.85
pH7:NAL	20.45	20.44	-
pH7:NAL+PTM-HMS-SP	20.1	19.08	1.02

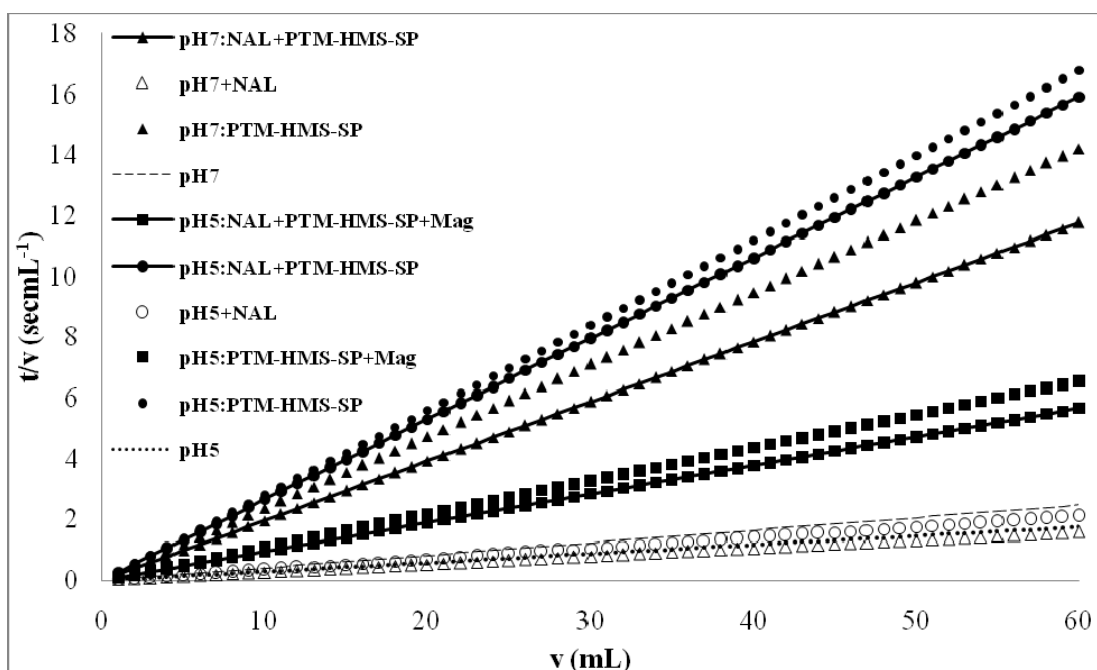


**Figure 4.17** Relations between filtrate volume and time per filtrate volume,  
at at  $25^{\circ}\text{C}$ , IS = 0.01 M, pH =  $5 \pm 0.2$ ,  $7 \pm 0.2$ .

From Figure 4.17 and Table 4.15, obtained slopes and very low  $R_c$  in case of no PTM-HMS-SP was not significantly different between pH 5 and 7, which indicated no cake formation in the system. Presence of PTM-HMS-SP at pH 7 provided less  $R_c$  than at pH 5 as shown in table 4.15, which might be caused by the role of electrostatic interaction. Negative surface charge of PTM-HMS-SP under pH 7 performed

repulsive electrostatic interaction with negative charge of UF membrane that might reduce the cake formation.

**Table 4.15** The Filter Media Resistance and the Specific Cake Resistance at pH = 5±0.2, 7±0.2

Experiment	$R_c$ (1/m <sup>2</sup> )	$R_m$ (1/m)
pH5	1.075	13.057
pH5:NAL	1.285	18.133
pH5:PTM-HMS-SP	10.294	5.079
pH5:PTM-HMS-SP+mag	4.021	15.238
pH5:NAL+PTM-HMS-SP	9.771	2.532
pH5:NAL+PTM-HMS-SP+Mag	3.479	10.789
pH7	1.513	14.335
pH7:NAL	0.965	17.431
pH7:PTM-HMS-SP	8.718	4.325
pH7:NAL+PTM-HMS-SP	7.216	7.662

The filtrate volume was also illustrated in Figure 4.18 to ensure the slow-down of membrane fouling caused by repulsive electrostatic interaction. Highest repulsive electrostatic interaction of PTM-HMS-SP with NAL adsorbed under pH 7 performed the highest filtrate flux following by PTM-HMS-SP without NAL under pH 7, PTM-HMS-SP with NAL under pH 5 and without NAL under pH 5 respectively.

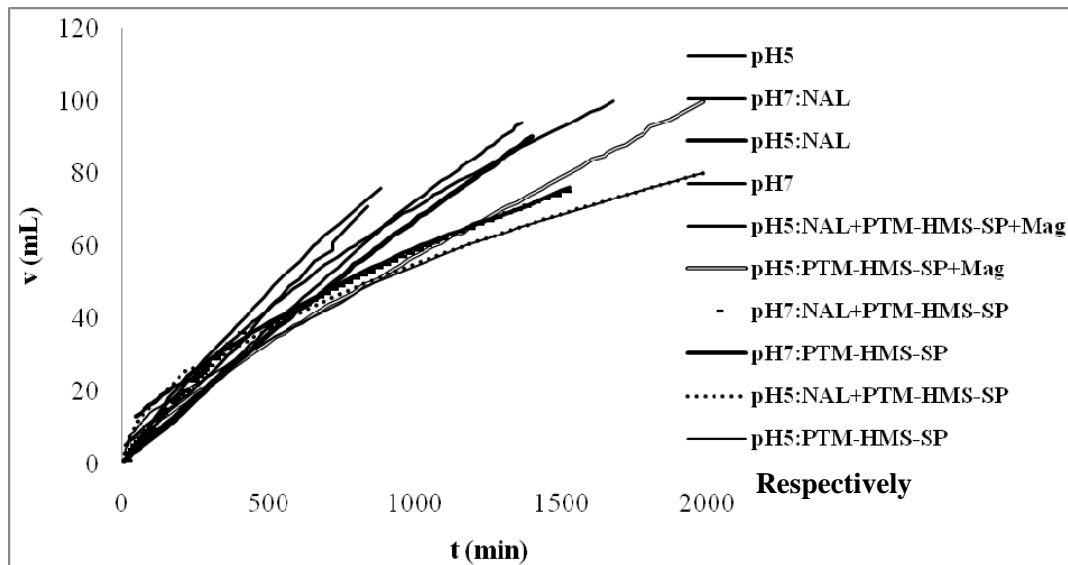


**Figure 4.18** Relations between Filtrate Volume Versus Time, at 25°C, IS = 0.01 M, pH = 5±0.2, 7±0.2.

Moreover, NAL adsorption on PTM-HMS-SP under pH7 also can greatly reduce  $R_c$  compare to PTM-HMS-SP without NAL under pH7 (8.72 to 7.22 m<sup>2</sup>) due to stronger repulsive electrostatic interaction caused by negative charges of NAL. Although existing of NAL on PTM-HMS-SP under pH5 can provide lower  $R_c$  than of which without NAL (10.92 to 9.77 m<sup>2</sup>), PTM-HMS-SP under pH 7 without NAL still performed much lower value of  $R_c$  (8.72 m<sup>2</sup>). Thus, greatly effect of electrostatic interaction to cake building on UF membrane surface can be implied. However, magnetic system applied on UF process for PTM-HMS-SP under pH 5 both with and without NAL still performed pretty much lower of  $R_c$  (3.48 and 4.02 m<sup>2</sup> respectively) compare to the case that performed under pH 7 without magnetic system. Thus, this also can indicated stronger effect of magnetic system than electrostatic interaction on  $R_c$  value.

Therefore, combination of magnetic system and repulsive electrostatic interaction between particles surface and UF membrane surface was suggested to enhance UF process by slow-down the cake formation.

## CHAPTER V

### CONCLUSION AND RECOMMENDATIONS

#### 5.1 Conclusion

The main objective of this research is to evaluate removal efficiency of nalidixic acid (NAL) residues in synthetic wastewater by adsorption on functionalized superparamagnetic mesoporous silicates (F-HMS-SP) and to study effect of magnetic field on cake formation of ultrafiltration (UF). In this study, F-HMS-SP was synthesized and characterized their physico-chemical properties. Adsorption capacities of Nalidixic acid (NAL) on functionalized superparamagnetic mesoporous silicates at high concentration (0-30 mg/L) were investigated including the impact of surface functional groups and pH, and then compared with powdered activated carbon (PAC). After adsorption process, magnetic system which consists of external magnetic field, was applied to enhance ultrafiltration (UF) in order to separate the used adsorbents. The slow-down cake formation of applied superparamagnetic (SP) adsorbents under external magnetic field was investigated.

From the investigation, crystalline structure of F-HMS-SP was collapsed during functional group modification via post-grafting method, comparing with the pristine HMS-SP. The synthesized adsorbent had their average pore size in mesoporous structure category (2-50 nm).

From the kinetic study at  $\text{pH} = 7 \pm 0.2$ , the equilibrium stages of NAL adsorption on F-HMS-SP were achieved at 15 min except for PTM-HMS-SP (20 min) and PAC (3 hr). The kinetic results were implied that the NAL adsorption on F-HMS-SP is controlled by the intraparticle diffusion process; for NAL adsorption on PAC, some degree of boundary layer control was found. All kinetic cases in this study were compatible with the pseudo-second order model with high correlation co-efficients ( $>0.9$ ).

According to adsorption isotherm study, the highest adsorption capacities of NAL at  $\text{pH} = 7 \pm 0.2$  were performed by hydrophobicity of n-octyldimethyl- groups grafted HMS-SP (OD-HMS-SP) following by phenyltrimethoxy group grafted HMS-SP (PTM-HMS-SP). It was still lower than adsorption capacity obtained from PAC. However, at low concentration (ppb level) which water drastically affected on the adsorption interaction, M-HMS-SP, OD-HMS-SP and PTM-HMS-SP has more opportunities to yield higher adsorption capacity than PAC due to higher hydrophobicity on these F-HMS-SP surface. Although, NAL adsorption capacities on F-HMS-SP complied with electrostatic interaction role at various pH, but the results indicated the stronger effect of van der Waals force due to hydrophobicity. Thus, van der Waals force due to hydrophobicity and electrostatic interaction might be the major role and were suggested to enhance NAL adsorption capacities.

PTM-HMS-SP performed highest NAL adsorption capacity was selected to study separation efficiency by UF process. After applied magnetic system, greatly reduction of cake resistance ( $R_c$ ) can be observed which indicated reducing of membrane fouling. A special configuration of the magnet system caused a slow down of the cake built-up due to by an external magnetic force and interparticulate magnetic force. Moreover, electrostatic interaction between adsorbent and membrane surface was found to affect on  $R_c$  value.

This research can prove that surface modification on F-HMS-SP such as hydrophobicity and attractive electrostatic interaction has high possibility to enhance adsorption capacity of nalidixic acid. Moreover, superparamagnetic properties of synthesized adsorbent under external magnetic field together with repulsive electrostatic interaction between adsorbent and membrane surfaces can enhance UF separation process by reducing membrane fouling via slow-down cake formation.



For further research, HMS-SP and A-HMS-SP was suggested to apply to other pollutants which have hydrophilic surface. These F-HMS-SPs may provide advantages on high selectivity, high surface area and easier separation using their superparamagnetic property.

## **5.2 Recommendations**

- 5.2.1 Selective adsorption between NAL and other pharmaceuticals on adsorption capacity of F-HMS-SP should be further investigated.
- 5.2.2 NAL adsorption on F-HMS-SP should be further investigated at low concentration (ppb level) to study adsorption mechanisms which greatly affected by water molecules and might provide different results compare to high concentration (ppm level).
- 5.2.3 Hydrophilic surfaces such as HMS-SP and A-HMS-SP have high opportunities to provide high adsorption capacity of hydrophilic pollutants and should be further studied.

## REFERENCES

- Al-Ahmad, A., Daschner, F. D., Kümmerer, K. 1999. Biodegradability of cefotiam, ciprofloxacin, meropenem, penicillin G, and sulfamethoxazole and inhibition of waste water bacteria. Archives of Environmental Contamination and Toxicology 37: 158–163
- Beck, J. S., and Vartuli, J. C. 1996. Recent advances in the synthesis, characterization and applications of mesoporous molecular sieves. Current Science 1: 76-87.
- Chakrapani, C., and Suresh babu, C. 2010. Adsorption kinetics for the removal of fluoride from aqueous Solution by activated carbon adsorbents derived from the peels of selected citrus fruits. E-Journal of Chemistry 7(S1): S419-S427.
- Charles, S. 1988. Aggregation in magnetic fluids and magnetic fluid composites. Chemical Engineering Communications 67: 145-180.
- Chen, V., and Fane, A. G. 1997. Particle deposition during membrane filtration of collids: transition between concentration polarization and cake formation. Membrane Science 125: 109-122.
- Cheung, W. H., and Szeto, Y. S. 2007. Intraparticle diffusion processes during acid dye adsorption onto chitosan. Bioresource Technology 98(15): 2897-2904.
- Chong, A. S. M., and Zhao, X. S. 2004. Functionalization of large-pore mesoporous silicas with organosilanes by direct synthesis. Microporous and Mesoporous Materials 72(1-3): 33-42.
- Ciesla, U. and Schüth, F. 1999. Ordered mesoporous materials. Microporous and Mesoporous Materials 27(2-3): 131-149.
- Deng, Y., and Qi, D. 2008. Superparamagnetic High-Magnetization Microspheres with an Fe<sub>3</sub>O<sub>4</sub>@SiO<sub>2</sub> Core and Perpendicularly Aligned Mesoporous SiO<sub>2</sub> Shell for Removal of Microcystins. American Chemical Society 130.

- Eichholz, C., Stolarski, M., Goertz, V., and Nirschl, H. 2008. Magnetic field enhanced cake filtration of superparamagnetic PVAc-particles. Chemical Engineering Science 63(12): 3193-3200.
- Heberer, T. 2002. Tracking persistent pharmaceutical residues from municipal sewage to drinking water. Journal of Hydrology 266(3-4): 175-189.
- Hu, J., Chen, G., and Lo, I.M.C. 2006. Selective Removal of Heavy Metals from Industrial Wastewater Using Maghemite Nanoparticle: Performance and Mechanisms. Journal of Environmental Engineering. 132(7) : 709-715.
- Hydrotech, Inc. 2005. Membrane Technology [Online]. Available from : <http://www.hydrotech.cn/English/index.asp>, [2010, January 9]
- Jürgensen, S. E., and Halling-Sørensen, B. 2000. Drugs in the environment. Chemosphere 40: 691-699.
- Kim, A. S., and Hoek, E. M. V. 2002. Cake Structure in Dead-End Membrane Filtration: Monte Carlo Simulations. Environmental Engineering Science 19, Number 6.
- Kim, Ilho, Yamashita, Naoyuki, and Tanaka, Hiroaki. 2009. Performance of UV and UV/H<sub>2</sub>O<sub>2</sub> processes for the removal of pharmaceuticals detected in secondary effluent of a sewage treatment plant in Japan. Journal of Hazardous Materials 166(2-3): 1134-1140.
- Kim, K. J., Fane, A. G., Nystrom, M., Pihlajamaki, A., Bowen, W. R., and Mukhtar, H. 1996. Evaluation of electroosmosis and streaming potential for measurement of electric charges of polymeric membranes. Journal of Membrane Science 116(2): 149-159.
- Kümmerer, K. 2003. Significance of antibiotics in the environment. Antimicrobial Chemotherapy 52: 5-7.
- Kümmerer, K. 2009. The presence of pharmaceuticals in the environment due to human use - present knowledge and future challenges. Journal of Environmental Management 90(8): 2354-2366.

- Kümmerer, K., Al-Ahmad, A., and Mersch-Sundermann, V. 2000. Biodegradability of some antibiotics, elimination of the genotoxicity and affection of wastewater bacteria in a simple test. Chemosphere 40: 701–710.
- Lin, Angela, Yu-Chen, Yu, Tsung-Hsien Lateef, and Shaik Khaja. 2009. Removal of pharmaceuticals in secondary wastewater treatment processes in Taiwan. Journal of Hazardous Materials 167(1-3): 1163-1169.
- Lee, B.H., Kim, Y.H., Lee, H.J., and Yi, J.H. 2001. Synthesis of functionalized porous silicas via templating method as heavy metal ion adsorbents: the introduction of surface hydrophilicity onto the surface of adsorbents. Microporous Mesoporous Mater 50 (1): 77-90.
- Linssen, T., Cassiers, K., Cool, P., and Vansant, E. F. 2003. Mesoporous templated silicates: an overview of their synthesis, catalytic activation and evaluation of the stability. Advances in Colloid and Interface Science 103(2): 121-147.
- Lorphensri, Oranuj, Intravijit, Jittipong, Sabatini, David A., Kibbeyb, Tohren C.G., Osathaphanc, Khemarath, and Saiwand, Chintana. 2006. Sorption of acetaminophen, 17[alpha]-ethynyl estradiol, nalidixic acid, and norfloxacin to silica, alumina, and a hydrophobic medium. Water Research 40(7): 1481-1491.
- Maaz, K., Karim, S., Mumtaz, A., Hasanain, S. K., Liu, J., and Duan, J. L. 2009. Synthesis and magnetic characterization of nickel ferrite nanoparticles prepared by co-precipitation route. Journal of Magnetism and Magnetic Materials 321(12): 1838-1842.
- Mahmoudi, Morteza, Sant, Shilpa, Wang, Ben, Laurent, Sophie, and Sen, Tapas. 2010. Superparamagnetic iron oxide nanoparticles (SPIONs): Development, surface modification and applications in chemotherapy. Advanced Drug Delivery Reviews In Press, Corrected Proof.
- Mamishi, S., Mashoori, N., Mahboobi, N., and Pour, Akbari B. 2009. Increasing resistance to nalidixic acid in Shigella subgroups in a comparative study between 2001–2003 and 2004–2006. Singapore Med J 50(8): 791-793.

- Mascolo, G., Balest, L., Cassano, D., Laera, G., Lopez, A., Pollice, A., and Salerno, C. 2010. Biodegradability of pharmaceutical industrial wastewater and formation of recalcitrant organic compounds during aerobic biological treatment. Bioresource Technology 101(8): 2585-2591.
- Nakada, Norihide, Tanishima, Toshikatsu, Shinohara, Hiroyuki, Kiri, Kentaro, and Takada, Hideshige. 2006. Pharmaceutical chemicals and endocrine disrupters in municipal wastewater in Tokyo and their removal during activated sludge treatment. Water Research 40(17): 3297-3303.
- Pérez-Quintanilla, D.del Hierro, I., Fajardo, M., and Sierra, I. 2006. Mesoporous silica functionalized with 2-mercaptopyridine: Synthesis, characterization and employment for Hg(II) adsorption. Microporous and Mesoporous Materials 89(1-3): 58-68.
- Punyapalakul, P., and Sitthisorn, T. 2010. Removal of Ciprofloxazin and Carbamazepine by Adsorption on Functionalized Mesoporous Silicates. World Academy of Science, Engineering and Technology 69: 546-550.
- Punyapalakul, P., and Takizawa, S. 2006. Selective adsorption of nonionic surfactant on hexagonal mesoporous silicates (HMSs) in the presence of ionic dyes. Water Research 40(17): 3177-3184.
- Qu, Jingmiao, Liu, Guang, Wang, Yiming, and Hong, Ruoyu. 2010. Preparation of Fe<sub>3</sub>O<sub>4</sub>-chitosan nanoparticles used for hyperthermia. Advanced Powder Technology In Press, Corrected Proof.
- Massart, R. 1981. Preparation of aqueous magnetic liquids in alkaline and acidic media. IEEE Transactions on Magnetics 17(2): 1247-1248.
- Ruth, B., Montillo, G., and Montonna, H. 1933. Studies in filtration, II. Fundamental axiom of constant-pressure filtration. Industrial Engineering Chemistry 25(2): 153-161.

- Sirtori, C., Zapata, A., Oller, I., Gernjak, W., Agüera, A., and Malato, S. 2009. Decontamination industrial pharmaceutical wastewater by combining solar photo-Fenton and biological treatment. Water Research 43(3): 661-668.
- Shepherd, Austin. 2001. Activated Carbon Adsorption for Treatment of VOC Emissions. The 13th Annual EnviroExpo, Boston Massachusetts (May 2001).
- Tanev, P. T., and T. J. Pinnavaia. 1996. Mesoporous Silica Molecular Sieves Prepared by Ionic and Neutral Surfactant Templating: A Comparison of Physical Properties. Chemistry of Materials 8(8): 2068-2079.
- Theivarasu, C., and S. Mysamy. 2010. Equilibrium and kinetic adsorption studies of rhodamine-B from aqueous solutions using cocoa (theobroma cacao) shell as a new adsorbent International journal of engineering science and technology 2(11): 6284-6292.
- Tian, Hua, Li, Jinjun, Shen, Qun, Wang, Hailin, Hao, Zhengping, Zou, Linda, and Hu, Qin. 2009. Using shell-tunable mesoporous Fe<sub>3</sub>O<sub>4</sub>@HMS and magnetic separation to remove DDT from aqueous media. Journal of Hazardous Materials 171(1-3): 459-464.
- University of Missouri-St. Louis. 2010. Analysis of IR Spectra [Online]. Available from : <http://www.umsl.edu/~orglab/documents/IRIR2.html> [2011, March 17]
- Wang, Chao, Ao, Yanhui, Wang, Peifang, Qian, Jin, Hou, Jun, and Zhang, Songhe. 2010. A simple method for preparation of superparamagnetic porous silica. Journal of Alloys and Compounds 493(1-2): 410-414.
- Wang, Zhan, Liu, Dezhong, Wu, Wenjuan, and Liu, Mei. 2006. Study of dead-end microfiltration flux variety law. Desalination 201(1-3): 175-184.
- Wankat, Phillip C. 1944. Separation process engineering. United States: Pearson.
- Wanitkorkul, Ananya, Osathaphan, Khemarath, and Sabatini, David A. 2005. Pharmaceutical removal by ion exchange process, Master's Thesis, Environmental Management Chulalongkorn University.

- Watson, D. G. 1999. Pharmaceutical analysis. London: Churchill Livingstone.
- Weber, J. W. J., and Morris, J. C. 1963. Kinetics of adsorption on carbon from solution. Sanit Eng Div 89(SA2): 31-59.
- Yan, Aiguo, Liu, Xiaohe, Qiu, Guanzhou, Wu, Hongyi, Yi, Ran, Zhang, Ning, and Xu, Jing. 2008. Solvothermal synthesis and characterization of size-controlled Fe<sub>3</sub>O<sub>4</sub> nanoparticles. Journal of Alloys and Compounds 458(1-2): 487-491.
- ONDCP. 2010. National Drug Control Strategy [Online]. Available from : [http://www.whitehousedrugpolicy.gov/drugfact/factsht/proper\\_disposal.html](http://www.whitehousedrugpolicy.gov/drugfact/factsht/proper_disposal.html) [2010, January 7]

## **APPENDICES**



## APPENDIX A

**Table A-1** NAL Concentration Versus Time in Kinetic Study on Adsorbents  
at pH = 7±0.2, 0.01 M Ionic Strength, 25°C

Time	NAL concentration (mg/l)							Time(PAC)
(min.)	HMS-SP	A-HMS-SP	M-HMS-SP	OD-HMS-SP	N-HMS-SP	PTM-HMS-SP	PAC	(min.)
0	20.01	20.01	20.01	20.01	20.01	20.01	37.43	0
1	19.75	19.63	19.55	19.40	19.67	19.68	26.49	1
2	19.71	19.40	19.36	19.07	19.48	19.54	23.45	3
3	19.66	19.25	19.23	18.69	19.29	19.12	18.82	5
4	19.64	19.13	19.15	18.85	19.01	18.96	15.47	10
5	19.63	19.14	19.02	18.76	19.01	18.93	13.23	15
10	19.63	19.13	19.13	18.67	18.99	18.89	11.46	20
15	19.63	19.12	19.14	18.73	18.99	18.82	11.2	25
20	19.63	19.13	19.14	18.65	18.99	18.78	9.23	30
25	19.63	19.13	19.13	18.66	19.01	18.8	8.29	45
30	19.63	19.12	19.14	18.64	19.01	18.76	7.21	60
45	19.64	19.14	19.14	18.66	19.01	18.79	5.72	120
60	19.63	19.12	19.15	18.65	18.99	18.78	5.00	180
120	19.64	19.13	19.13	18.65	18.98	18.78	4.83	1440

## APPENDIX B

**Table B-1** NAL Adsorption capacity Versus NAL Equilibrium Concentration in Isotherm  
Study on HMS-SP at pH = 5±0.2, 7±0.2, 9±0.2, 0.01 M Ionic Strength, 25°C

HMS-SP					
pH 5		pH7		pH9	
<i>C<sub>e</sub></i> (mg/L)	<i>q</i> (mg/g)	<i>C<sub>e</sub></i> (mg/L)	<i>q</i> (mg/g)	<i>C<sub>e</sub></i> (mg/L)	<i>q</i> (mg/g)
0.22	0.0241	0.20	0.0031	0.24	0.0156
3.12	0.2423	1.11	0.0744	2.26	0.1656
7.51	0.5110	6.33	0.2184	2.50	0.1664
10.24	0.7344	12.06	0.3374	9.55	0.2572
12.35	0.8733	15.02	0.414	15.14	0.4305
15.43	0.9255	20.12	0.4494	23.24	0.4456
18.56	0.9354	24.17	0.4428	28.13	0.4519
22.78	0.9804	26.70	0.4420	32.46	0.4751
0.22	0.0241	0.20	0.0031	0.24	0.0156
3.12	0.2423	1.11	0.0744	2.26	0.1656
-	-	6.33	0.2184	2.50	0.1664

**Table B-2** NAL Adsorption capacity Versus NAL Equilibrium Concentration in Isotherm  
Study on A-HMS-SP at pH = 5±0.2, 7±0.2, 9±0.2, 0.01 M Ionic Strength, 25°C

A-HMS-SP					
pH 5		pH7		pH9	
<i>C<sub>e</sub></i> (mg/L)	<i>q</i> (mg/g)	<i>C<sub>e</sub></i> (mg/L)	<i>q</i> (mg/g)	<i>C<sub>e</sub></i> (mg/L)	<i>q</i> (mg/g)
0.24	-	0.24	0.0237	0.24	-
1.73	-	1.73	0.2496	1.73	-
5.13	-	5.13	0.4803	5.13	-
9.59	-	9.59	0.6807	9.59	-
13.28	-	13.28	0.8130	13.28	-
22.02	-	22.02	0.8712	22.02	-
29.43	-	29.43	0.9464	29.43	-

**Table B-3** NAL Adsorption capacity Versus NAL Equilibrium Concentration in Isotherm  
Study on M-HMS-SP at pH = 5±0.2, 7±0.2, 9±0.2, 0.01 M Ionic Strength, 25°C

M-HMS-SP					
pH 5		pH7		pH9	
<i>C<sub>e</sub></i> (mg/L)	<i>q</i> (mg/g)	<i>C<sub>e</sub></i> (mg/L)	<i>q</i> (mg/g)	<i>C<sub>e</sub></i> (mg/L)	<i>q</i> (mg/g)
0.52	0.0687	0.23	0.0216	0.24	0.0142
1.47	0.4335	2.25	0.2801	2.61	0.1640
4.28	0.8518	4.02	0.4232	5.02	0.2353
8.16	1.0906	8.77	0.6552	9.45	0.4233
12.69	1.3074	17.23	0.8766	15.34	0.6628
18.28	1.3109	24.15	0.8900	12.59	0.5444
25.10	1.3153	26.88	0.8889	17.90	0.7030
33.09	1.2906	30.95	0.889	26.04	0.7331
0.52	0.0687	0.23	0.0216	0.24	0.0142
1.47	0.4335	2.25	0.2801	2.61	0.164
4.28	0.8518	4.02	0.4232	5.02	0.2353

**Table B-4** NAL Adsorption capacity Versus NAL Equilibrium Concentration in Isotherm  
Study on OD-HMS-SP at pH = 5±0.2, 7±0.2, 9±0.2, 0.01 M Ionic Strength, 25°C

OD-HMS-SP					
pH 5		pH7		pH9	
<i>C<sub>e</sub></i> (mg/L)	<i>q</i> (mg/g)	<i>C<sub>e</sub></i> (mg/L)	<i>q</i> (mg/g)	<i>C<sub>e</sub></i> (mg/L)	<i>q</i> (mg/g)
0.22	0.219	0.23	0.0216	0.35	0.1580
0.44	0.4098	2.25	0.2801	0.67	0.2255
3.71	1.1913	4.02	0.4232	4.42	0.5476
7.01	1.514	8.77	0.6552	9.57	0.9433
12.23	1.7286	17.23	0.8766	13.42	1.1416
18.10	1.8806	24.15	0.89	18.39	1.3647
21.56	1.8204	26.88	0.8889	23.31	1.3765
26.91	1.8749	30.95	0.889	-	-
30.50	1.8794	-	-	-	-

**Table B-5** NAL Adsorption capacity Versus NAL Equilibrium Concentration in Isotherm Study on N-HMS-SP at pH = 5±0.2, 7±0.2, 9±0.2, 0.01 M Ionic Strength, 25°C

N-HMS-SP					
pH 5		pH7		pH9	
<i>C<sub>e</sub></i> (mg/L)	<i>q</i> (mg/g)	<i>C<sub>e</sub></i> (mg/L)	<i>q</i> (mg/g)	<i>C<sub>e</sub></i> (mg/L)	<i>q</i> (mg/g)
0.28	0.0470	0.58	0.0746	0.32	0.0082
0.98	0.3411	1.02	0.0920	2.02	0.0100
4.07	0.6364	3.85	0.2013	4.97	0.0239
9.12	0.7942	8.10	0.3346	9.83	0.0737
14.18	0.9126	10.01	0.3873	12.16	0.0938
18.35	0.9893	12.49	0.4235	15.28	0.1232
23.80	1.0007	17.05	0.5151	20.22	0.1510
-	-	21.45	0.6189	25.09	0.1900

**Table B-6** NAL Adsorption capacity Versus NAL Equilibrium Concentration in Isotherm Study on PTM-HMS-SP at pH = 5±0.2, 7±0.2, 9±0.2, 0.01 M Ionic Strength, 25°C

PTM-HMS-SP					
pH 5		pH7		pH9	
<i>C<sub>e</sub></i> (mg/L)	<i>q</i> (mg/g)	<i>C<sub>e</sub></i> (mg/L)	<i>q</i> (mg/g)	<i>C<sub>e</sub></i> (mg/L)	<i>q</i> (mg/g)
0.20	0.1451	0.26	0.0164	0.31	0.0024
0.42	0.2708	2.02	0.0504	0.64	0.0197
2.82	1.4796	4.53	0.1676	4.58	0.1632
6.40	2.2299	9.36	0.5204	9.76	0.2988
1.53	1.0183	14.26	0.8415	12.39	0.3727
10.59	2.5783	20.35	1.1336	15.83	0.4284
14.86	2.6864	23.50	1.2872	19.83	0.4716
20.04	2.7101	-	-	24.50	0.5416

**Table B-7** NAL Adsorption capacity Versus NAL Equilibrium Concentration in Isotherm Study on PAC at pH = 5±0.2, 7±0.2, 9±0.2, 0.01 M Ionic Strength, 25°C

PAC					
pH 5		pH7		pH9	
<i>C<sub>e</sub></i> (mg/L)	<i>q</i> (mg/g)	<i>C<sub>e</sub></i> (mg/L)	<i>q</i> (mg/g)	<i>C<sub>e</sub></i> (mg/L)	<i>q</i> (mg/g)
1.92	28.51	0.76	30.4096	6.94	24.8144
10.04	29.45	4.22	33.2800	14.28	29.4400
35.17	33.63	27.60	35.1104	39.93	34.2368
-	-	35.02	38.7816	6.938	24.8144

## APPENDIX C

**Table C-1** UF Study at pH = 5±0.2, 0.01 M Ionic Strength, 25°C

pH5		pH5:NAL		pH5: PTM-HMS-SP		pH5:PTM-HMS-SP+Magnet		pH5:PTM-HMS-SP+NAL		pH5:PTM-HMS-SP+NAL+Mag	
t(sec)	v(mL)	t(sec)	v(mL)	t(sec)	v(mL)	t(sec)	v(mL)	t(sec)	v(mL)	t(sec)	v(mL)
51	4	7	1	8	3	36	7	9	3	11	5
64	6	21	2	15	5	88	10	16	5	79	10
78	8	34	3	28	8	107	11	28	8	92	11
91	10	53	4	40	9	125	12	36	9	107	12
98	11	68	5	50	10	157	14	44	10	120	13
106	12	84	6	60	11	176	15	55	12	128	14
115	13	146	10	70	12	210	17	66	13	140	15
132	15	205	14	82	13	228	18	85	15	148	16
144	16	228	16	95	14	245	19	97	16	161	17
155	18	254	18	109	15	285	21	108	17	173	18
178	20	281	20	129	16	297	22	116	18	199	20
191	21	303	22	169	18	317	23	131	19	218	22
201	22	337	24	191	19	336	24	150	20	230	23
236	25	388	28	211	20	351	25	171	22	243	24
252	26	423	30	247	22	382	27	183	23	256	25
263	27	462	33	274	23	419	29	195	24	268	26
283	29	530	38	292	24	434	30	208	25	298	28
306	31	570	40	310	25	456	31	220	26	320	30
320	32	594	42	352	27	491	33	289	27	360	33
343	34	629	44	459	32	509	34	307	28	375	34
370	36	647	45	520	35	523	35	325	29	392	35
389	38	666	46	636	40	549	36	344	30	406	36
425	41	708	49	740	44	586	38	364	31	446	39
448	43	726	50	760	45	612	39	384	32	463	40
484	46	755	52	812.4	48	650	41	405	33	494	42
516	49	771	53	867	50	708	44	426	34	518	44
554	52	789	55	1023	55	736	45	448	35	537	45
653	60	834	57	1327.2	64	819	49	494	37	584	48

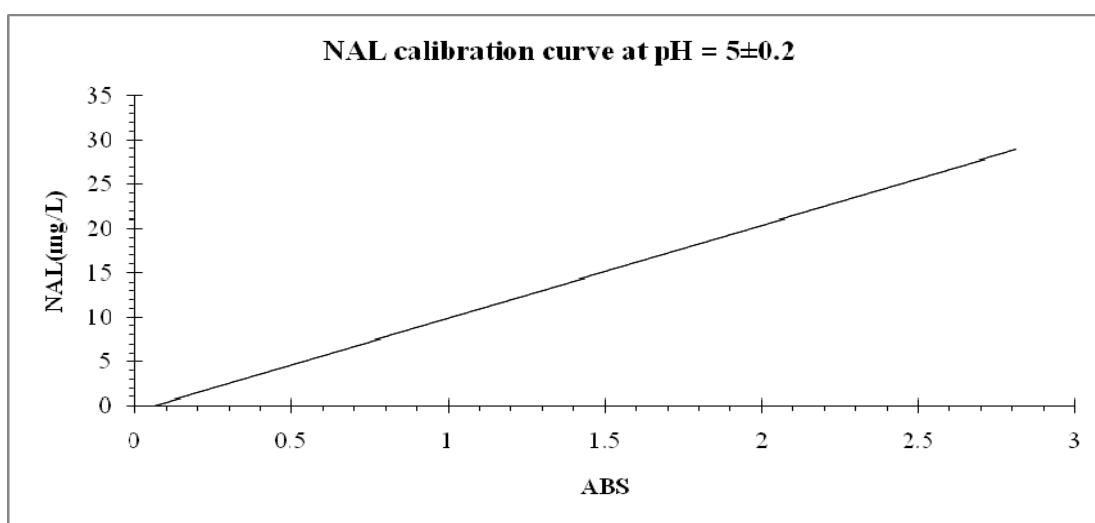
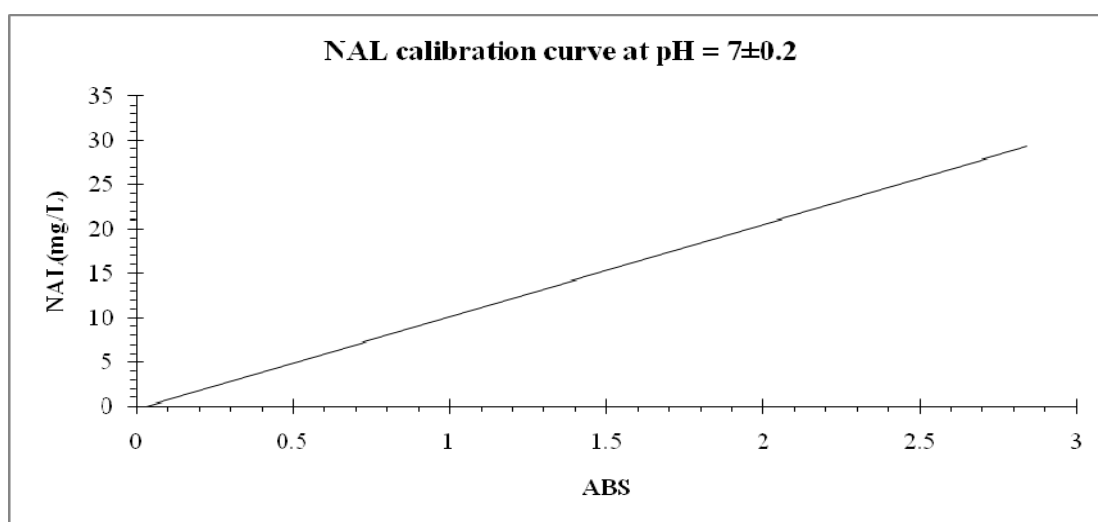
pH5		pH5:NAL		pH5: PTM-HMS-SP		pH5:PTM-HMS-SP+Magnet		pH5:PTM-HMS-SP+NAL		pH5:PTM-HMS-SP+NAL+Mag	
t(sec)	v(mL)	t(sec)	v(mL)	t(sec)	v(mL)	t(sec)	v(mL)	t(sec)	v(mL)	t(sec)	v(mL)
667	61	848	58	1350	65	850	50	517	38	623	50
695	63	864	59	1563	70	876	51	541	39	650	52
741	66	881	60	1752	75	912	53	565	40	664	53
807	71	911	62	1980	80	937	54	590	41	695	55
883	76	926	63	-	-	955	55	616	42	719	56
-	-	944	64	-	-	972	56	642	43	738	57
-	-	966	65	-	-	990	57	669	44	773	59
-	-	986	66	-	-	1012	58	696	45	795	60
-	-	1012	68	-	-	1058	60	724	46	810	61
-	-	1032	69	-	-	1088	61	752	47	833	62
-	-	1053	70	-	-	1126	63	780	48	850	63
-	-	1085	72	-	-	1164	64	810	49	885	65
-	-	1100	73	-	-	1197	66	840	50	906	66
-	-	1120	74	-	-	1227	67	870	51	926	67
-	-	1137	75	-	-	1251	68	901	52	945	68
-	-	1153	76	-	-	1288	70	932	53	960	69
-	-	1172	77	-	-	1317	71	964	54	989	70
-	-	1206	79	-	-	1349	72	996	55	1050	73
-	-	1221	80	-	-	1389	74	1029	56	1063	74
-	-	1263	82	-	-	1410	75	1063	57	1090	75
-	-	1306	85	-	-	1434	76	1097	58	1106	76
-	-	1327	86	-	-	1454	77	1132	59	1151	78
-	-	1347	87	-	-	1497	79	1167	60	1203	80
-	-	1361	88	-	-	1568	82	1202	61	1245	82
-	-	1377	89	-	-	1604	84	1238	62	1264	83
-	-	1396	90	-	-	1644	85	1275	63	1308	85
-	-	-	-	-	-	1655	86	1312	64	1334	86
-	-	-	-	-	-	1687	87	1350	65	1354	87
-	-	-	-	-	-	1718	88	1388	66	1380	88
-	-	-	-	-	-	1758	90	1427	67	1433	90
-	-	-	-	-	-	1778	91	1467	68	1456	91
-	-	-	-	-	-	1800	93	1506	69	1478	92
-	-	-	-	-	-	1866	95	1547	70	1533	94
-	-	-	-	-	-	1983	100	1588	71	1555	95
-	-	-	-	-	-	-	-	1629	72	1598	97
-	-	-	-	-	-	-	-	1671	73	1633	98
-	-	-	-	-	-	-	-	1714	74	1657	99

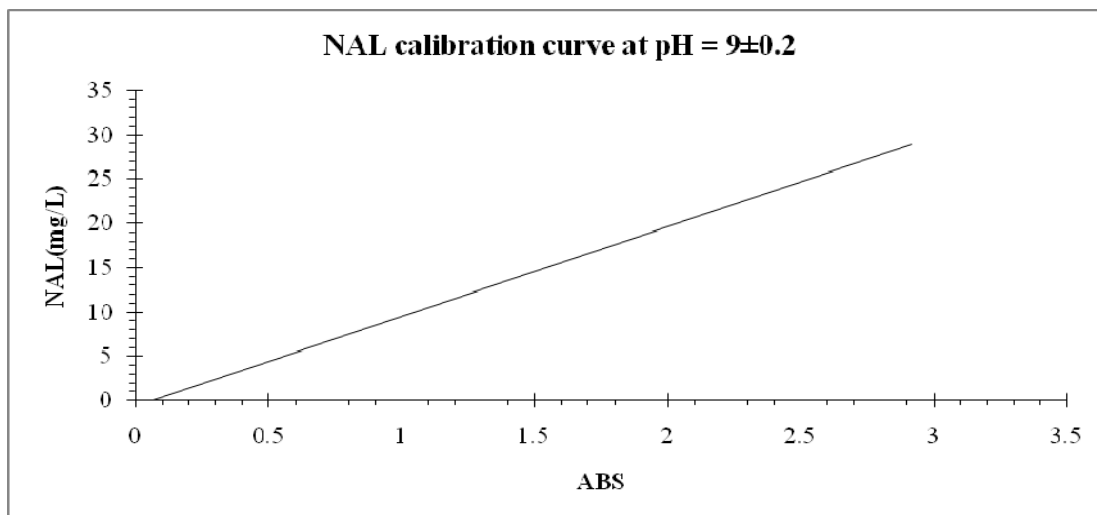
**Table C-2** UF Study at pH = 7±0.2, 0.01 M Ionic Strength, 25°C

pH7		pH7:NAL		pH7:PTM-HMS-SP		pH7:PTM-HMS-SP+NAL	
t(sec)	v(mL)	t(sec)	v(mL)	t(sec)	v(mL)	t(sec)	v(mL)
7	1	35	4	44	13	4	1
23	3	55	5	62	14	12	3
38	4	61	6	77	15	18	4
46	5	75	7	89	16	27	5
69	7	110	9	112	17	38	6
83	8	132	10	124	18	47	7
107	10	140	11	137	19	59	8
137	13	156	12	156	20	71	9
159	15	172	13	171	21	84	10
175	16	185	14	202	22	104	12
206	18	199	15	222	24	117	13
227	19	213	16	252	26	127	14
253	21	250	19	270	27	138	15
287	24	269	20	299	29	162	17
303	25	304	23	339	31	171	18
316	26	324	24	363	32	183	19
328	27	344	26	402	34	202	20
361	30	360	27	422	35	232	23
377	31	389	29	441	36	246	24
398	33	415	31	462	37	258	25
410	34	437	33	483	38	268	26
420	35	460	34	505	39	281	27
460	39	477	36	528	40	306	29
469	40	519	39	550	41	320	30
481	41	546	41	570	42	354	33
500	43	592	44	594	43	394	36
521	45	606	45	640	45	485	38
540	46	619	46	663	46	506	39
572	49	634	47	676	47	527	40
603	51	664	49	702	48	548	41
633	54	676	50	732	49	569	42
657	56	703	52	802	52	591	43
717	59	736	54	853	54	614	44
720	61	760	56	884	55	637	45





**APPENDIX D****Table D-1** NAL Calibration Curve at pH = 5±0.2, 0.01 M Ionic Strength, 25°C**Table D-2** NAL Calibration Curve at pH = 7±0.2, 0.01 M Ionic Strength, 25°C

**Table D-3** NAL Calibration Curve at pH = 9±0.2, 0.01 M Ionic Strength, 25°C

## BIOGRAPHY

**Name:** Ms. Vichuda Tipsunave  
**Date of Birth:** October, 20, 1987  
**Place of Birth:** Bangkok, Thailand  
**Nationality:** Thai  
**Education:**  
**2009** Bachelor Degree of Environmental Engineering,  
Faculty of Engineering, Chulalongkorn University,  
Bangkok, Thailand